NORTHWESTERN UNIVERSITY

Improving Biological Properties of Spherical Nucleic Acids Through Structural Control

A DISSERTATION

SUBMITTED TO THE GRADUATE SCHOOL
IN PARTIAL FULFILLMENT OF THE REQUIREMENTS

for the degree

DOCTOR OF PHILOSOPHY

Field of Biomedical Engineering

By

Matthew K. Vasher

EVANSTON, ILLINOIS

December 2022

Abstract

Nucleic acid therapeutics can be drug molecules with high programmability, minimal off-target effects, and the capability to address “undruggable” targets for diseases. In addition, each time a new drug is needed, one needs to only change the sequence as opposed to finding an entirely new structure. One nucleic acid type in particular, small interfering RNA (siRNA), has shown particular promise as a therapeutic. siRNAs are short, double-stranded RNA molecules that can be designed to silence any gene of interest. Due to their programmability, specificity, and potency, siRNAs have tremendous potential as therapeutics for cancers, autoimmune disorders, and any other diseases that are driven by the overexpression of a gene. However, despite over two decades of research, siRNAs have yet to reach widespread clinical use, with the first siRNA drug receiving FDA approval in 2018 and only four more being approved since then, all for treating the liver. The clinical success of siRNAs has been severely restricted by poor stability and delivery: unmodified siRNAs are rapidly degraded in biological fluids by nucleases, have poor pharmacokinetics, and cannot enter cells without transfection agents.

To overcome these limitations, siRNAs can be radially arranged around a nanoparticle core to form a spherical nucleic acid (SNA). siRNA-based SNAs (siRNA-SNAs) gain unique properties that linear siRNAs lack, such as resistance to nuclease degradation and efficient entry into cells. At the start of my PhD, all published siRNA-SNAs followed a prototypical design: thiolated passenger strands were attached to a ~13-nm gold nanoparticle core, and complementary guide strands were hybridized to the passenger strands. Prototypical siRNA-SNAs have shown some success in mouse models of disease and even progressed to a first-in-human clinical trial, but they are limited in their performance and widespread applicability. Important biological properties critical to the efficacy of the siRNA-SNA include structural

stability, nuclease resistance, biocompatibility, pharmacokinetics, cellular uptake, cytosolic delivery, and therapeutic activity, and all of these properties are limited by the prototypical siRNA-SNA's structure.

This dissertation investigates how structural changes to the siRNA-SNA can be used to improve its biological properties. Chapter 1 introduces siRNA, current delivery strategies, prototypical siRNA-SNAs, and the structure-function relationships of SNAs. In Chapter 2, a hairpin-like architecture for attaching siRNAs to the nanoparticle core is introduced, leading to improved structural stability, nuclease resistance, biocompatibility, cellular internalization, and therapeutic activity. In Chapter 3, the effect of core size on SNA behavior is investigated, with the finding that an ultrasmall 1.4-nm gold nanocluster core improves the SNA's drug-to-carrier ratio, pharmacokinetics, and cellular uptake. In Chapter 4, lipid-based cores are explored as a biocompatible alternative to gold-based cores for siRNA-SNAs, leading to the design of next-generation siRNA-SNAs with improved biocompatibility, potential suitability as an ocular drug, and efficient cytosolic delivery. Finally, Chapter 5 concludes the dissertation with a summary of the findings and a description of future work in the development of next-generation SNAs. While this work primarily focuses on siRNA-SNAs, many of the structure-function relationships characterized herein will apply to SNAs composed of other nucleic acids as well. Overall, this dissertation shows that control over chemical structure can be used to significantly enhance the biological properties of SNAs, improving their therapeutic suitability. These findings will play an important role in the design of next-generation SNAs as well as drive the progression of siRNAs toward widespread clinical use.

Acknowledgments

It is no secret that a PhD can be filled with challenges, and my time in graduate school was no exception. There were many times when I felt like I would not be able to finish this degree. While writing this dissertation, I reflected on the fact that it was the people I interacted with along the way that enabled not only my success, but my sanity. My advisors, labmates, friends, and family provided the support, wisdom, and fun I needed to get through graduate school and actually enjoy my time during it. I thank the following people for helping me complete this PhD.

First, I extend gratitude to my advisor, Prof. Chad Mirkin. Chad provided a lab environment with immense resources, freedom to pursue the research I was passionate about, and interdisciplinary collaborative opportunities. Whenever I discussed a project with him, he taught me to focus on both a fundamental understanding of the science behind a technology and its real-world applications, and that a project is not complete without both. Our meetings were concise and highly impactful, which developed my ability to tell a story and sell a project and allowed me to work at my own pace. Perhaps most importantly, he taught me how to present in a straightforward, compelling, professional manner, which has already significantly impacted my career, and I am certain I will continue to benefit from it. He also taught me to respectfully disagree and defend my perspective if I believe I am correct, no matter how famous the other person is (even him!). Because of Chad, I am a better scientist, leader, and presenter.

I thank the other members of my thesis committee, Prof. Evan Scott, Prof. Neha Kamat, and Prof. Milan Mrksich, for providing fresh perspectives and helpful feedback on my research. I thank Prof. Casey Ankeny for being a terrific professor to do my teaching assistantship under during spring 2020. I was inspired by her flexibility and professionalism during the abrupt

transition to virtual classes at the start of the COVID-19 pandemic, and I had a great experience teaching during what was an otherwise hectic time. I thank my career advisor, Elysse Longiotti, for providing crucial guidance and feedback during my job hunt.

There are many people in the Mirkin lab that were essential to my success. I thank the Mirkin office staff for keeping the lab running like a well-oiled machine. Dr. Tanushri Sengupta, Dr. Jenny Orbeck, Pam Watson, Bethany Hexom, Dr. Sarah Petrosko, Dr. Sara Rupich, and Elizabeth Forest ensured that I was able to set up meetings, complete my research, and fulfill my degree requirements. I thank the technicians I worked with, Vinz Mayer, Jenny Delgado, Matt Capek, and Rob Stawicki for synthesizing all of the oligonucleotides (especially RNA) that I needed for my projects.

I am grateful to Dr. Gokay Yamankurt for mentoring me during the first three years of my PhD, and especially for his valuable advice. Gokay completely shaped the way I approach research. He taught me how to prioritize my experiments, decide what was and was not worth my time and effort, and plan a path to completing a project. He also taught me how to think of each project as a story and figure out how each experiment would help me tell that story in a convincing and compelling way. His guidance set me up for success in my PhD.

I thank my labmates for providing an excellent work environment and making it fun to go into the lab. I thank my collaborators Dr. Gokay Yamankurt, Jungsoo Park, and Justin Kim for their work on Chapter 2; Prof. Cassi Callmann, Prof. Dia Das, and Dr. Caroline Kusmierz for their work on Chapter 3; Michael Evangelopoulos, Dr. Gokay Yamankurt, Dr. Alex Anderson, and Absorption Systems for their work on Chapter 4; and Prof. Michelle Teplensky, Dr. Andrew Sinegra, Dr. Ziyin Huang, and Dr. Shuya Wang for their work on other projects. I thank my coleaders of the Nanomedicine Subgroup, Michael Evangelopoulos and Prof. Michelle

Teplensky, for ensuring the success of our subgroup and helping me build my leadership skills. Thanks to Jasper Dittmar, Dr. Andrew Sinegra, Jungsoo Park, Dr. Sasha Ebrahimi, Jenny Delgado, Michael Evangelopoulos, Ben Coleman, Vinz Mayer, Namrata Ramani, Dr. Adam Ponedal, and Melissa Puga for being great friends to hang out with both inside and outside the lab. I thank my mentees Justin Kim and T Ocampo for their fresh perspectives and willingness to carry on my research, and I thank the countless other people I met at Northwestern that I did not have space to mention here. It was a joy to discuss research with you, bounce ideas off of each other, and do fun activities together.

My friends were essential to my mental health throughout graduate school, and it was a joy to celebrate victories, drown sorrows, and laugh in the face of failure with them. I am grateful to have met my fellow biomedical engineering PhD students Jasper Dittmar, Dr. Dan Sykora, Dr. Maggie Boyd, Dr. Joey Bruns, and Dr. Andrew Sinegra. They showed me that we do not have to go through our struggles alone. Thanks to my friends Max Greenberg and Michael Kinsey for reminding me that there is life outside of graduate school. Thanks to Dr. Al Hassan and Dr. Hussain Sangji for being amazing roommates during my first three years in Chicago. They were a great source of wisdom for navigating both graduate school and the city of Chicago. They also introduced me to the world of consulting, which had a monumental impact on my career path. Thanks to my college buddies Ian Lane, Alex Chafetz, and Eric Bargiel for always making the effort to meet up and being true lifelong friends.

I am grateful to my girlfriend Jackie Tapia for always sticking by my side throughout my PhD. She always provided the love and support I needed to persevere. She is a great person to discuss my problems and ideas with and provided a much needed outside perspective when it came to my research and career decisions. She was also always willing to escape with me when I

needed a break from graduate work. She has always been there to remind me that I am not going through this journey alone.

Last but certainly not least, I thank my family for their endless support. My dad made the effort to always talk with me and served as a sounding board for all of my problems and decisions. My mom gave me words of encouragement and understood my interests. My sister Holly has always been a friend and peer that has given me much-needed perspective. My (soon-to-be) brother-in-law Daniel Castro has become a true member of the family who has supported me and been a lot of fun to hang out with. My grandparents, aunts, uncles, and cousins have been supportive, and I always look forward to our family reunions. I appreciate everything my family has done for me, and I hope I have made them proud.

List of Abbreviations

A: adenine

ALAS1: aminolevulinate synthase 1

AMD: age-related macular degeneration

ANOVA: analysis of variance

ASGPR: asialoglycoprotein receptors

ATP: adenosine triphosphate

AuNC: gold nanocluster

AuNC-SNA: gold nanocluster-core spherical nucleic acid

AuNP: gold nanoparticle

AuNP-SNA: 10-nm gold nanoparticle-core spherical nucleic acid

AuSNA: 13-nm gold nanoparticle-core spherical nucleic acid

C: cytosine

calc.: calculated

CD31: cluster of differentiation 31

chol: cholesterol

CI: confidence interval

DAPI: 4′,6-diamidino-2-phenylindole

DHAP: 2',4'-dihydroxyacetophenone

D-Lin-MC3-DMA: (6Z,9Z,28Z,31Z)-heptatriacont-6,9,28,31-tetraene-19-yl 4-(dimethylamino) butanoate

DLS: dynamic light scattering

DMT: dimethoxytrityl

DNA: deoxyribonucleic acid

DOPC: 1,2-dioleoyl-*sn*-glycero-3-phosphorethanolamine

DPBS: Dulbecco's phosphate-buffered saline

DPPC: 1,2-dipalmitoyl-sn-glycero-3-phosphocholine

DS: dithiol serinol

DSPC: 1,2-distearoyl-*sn*-glycero-3-phosphocholine

DTT: dithiothereitol

EDC: 1-ethyl-3-(3-dimethylaminopropyl)carbodiimide

EGM-2: Endothelial Cell Growth Medium-2

ELISA: enzyme-linked immunosorbent assay

exp.: expression

FBS: fetal bovine serum

FDA: Food and Drug Administration

G: guanine

GalNAc: N-acetylgalactosamine

HEPES: 4-(2-hydroxyethyl)-1-piperazineethanesulfonic acid

HER2: human epidermal growth factor receptor 2

HP: hairpin-like

HRP: horseradish peroxidase

HUVEC: human umbilical vein endothelial cells

hyb.: hybridized

IC_{50}: half maximal inhibitory concentration

ICP-MS: inductively coupled plasma mass spectrometry

IV: intravenous

LD_{50}: median lethal dose

LDL-C: low-density lipoprotein cholesterol

LNA: locked nucleic acid

LNP: lipid nanoparticle

LNP-SNA: lipid nanoparticle-core spherical nucleic acid

LSNA: liposome-core spherical nucleic acid

Luc: luciferase

Luc2: luciferase 2

MALDI-TOF: matrix-assisted laser desorption/ionization time-of-flight

MPS: mononuclear phagocyte system

mRNA: messenger ribonucleic acid

MW: molecular weight

Obs.: observed

PAGE: polyacrylamide gel electrophoresis

PBS: phosphate-buffered saline

PC: phosphatidylcholine

PCSK9: proprotein convertase subtilisin/kexin type 9

PEG: polyethylene glycol

PLGA: poly(lactic-*co*-glycolic acid)

PLGA-SNA: poly(lactic-*co*-glycolic acid) nanoparticle-core spherical nucleic acid

***p*-MBA:** *p*-mercaptobenzoic acid

POSS: polyoctahedral silsesquioxane

rel.: relative

RISC: ribonucleic acid-induced silencing complex

RNA: ribonucleic acid

RNAi: ribonucleic acid interference

RT-qPCR: reverse transcription quantitative polymerase chain reaction

SD: standard deviation

SDS: sodium dodecyl sulfate

siRNA: small interfering ribonucleic acid

siRNA-SNA: small interfering ribonucleic acid-based spherical nucleic acid

SNA: spherical nucleic acid

Sp18: spacer 18

SSC: saline-sodium citrate

STAT3: signal transducer and activator of transcription 3

T: thymine

TBE: tris/borate/ethylenediaminetetraacetic acid

TE: tris/ethylenediaminetetraacetic acid

TLR9: toll-like receptor 9

TMB: 3,3',5,5'-tetramethylbenzidine

TNBC: triple-negative breast cancer

toc: tocopherol

TTR: transthyretin

U: uracil

US: ultrasmall

UV-vis: ultraviolet-visible

VEGF: vascular endothelial growth factor

λ_{em}**:** emission wavelength

λ_{ex}**:** excitation wavelength

Table of Contents

List of Figures

List of Tables

CHAPTER 1

Introduction

1.1. Classes of Therapeutics

1.1.1. Small Molecule Therapeutics

Historically, the vast majority of medicines have been small molecules, which still make up 90% of current on-the-market drugs.[1] However, the development of small molecule drugs is expensive, lengthy, risky, and inefficient. The discovery of a drug candidate involves screening a library of small molecules against an array of targets (usually proteins) in the search for an interaction that indicates an ability to treat a disease.[2] The following processes of research, development, clinical trials, and regulatory approval are time consuming, labor intensive, and expensive, and during each stage a large fraction of drug candidates are eliminated; the overall failure rate in drug development is over 96%.[3] Usually, it takes 10 to 15 years and hundreds of millions of dollars for a single drug to finally reach the market.[4] Even for small molecule drugs that do manage to reach the market, the interactions between small molecules and their targets are not perfectly specific and small molecules often bind to off-target sites, leading to harmful side effects.[5] Beyond the diseases and conditions that can be treated by small molecule drugs, many potential targets including a broad variety of disease-causing proteins are currently considered "undruggable."[6] The strategy of trying to develop random small molecules for disease targets is highly inefficient and only effective for a narrow range of targets.

1.1.2. Biologic Therapeutics

Biologics such as antibodies are another established class of therapeutics. Unlike the serendipitous development process of small molecule drugs, biologics are extracted from living organisms with a known target already in mind.[7] For example, antibodies that target specific antigens are produced in animals and can be used as a therapeutic for humans. Because of this, development of biologics is much more focused than the broad screening of small molecule

drugs against random targets, which often results in shorter development times.[8] While targeted development may help with the efficiency of biologic drug development, production of biologics is difficult due to their complexity and instability as well as strict quality controls from generating drugs from living organisms. Since biologics naturally bind to their targets in a manner that has been optimized by evolution, biologics are more specific to their targets and are less prone to off-target binding than small molecule drugs.[9] However, the large size of antibodies and other biologics makes delivery to their targets difficult, and they can still cause a harmful off-target immune response.[10] Like small molecule drugs, biologics often target proteins. The three-dimensional interactions between biologics and their targets are highly complex and development usually relies on biologic-target interactions that exist in nature. Thus, biologics are primarily limited to known targets (e.g., antibodies with known antigens) and the vast majority of potential targets remain undruggable. Therefore, the development of intentionally designed drug molecules for targets beyond those currently accessible by small molecules and biologics would vastly expand the range of diseases that can be treated, improve drug development efficiency, and increase the specificity of the final therapeutic.

1.1.3. Nucleic Acid Therapeutics

Nucleic acids such as deoxyribonucleic acid (DNA) and ribonucleic acid (RNA) have tremendous potential as highly specific, intentionally designed therapeutic agents for a wide range of diseases. Nucleic acids are primarily known as naturally occurring molecules that function as information carriers in all living things on Earth.[11] However, nucleic acids can also be synthetically designed and constructed for therapeutic purposes.[12] Unlike most small molecules and biologics which primarily target proteins, nucleic acids can be designed to target DNA and RNA in the body. Many diseases arise from or are exacerbated by abnormal genes or

gene expression, including cancers, immune disorders, and degenerative diseases.[13,14] Nucleic acid drugs are designed to specifically manipulate these genetic defects in order to alleviate the disease state. Since nucleic acids are composed of a simple "alphabet" of nitrogenous bases (adenine (A), thymine (T)/uracil (U), cytosine (C), and guanine (G)), it is straightforward to develop nucleic acid drugs with a sequence that will interact with the disease-causing gene and either alter, eliminate, or change the expression of it.[15] In contrast to relying on the complex interactions of small molecules and biologics with a limited range of targets, nucleic acid drugs can be easily designed to target any problematic gene using the simple knowledge of sequence complementarity (A binds to T and U, C binds to G) and can potentially target the entire genome. There is also an inherent advantage to inhibiting the production of disease-associated proteins by targeting genes, rather than interacting with disease-associated proteins that are already abundant in the body and continue to be produced. The ultimate promise of the field is that nucleic acid therapeutics can be intentionally and precisely designed to treat a wide range of diseases. A variety of synthetic nucleic acid structures are being developed as gene regulatory agents,[16–18] gene editing agents,[19] immunomodulatory agents,[20] and aptamers,[21] and several have reached clinical use.[12]

1.2. siRNA as a Nucleic Acid Therapeutic

1.2.1. siRNA

One nucleic acid molecule in particular, small interfering RNA (siRNA), has shown significant therapeutic promise due to its ability to silence genes via RNA interference (RNAi) (**Figure 1.1**). siRNA is a short (roughly 20 base pairs in length) double-stranded RNA molecule consisting of a guide strand and a passenger strand.[22] RNAi is an endogenous pathway in which a protein complex in the cytosol called the RNA-induced silencing complex (RISC) processes

the siRNA molecule, hybridizes the guide strand of the siRNA to complementary messenger RNA (mRNA), and cleaves the mRNA, preventing it from being translated into the protein it codes for. Through this cleavage, the gene carried by the mRNA is "silenced" and the expression of that gene and the protein it codes for are reduced.[23,24]

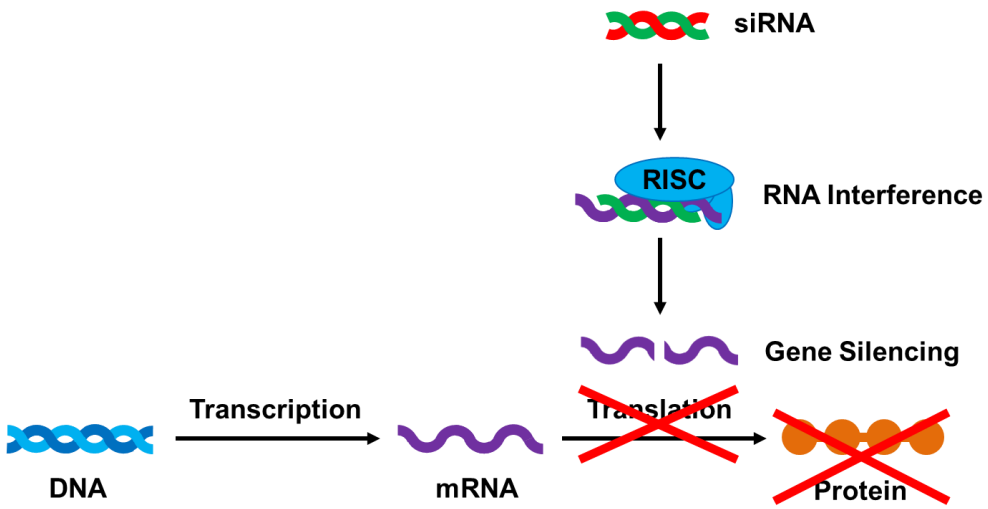

Figure 1.1. siRNA silences genes through RNAi. DNA is transcribed into mRNA, which is then translated into proteins. siRNA (red: passenger strand, green: guide strand) is processed by the RISC, the guide strand is hybridized to complementary mRNA, and the mRNA is cleaved, preventing translation into the protein it codes for and silencing that gene.

1.2.2. siRNA as a Therapeutic

In principle, siRNAs can be synthetically designed to silence any gene of interest through the RNAi pathway by designing the guide strand of the siRNA to be complementary to the mRNA for the target gene.[25–27] Since many diseases such as cancer and autoimmunity arise from, or are exacerbated by, the abnormal overexpression of specific genes, siRNAs have tremendous potential as a broadly applicable therapeutic class that can silence genes to treat a wide range of diseases.[13,14,28] In addition to its programmability, since RNAi is enzymatically driven, siRNAs are more potent and specific than other nucleic acid therapeutics such as antisense oligonucleotides.[29,30] The discovery of the RNAi mechanism in 1998[23] was eventually awarded

the 2006 Nobel Prize in Physiology or Medicine, with anticipation that siRNAs would lead to a therapeutic revolution.[31] However, due to several limitations and challenges of developing siRNAs as a therapeutic, it took until 2018 for the first siRNA drug to be approved by the U.S. Food and Drug Administration,[32,33] and there are still only a small number of siRNA drugs available for a very narrow range of targets.[34]

1.2.3. Current siRNA Therapeutic Strategies

Despite the promise of siRNAs as a therapeutic, clinical development of siRNAs has been severely restricted by several limitations. siRNAs are highly susceptible to rapid degradation by nucleases in biological fluids, particularly serum nucleases in blood (the half-life of siRNAs in serum can be as low as several minutes).[35] This means that after the administration of an siRNA drug, much of the siRNA molecule is degraded before it can reach its target site. siRNAs also have unfavorable pharmacokinetics with low accumulation in tissues of interest and rapid clearance from the body.[36,37] Finally, due to their large size (~13 kDa) and negative charge, siRNAs are unable to independently cross cell membranes to enter cells.[38,39] Consequently, even if a sufficient amount of siRNAs reach the target site, they cannot enter the cells to interact with RNAi proteins and silence target mRNA in the cytosol. These limitations have rendered unmodified siRNA molecules unsuitable for therapeutic use. Researchers have developed a variety of strategies to overcome these limitations. However, it is important to consider that any structural change to siRNA that improves nuclease resistance, pharmacokinetics, or cellular internalization could also interfere with the RNAi pathway by inhibiting interactions with the RISC or target mRNA.[40,41]

siRNA molecules can be chemically modified by altering their phosphate backbone, sugar moieties, or bases in order to improve stability, pharmacokinetics, and uptake.[42–44] For

example, replacing the phosphodiester backbone with a phosphorothioate increases resistance to nuclease degradation. Modifying the 2' position of the sugar with 2'-O-methyl (2'-OMe), 2'-fluoro (2'-F), or 2'-O-methoxyethyl (2'-MOE) enhances stability and nuclease resistance and reduces off-target effects. However, these modifications can have a detrimental effect on gene silencing ability, especially when prominently used throughout the sequence. Only certain modification patterns at specific points in the sequence are tolerated by the RNAi pathway, requiring careful design and optimization of each modified siRNA sequence and limiting its broad applicability.[43,45]

Viral vectors can be used to efficiently delivery siRNAs, but they induce mutations, inflammation, and immunogenic responses, making them unsafe for clinical use.[46] As a non-viral delivery strategy, nanoparticles composed of materials such as polymers,[47] dendrimers,[48] and metal[49] have been used to encapsulate or attach siRNAs. These nanoparticle-based approaches have varied effects on protection from nuclease degradation, pharmacokinetics, and cellular internalization, and often come with drawbacks such as endosomal entrapment and low biocompatibility.[41] Lipid-based nanoparticles have become a popular approach due to their ease of synthesis and biocompatible composition, and can carry encapsulated siRNAs into cells via membrane fusion.[50] Neutrally charged liposomes are biocompatible but can be inefficient at transfecting siRNA into cells.[41] Cationic liposomes are exceptionally efficient at delivering siRNAs into cells, and have become the state-of-the-art transfection reagent for siRNA *in vitro* for cell culture gene silencing experiments.[51,39] However, they are not ideal for *in vivo* usage since their positive charge leads to inflammation, cytotoxicity, and rapid clearance due to interactions with negatively charged serum proteins.[52,53] Solid lipid nanoparticles provide siRNAs with effective protection from degradation and efficient cytosolic delivery.[54] Lipid

nanoparticles are one of the only siRNA delivery strategies to reach the clinic,[33] but they have several drawbacks that do not make them a universal solution. Lipid nanoparticles can lead to inflammation so severe that patients must be pre-treated with anti-inflammatory drugs before receiving the siRNA drug.[34] Additionally, the large size of lipid nanoparticles causes them to only accumulate in fenestrated tissues such as the liver, significantly restricting their use for treating diseases in other tissues.[55]

Finally, the strategy of bioconjugation involves attaching siRNAs to molecules that enhance delivery, such as targeting ligands.[56] For example, the approach of conjugating siRNAs to glycoproteins terminating with N-acetylgalactosamine (GalNAc) sugars that target asialoglycoprotein receptors (ASGPR) highly expressed in hepatocytes allows for exceptionally efficient delivery to the liver.[57] While GalNAc has shown impressive efficacy in the siRNA field, it is limited to targeting hepatocytes and has been associated with severe adverse effects.[58,59] Other targeting ligands that have been conjugated to siRNAs include cyclic arginyl-glycyl-aspartic acid for targeting integrins on cancer cells and antibodies for targeting cell-specific antigens. Beyond targeting ligands, siRNAs can be conjugated to cationic peptides to penetrate tissue barriers and cell membranes as well as lipophilic molecules to improve serum stability and pharmacokinetics.[60,34]

At the start of my PhD in 2017, there were no Food and Drug Administration (FDA)-approved siRNA drugs despite over two decades of development efforts, which motivated my pursuit of siRNA research. Since then, five siRNA drugs have finally broken into the pharmaceutical market, with several others following close behind in late-stage clinical trials. In 2018, Onpattro (patisiran) became the first siRNA drug to receive FDA approval.[33] Patisiran consists of chemically modified siRNAs encapsulated in a lipid nanoparticle, and it treats

polyneuropathy associated with hereditary transthyretin (TTR)-mediated amyloidosis, a fatal orphan disease.[32] Patisiran siRNA silences *TTR* mRNA in the liver, inhibiting the production of TTR protein in amyloid deposits. The siRNA molecule features 11 2'-OMe modifications and an unmodified phosphodiester backbone, which is fewer modifications than other prominent siRNA drugs that were in development at the time.[34] The lipid nanoparticle contains the ionizable lipid (6Z,9Z,28Z,31Z)-heptatriacont-6,9,28,31-tetraene-19-yl 4-(dimethylamino)butanoate (D-Lin-MC3-DMA), which facilitates the cellular uptake of the lipid nanoparticle as well as the release of siRNA into the cytosol.[61] Due to their large size, the lipid nanoparticles highly accumulate in the liver, making the patisiran lipid nanoparticle strategy well-suited for treating this liver disease but not ideal for treating other tissues. In clinical trials, patisiran was highly effective and caused only some mild adverse effects.[32] Patisiran is administered through intravenous infusion over 80 min every three weeks and requires premedication with anti-inflammatory drugs.[33]

The second siRNA drug to receive FDA approval was Givlaari (givosiran), a fully chemically modified siRNA conjugated to GalNAc that silences aminolevulinate synthase 1 (*ALAS1*) mRNA in the liver to treat acute hepatic porphyria, a rare genetic disorder driven by the overproduction of ALAS1 enzymes.[62,59] Every nucleotide of givosiran is chemically modified, consisting of a combination of 2'-F, 2'-OMe, and phosphorothioate modifications. When givosiran is subcutaneously injected, GalNAc targets ASGPR prominently expressed in hepatocytes, resulting in high uptake in the liver. While givosiran was highly effective in clinical trials and most adverse effects were mild, several participants experienced severe renal and hepatic side effects.[58,63] Given that the drug was rapidly reviewed and approved in 2019, more time is needed to evaluate its long-term efficacy due to the chronic nature of acute hepatic porphyria and its long-term safety due to the severe adverse effects observed in clinical trials.

Oxlumo (lumasiran) received FDA approval in 2020 as a treatment for the orphan disease primary hyperoxaluria type 1.[64] Like givosiran, lumasiran is a fully chemically modified siRNA conjugated to GalNAc and it follows a similar chemical modification pattern.[65] Lumasiran targets glyoxylate oxidase mRNA in the liver. In clinical trials, lumasiran showed high efficacy and resulted in only mild adverse effects.[66,67,65]

The first three FDA-approved siRNA drugs treat orphan diseases, meaning siRNA was far from reaching the status of a widespread therapeutic class. This began to shift when Leqvio (inclisiran) became the fourth siRNA drug to receive FDA approval in late 2021.[68] Inclisiran is a fully chemically modified siRNA conjugated to GalNAc that treats the highly prevalent disease hypercholesterolemia (high cholesterol), which can lead to life-threatening cardiovascular diseases.[69,70] Following subcutaneous injection, inclisiran is taken up by hepatocytes and silences proprotein convertase subtilisin/kexin type 9 (*PCSK9*) mRNA to inhibit the low-density lipoprotein cholesterol (LDL-C) metabolic pathway. In clinical trials, inclisiran demonstrated a favorable safety profile and effectively reduced PCSK9 and LDL-C levels.[71,72,69] However, while decreased PCSK9 and LDL-C levels indicate successful gene silencing, they are not guaranteed to translate into improved cardiovascular outcomes. The effect of inclisiran on cardiovascular morbidity and mortality has not been demonstrated, and some studies show that LDL-C reduction alone is not enough to substantially prevent cardiovascular disease.[73–75] Thus, while it is exciting that an siRNA drug for a widespread disease has finally reached the clinic, its ultimate long-term therapeutic efficacy in terms of cardiovascular outcomes has yet to be proven.

Amvuttra (vutrisiran) was the fifth and most recent siRNA drug to enter the clinic, receiving FDA approval in June 2022.[76] Like patisiran, vutrisiran is also a treatment for hereditary TTR-mediated amyloidosis through silencing *TTR* mRNA.[77] However, while patisran

is a partially chemically modified siRNA encapsulated in a lipid nanoparticle, vutrisiran is a fully chemically modified siRNA conjugated to GalNAc, similar to the previous three FDA-approved siRNA drugs. In clinical trials, vutrisiran demonstrated efficacy and a favorable safety profile.[78,77,79] Compared to patisiran, vutrisiran was more stable and more efficiently taken up by hepatocytes, enabling less frequent dosing: patisiran is intravenously injected every three weeks while vutrisiran is subcutaneously injected every three months.[80] Vutrisiran's advantages over patisiran have cemented full chemical modification and GalNAc conjugation as the current state-of-the-art strategy for clinical siRNA drugs.

Overall, the five clinically approved siRNA drugs have many things in common. They were all developed by Alnylam Pharmaceuticals, Inc., resulting in drugs with a very similar composition and structure utilizing the company's proprietary technology. They were all developed quickly, with several of the drugs receiving fast-track approval pathways from the FDA such as Orphan Drug, Breakthrough Therapy, or Priority Review designations, raising some questions about long-term safety and efficacy.[34] They all caused adverse effects in clinical trials; most were mild to moderate, but there were some severe adverse effects.[59] Four out of the five siRNA drugs treat orphan diseases, while the one that does treat a widespread disease has been met with skepticism regarding its ability to improve long-term therapeutic outcomes.[73–75] The most recent four out of the five clinically approved siRNA drugs are fully chemically modified siRNAs conjugated to GalNAc. Extensive chemical modifications have been shown to inhibit gene silencing activity for some sequences, which may limit the genes that can be targeted using this strategy.[43,45] While GalNAc efficiently delivers siRNA to the liver, it is not an effective strategy for targeting other parts of the body. Importantly, all clinically approved siRNA drugs target the liver. Current clinically approved siRNA delivery strategies can only be

used for diseases in which mRNA silencing in liver cells is the therapeutic mechanism; the vast majority of diseases that could potentially be treated by gene silencing are excluded from this mechanism, including cancers, neurological disorders, skin diseases, and countless others. Thus, siRNAs still have a long way to go before achieving the broad applicability promised by the nucleic acid therapy field. There is a need for an siRNA drug formulation that has favorable pharmacokinetics and cellular internalization to targets beyond the liver, as well as minimal off-target effects. It would also be ideal if the siRNA drug is modular, consisting of a structure that can be precisely controlled to strengthen the properties needed for treating a multitude of diseases, rather than relying on an identical structure for all treatments.

1.3. Spherical Nucleic Acids

1.3.1. Properties of Spherical Nucleic Acids

Spherical nucleic acids (SNAs) have emerged as an exceptionally promising strategy for delivering nucleic acid therapeutics.[81,82] SNAs are composed of oligonucleotides radially arranged around a nanoparticle core (**Figure 1.2**).[81,83] This is in contrast to other nanoparticle-oligonucleotide constructs in which the oligonucleotides are encapsulated within the nanoparticle. In this densely functionalized radial geometry, SNAs exhibit unique properties distinct from their linear counterparts. Linear oligonucleotides are rapidly degraded in serum, but SNAs are resistant to nuclease degradation due to the negatively charged nanoparticle surface and resultant high local salt concentration.[84,85] SNAs have longer circulating half-lives than linear oligonucleotides, with favorable pharmacokinetics that have shown the penetration of biological barriers such as the epidermis and the blood-brain barrier, as well as accumulation in tumors.[86–89] While many linear oligonucleotides are unable to cross cell membranes and enter cells, SNAs efficiently enter cells via scavenger receptor-mediated endocytosis.[84,90] SNAs have

exhibited the ability to enter over 50 different cell types, demonstrating that they can be used to deliver nucleic acids to a wide range of targets.[81] Finally, SNAs have shown fewer off-target effects than linear oligonucleotides, implying better clinical safety.[91]

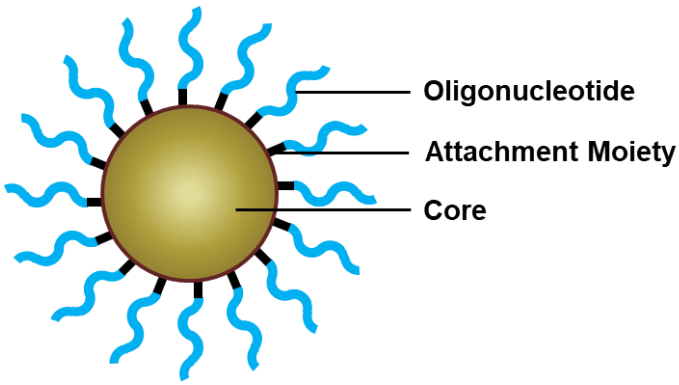

Figure 1.2. SNA structure. SNAs consist of oligonucleotides radially arranged around a nanoparticle core.

SNAs have been composed of a variety of nucleic acids, such as fluorescently labeled probes,[92,93] antisense oligonucleotides,[84] immunomodulatory oligonucleotides,[94] and linker strands,[83] as well as a variety of core materials, such as gold nanoparticles (AuNPs),[84] liposomes,[95] polymeric nanoparticles,[96] and proteins.[97] These SNAs have been developed as mRNA detectors,[92,93] gene regulation agents,[84] cancer vaccines,[94] and nanomaterial building blocks.[83] The SNA structure is highly modular; as long as the oligonucleotides are densely functionalized around a spherical nanoparticle core, the SNA will retain its signature behavior regardless of composition, e.g., it will protect its nucleic acids from degradation by serum nucleases and enter cells. The behavior of the SNA arises from the dense, radial geometry of the oligonucleotides, not the core, as demonstrated by a study of coreless SNAs.[98] However, altering the structure of the SNA can significantly impact the magnitude of its properties, such as the degree of nuclease resistance[85,99] or cellular internalization,[100,101] and ultimately the efficacy of the final therapeutic construct.[81,82] This phenomenon has necessitated the effort to understand the

structure-function relationships of SNAs and create design rules for controlling their properties by altering their structure.

1.3.2. siRNA-SNAs

siRNAs can be radially arranged around a spherical nanoparticle core to form siRNA-SNAs, in which they benefit from the properties of the spherical architecture including enhanced cellular uptake and resistance to degradation by serum nucleases while still demonstrating gene silencing activity.[102] siRNA-SNAs have also shown advantageous pharmacokinetics in mice, with tumor accumulation and the ability to cross the epidermis and the blood-brain barrier.[82,86–89] Due to these benefits, siRNA-SNAs have demonstrated therapeutic success in animal models of skin diseases[86,88,89] and glioblastoma multiforme,[87] and have progressed to a first-in-human clinical trial for glioblastoma.[103] However, there has been difficulty developing siRNA-SNAs for applications and diseases beyond these targets, limiting their broad usage. All siRNA-SNAs developed for therapeutic applications have used the same prototypical structure (**Figure 1.3**). These siRNA-SNAs consist of a ~13-nm gold nanoparticle core, with a thiolated passenger strand of the siRNA attached to the core and the guide strand hybridized to the passenger strand.[102,86–89] Prototypical siRNA-SNAs are easy to synthesize and characterize. However, this design limits the performance of several key properties of the siRNA-SNA.

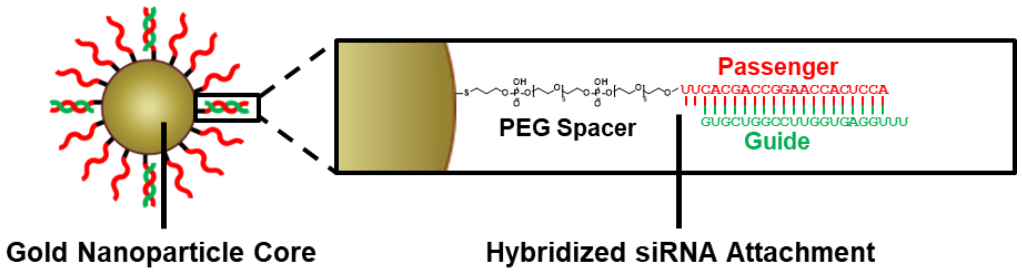

Figure 1.3. Prototypical siRNA-SNA structure. Prototypical siRNA-SNAs consist of a 13-nm gold nanoparticle core functionalized with thiolated passenger strands with hybridized guide strands.

1.3.3. Biological Properties of siRNA-SNAs

The most important property of the siRNA-SNA is its gene silencing activity. However, there are many other properties in which the siRNA-SNA must be sufficient in order to achieve efficacy (**Figure 1.4**). In the pathway from synthesis to delivery to therapeutic activity, each biological property is critically important, and low performance in any one of these properties significantly restricts the efficacy of the siRNA-SNA.

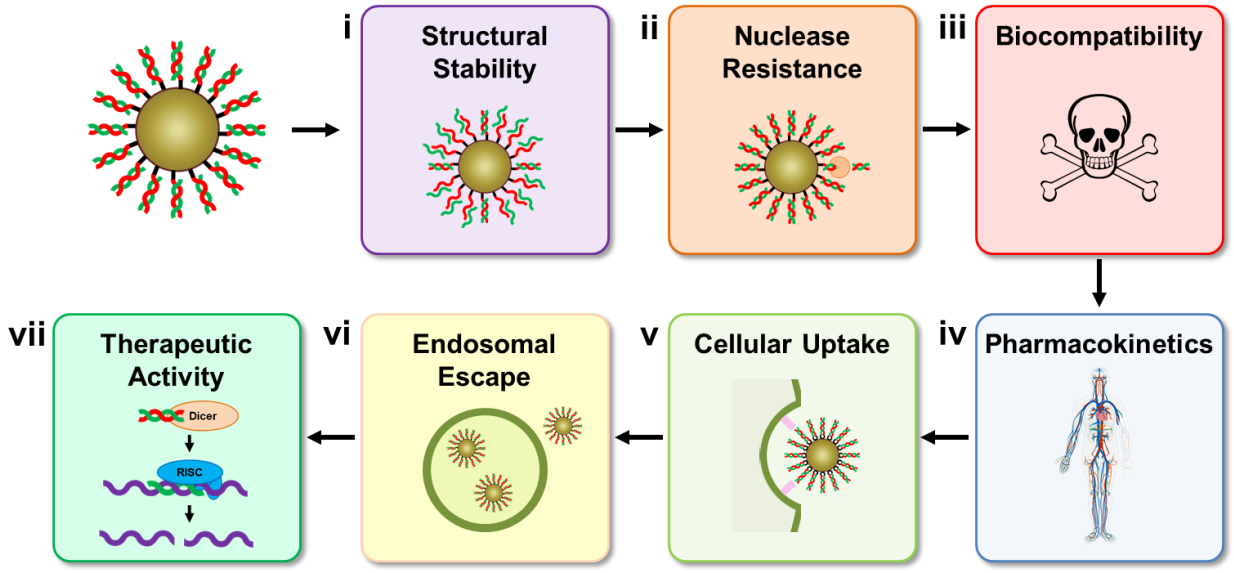

Figure 1.4. Biological properties of siRNA-SNAs. siRNA-SNAs have biological properties that play a critical role in each step of the pathway from synthesis to delivery to therapeutic efficacy. The properties in this pathway include (i) structural stability, (ii) nuclease resistance, (iii) biocompatibility, (vi) pharmacokinetics, (v) cellular uptake, (vi) endosomal escape, and (vii) therapeutic activity. All of these properties play a significant role in the eventual therapeutic efficacy of the siRNA-SNA.

Structural stability (**Figure 1.4i**) is the ability of the siRNA-SNA to stay intact. Structural stability affects the number of nucleic acid strands that can be loaded onto the SNA and ultimately delivered to the target site. Since the nucleic acid is essentially the active ingredient of the SNA drug, the amount of nucleic acid on each SNA can have significant implications for therapeutic efficacy and potency. Additionally, the density of nucleic acid strands on the SNA

surface can in turn can affect downstream properties such as nuclease resistance, biocompatibility, and cellular uptake.[99,100] The hybridized architecture of the prototypical siRNA-SNA severely restricts structural stability. Due to the high charge density near the core, electrostatic repulsion causes the majority of the weakly hybridized guide strands to dissociate from the SNA, leaving behind lone passenger strands with no gene silencing activity.[104,105]

Upon administration to the body, siRNA drugs are vulnerable to degradation by nucleases present in biological fluids (especially serum nucleases in blood), which limits the amount of intact, active siRNAs that can reach target cells. The SNA architecture confers nuclease resistance (**Figure 1.4ii**) to the siRNAs due to the negatively charged nanoparticle surface and high local salt concentration.[102,85] siRNA-SNAs have been found to have a significantly greater half-life in serum compared to their linear counterparts.[102] However, since serum nucleases cleave nucleic acids at specific sequence motifs, the half-life of siRNAs as well as siRNA-SNAs can vary greatly between sequences.[106,107,99] For example, while firefly luciferase-targeting siRNA-SNAs have a serum half-life of 816 min,[102] human androgen receptor-targeting siRNA-SNAs have a serum half-life of only two min.[107] Thus, there are some siRNA-SNA sequences that are unsuitable for clinical development due to prohibitively short serum half-lives. Generalizable strategies to increase serum nuclease resistance would benefit the therapeutic suitability of siRNA-SNAs of all sequences.

Biocompatibility (**Figure 1.4iii**), including cytotoxicity, unintentional immune system activation, and off-target effects, can be detrimental to any drug's clinical success. Gold nanoparticle-core siRNA-SNAs have demonstrated low cytotoxicity and no harmful side effects at therapeutic concentrations both *in vitro* and *in vivo*.[102,108,86,87,89] However, gold accumulation can still lead to cytotoxicity from siRNA-SNAs at high concentrations.[105] Gold nanoparticles are

poorly eliminated from the body, accumulate in the liver, and are non-biodegradable, and thus there are concerns about the effects of their long-term retention in the body.[109] These issues have limited the number of active clinical trials for gold nanoparticle-based therapeutics, and the FDA has approved few gold nanodrugs.[110] The biocompatibility of SNAs would improve with a higher nucleic acid-to-gold ratio or a more biocompatible core material.

Pharmacokinetics (**Figure 1.4iv**), or the movement of drugs within the body, is also a critical property for a drug's efficacy. After administration, the drug must transport through the body, with the hope that there will be high accumulation in the target tissue and low accumulation in off-target organs. Prototypical siRNA-SNAs are able to cross the epidermis and blood-brain barrier, and have shown accumulation in tumors as well as the liver.[86–89] Efforts to increase delivery to the tumor and decrease gold accumulation in the liver will improve the therapeutic suitability of siRNA-SNAs.

Upon reaching target cells, the cellular uptake (**Figure 1.4v**) of siRNA-SNAs determines how much siRNA can enter the cell. SNAs have demonstrated an ability to efficiently enter over 50 different cell types, which makes them an ideal construct for delivering siRNAs to a broad range of targets.[81] Cellular uptake of SNAs is primarily driven by interactions with class A scavenger receptors, which bind to SNAs and transport them into the cell via endocytosis.[90] It has been found that these interactions and thus cellular uptake are affected by the sequence, secondary structure, and loading density of oligonucleotides on the SNA.[100,101]

Upon internalization, siRNA-SNAs localize in the endosome. A small fraction of siRNA-SNAs escape the endosome (**Figure 1.4vi**) and enter the cytosol, where they interact with the RNAi machinery and silence mRNA. The remaining majority of the siRNA-SNAs are trapped in the endosome and traffic through the endocytic pathway into late endosomes while being

degraded by enzymes.[111] Endosomal entrapment is a significant issue for most nanoparticle-based siRNA delivery systems that enter cells via endocytosis, and is often the bottleneck for the drug's efficacy. For many nanoparticle constructs, endosomal escape is so minimal that an insufficient amount of siRNA is able to enter the cytosol and silence genes. Endosomal escape is also poorly understood, with little information on the variables that affect it and no well-established method to measure it.[55,112] For siRNA-SNAs, it is apparent that some sequences in some cell types sufficiently escape the endosome,[102,86–89] but for other potential targets and disease applications, endosomal entrapment is the bottleneck that limits the therapeutic efficacy of siRNA-SNAs.

The final and most important property of the siRNA-SNA is therapeutic activity (**Figure 1.4vii**), including gene silencing magnitude, potency, and durability. siRNA-SNAs have demonstrated strong, potent gene silencing for several targets, at times exceeding the magnitude and potency of gene silencing from transfected linear siRNAs.[102,86–89] Interestingly, siRNA-SNAs exhibit slower, longer-lasting silencing than linear siRNAs.[86,105] This is due to an additional step in the RNAi pathway for siRNA-SNAs, in which the enzyme Dicer-2 cleaves siRNA duplexes from the SNA and traffics them to the RISC for RNAi, while linear siRNAs directly engage with the RISC.[105] Thus, if all other properties are sufficient, siRNA-SNAs are capable of achieving strong, potent, durable gene silencing. Conversely, any modifications used to increase other properties may have a detrimental effect on Dicer-2, RISC, or mRNA interactions, which could limit gene silencing activity.[40,41] When trying to improve other properties, one must be careful to not lose sight of the importance of therapeutic activity.

Several of these properties are siRNA sequence dependent, so the performance of siRNA-SNAs will differ for each new target.[107,99,101] The performance of each siRNA-SNA

sequence is hard to predict; in one study, only two out of five siRNA-SNAs showed gene silencing activity, even though all five sequences had demonstrated potent gene silencing as transfected linear siRNAs.[88] A sequence can negatively affect one or several properties, restricting the therapeutic suitability of that siRNA-SNA. While the prototypical design may work for a certain sequence or target, it may not work for others, leading to trail-and-error testing, extensive screening, and inefficient development of the siRNA-SNA as a drug. The siRNA-SNA would substantially benefit from strategies that greatly improve its biological properties to a point at which sequence dependency will no longer restrict the performance of the siRNA-SNA below a critical threshold for any property. Thus, strategies for significantly increasing all of these properties would strongly benefit the siRNA-SNA's suitability for broad applications.

1.3.4. Altering the Structure of SNAs Affects Their Behavior

The SNA is highly modular and its structural features can be precisely controlled (**Figure 1.5**). A key advantage of the SNA is that its structure can be altered to cause changes in properties and behavior.[81,82,113] The structure-function relationships of SNAs have been studied with the goal of developing design rules to tailor SNA structure to optimally function for specific applications. For example, it has been found that increasing the loading density of oligonucleotides on the SNA surface increases cellular uptake.[100] It has also been discovered that modifying the composition of liposome-core and lipid nanoparticle-core SNAs affects their biodistribution and immunomodulatory activity.[114–116] Finally, it has been shown that the structural arrangement of the components of SNA cancer vaccines significantly affects their therapeutic efficacy.[117,113] While the effects of structural changes on the properties of SNAs has been demonstrated, this relationship has not been extensively explored for siRNA-SNAs, and

thus development efforts for the siRNA-SNA have used the prototypical architecture.[102,86–89] A pair of initial studies showed that chemical modifications and loading density affect the nuclease resistance of siRNA-SNAs, demonstrating the potential benefit of structural changes to the siRNA-SNA.[107,99] The modularity of the siRNA-SNA provides opportunities to improve the stability and delivery of siRNA to meet the needs of a wide variety of diseases, providing a significant advantage over current clinically approved siRNA drugs that utilize a single structure that is only applicable to a narrow range of diseases. Thus, at the start of my PhD, I aimed to update the prototypical siRNA-SNA design with generalizable structural changes to develop next-generation siRNA-SNAs with improved properties and ultimately improved therapeutic suitability.

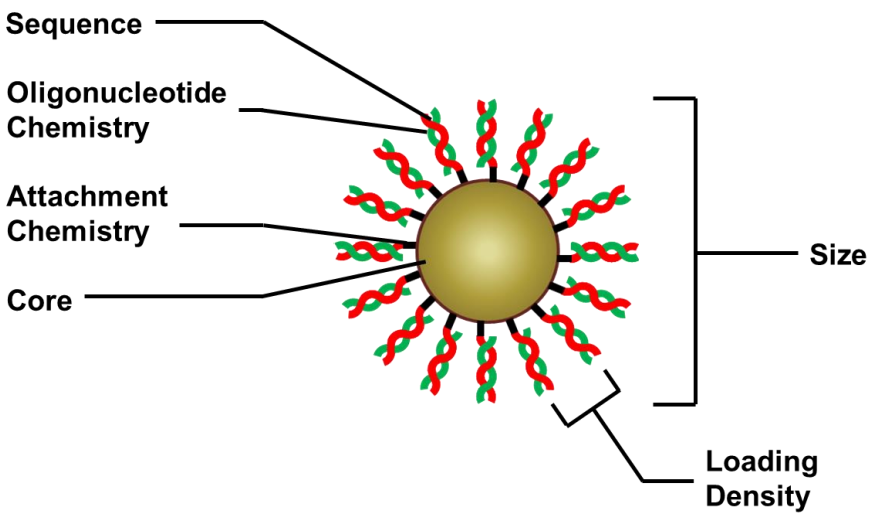

Figure 1.5. Structural features of siRNA-SNAs. Structural features of SNAs can be precisely controlled to cause changes in properties and behavior.

Herein, I describe how structural changes to the SNA architecture can improve these biological properties. Chapter 2 describes a hairpin-like architecture for siRNA-SNAs that significantly improves structural stability, leading to improved nuclease resistance,

biocompatibility, cellular uptake, calcium-enhanced cytosolic delivery, and therapeutic duration. Chapter 3 describes the enhanced drug-to-carrier ratio, pharmacokinetics, and cellular uptake of SNAs synthesized at an ultrasmall size regime. Chapter 4 introduces next-generation siRNA-SNAs with lipid-based cores and investigates their biocompatibility, pharmacokinetics, cellular uptake, cytosolic delivery, therapeutic activity, and suitability as an ocular nanomedicine. Finally, Chapter 5 summarizes the main takeaways from this work as well as future work for developing next-generation SNAs. While this dissertation primarily focuses on siRNA-SNAs, many of the design principles described herein can be applied to SNAs composed of other nucleic acids. The structural advances described in this work substantially improve the biological properties of SNAs, driving the development of next-generation SNA constructs and advancing siRNAs toward clinical use.

CHAPTER 2

Hairpin-like siRNA-Based Spherical Nucleic Acids

Reprinted with permission from Vasher, M. K.; Yamankurt, G.; Mirkin, C. A. Hairpin-like siRNA-Based Spherical Nucleic Acids. *J. Am. Chem. Soc.* **2022**, *144* (7), 3174–3181. https://doi.org/10.1021/jacs.1c12750.

Full text access: http://pubs.acs.org/articlesonrequest/AOR-5ZGGGFHWNKDGDIU5AHSX

2.1. Introduction

2.1.1. siRNA

siRNAs are short, double-stranded RNA molecules that silence genes via RNAi.[23] Due to the efficiency and specificity of RNAi, in principle, siRNAs can be synthetically designed to silence any target sequence of interest, potentially serving as a gene regulation therapy for a broad range of diseases.[25,27,28] Unfortunately, clinical use of siRNA has been restricted because siRNAs have limited biodistribution, are rapidly degraded in biological fluids, and cannot enter cells as single entities.[49,118]

2.1.2. Prototypical siRNA-SNAs

SNAs consist of oligonucleotides radially arranged around a nanoparticle core in high density, and they exhibit properties that distinguish them from their linear counterparts. In particular, their biodistribution is markedly different, allowing them to enter tissues and cells that linear structures do not access, and they are more resistant to nuclease degradation with longer circulating half-lives.[83,81,102,85,90] Thus, siRNA-SNAs have been shown to be promising as therapeutics in animal models of impaired wound healing and psoriasis as well as a first-in-human clinical trial for glioblastoma.[86–89,103]

Prototypical siRNA-SNA designs exhibit a hybridized (hyb.) architecture, in which only the passenger strand of the siRNA is directly attached to the nanoparticle core, and the complementary guide strand is attached to the SNA conjugate via hybridization to the passenger strand (**Figures 2.1A** and **2.2A**).[102] With this SNA design, the hybridization of the guide strands to densely packed passenger strands on the nanoparticle core occurs with negative cooperativity; each binding event increases the charge density near the surface of the core, ultimately limiting the number of guide strands that can be loaded on the SNA due to electrostatic repulsion.[104]

According to previous studies, these siRNA-SNAs have only as many as 40 guide strands hybridized to the >80 passenger strands on the surface of the particle, a duplex efficiency of <50%.[87,88] It is also possible that the guide strand can dehybridize before reaching the target cell with this design.[22] Because intact siRNA duplexes are necessary for efficient gene silencing, the low functional siRNA concentrations delivered using this SNA design ultimately leads to limited target site accumulation, and a large amount of SNA material is required to induce silencing. Thus, methods for preparing siRNA-SNAs that bear a greater amount of active, stable siRNA are needed so that these conjugates can be delivered to target cells and potent gene silencing can be realized.[119]

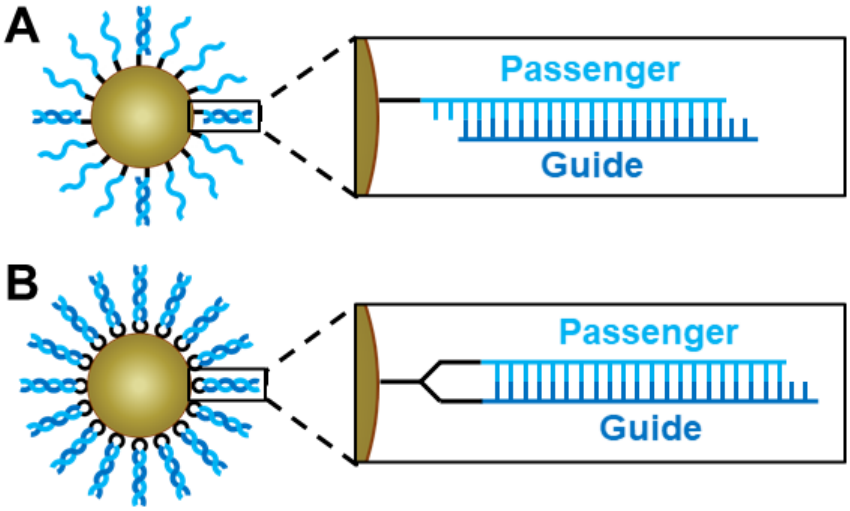

Figure 2.1. Attachment architectures of siRNA-SNAs. (A) Hybridized architecture, in which the passenger strand is attached to the core and the guide strand is hybridized to it with low duplexing efficiency, and (B) hairpin-like architecture, in which a hairpin-like siRNA, a single RNA strand composed of a duplex and a hairpin-like region of polyethylene glycol (PEG) spacers, is attached to the core with high duplexing efficiency. Detailed chemical structures are shown in **Figure 2.2**.

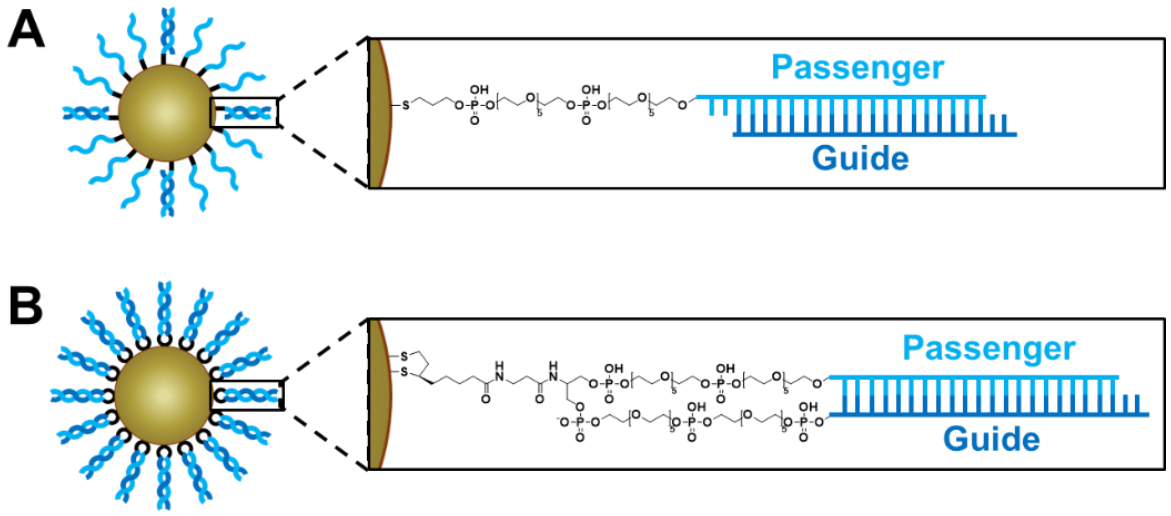

Figure 2.2. Chemistry of siRNA-SNA attachment architectures. (A) Hybridized architecture, in which the passenger strand is attached to the core via a PEG linker with a thiol group. (B) Hairpin-like architecture, in which both strands are attached to the core via a PEG linker with a dithiol serinol group.

2.1.3. Hairpin-like Attachment Architecture for siRNA-SNAs

Researchers have shown that the enzyme Dicer-2 cleaves siRNA duplexes from the SNA for RNA-induced silencing complex (RISC) processing, opening up the possibility to explore new, more stable chemistries (**Figure 2.3**).[105] A straightforward approach involves attaching a thiol group to the end of both the passenger and guide strands so that both strands can be functionalized to the gold nanoparticle core (two points of chemical attachment). However, while such a strategy is suitable for gold nanoparticle cores, it is not extendable to many biocompatible cores, such as liposomes and poly(lactic-co-glycolic acid) (PLGA) nanoparticles.[95,96] Hydrophobic anchor-conjugated RNA strands can separate and laterally diffuse on liposomal cores, and the chemistry of PLGA-SNAs features separate, single points of covalent attachment that are not conducive to the hybridization of adjacent complementary RNA strands. Lateral diffusion is also possible with gold nanoparticle cores, so there is no guarantee that duplex

formation is maximized.[120] Thus, it is ideal that both the passenger and guide strand on an siRNA-SNA are attached to each other and to the nanoparticle core through a single functional group.

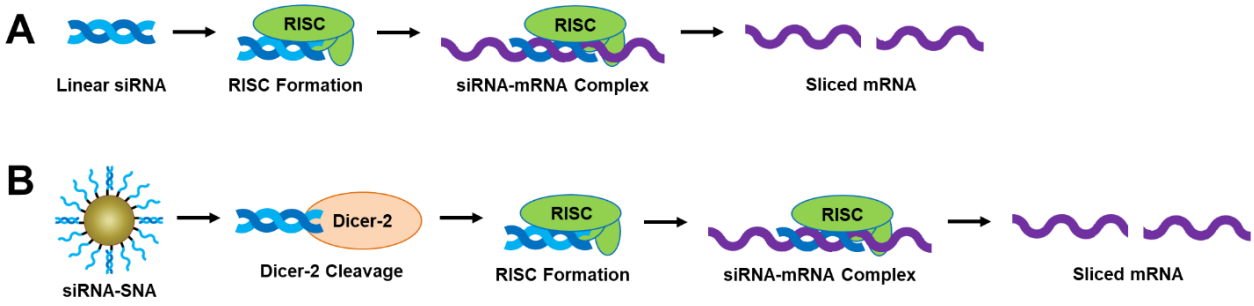

Figure 2.3. RNAi pathway for linear siRNAs and siRNA-SNAs. (A) Linear siRNAs are processed by the RISC and hybridize to complementary mRNA strands, which are then sliced, resulting in gene silencing. (B) For siRNA-SNAs, Dicer-2 cleaves off siRNA duplexes from the SNA. The cleaved siRNAs then proceed through the canonical RNAi pathway.

Herein, we describe the design and synthesis of a hairpin-like (HP) siRNA-SNA architecture that fulfills this key criterion. In this novel design, both strands of the siRNA duplex are components of a single hairpin-shaped molecule, allowing for their direct attachment to the nanoparticle core via a single functional group (**Figures 2.1B** and **2.2B**). This design prevents guide strand dehybridization and permits increased duplex loading compared to the previously utilized hybridized siRNA-SNA design. As a result, improved serum nuclease resistance, decreased cytotoxicity, and increased gene silencing duration are observed. This hairpin-like siRNA-SNA design can be translated for use on a variety of nanoparticle cores due to its single functional group, making it a very attractive synthon for the development of next-generation siRNA-SNAs.

2.2. Materials and Methods

Oligonucleotide Synthesis. RNA oligonucleotides were synthesized on a MerMade 12 system (BioAutomation) using 2'-*O*-triisopropylsilyloxymethyl-protected phosphoramidites (ChemGenes). In the hybridized siRNA system, the passenger and guide RNA strands were synthesized separately. The passenger strand consisted of RNA base cyanoethyl phosphoramidites (Glen Research), two spacer 18 (18-*O*-dimethyoxytritylhexaethyleneglycol,1-[(2-cyanoethyl)-(*N*,*N*-diisopropyl)] phosphoramidites (Glen Research), and a thiol modification added by using 1-*O*-dimethoxytrityl-propyl-disulfide,1'-succinyl-lcaa-controlled pore glass beads. The guide strand consisted of RNA base cyanoethyl phosphoramidites. For the hairpin-like siRNA system, the single strand consisted of RNA base cyanoethyl phosphoramidites (the guide portion of the strand), two spacer 18 phosphoramidites, a dithiol serinol phosphoramidite (the hairpin turn and nanoparticle attachment moiety) (Glen Research), two spacer 18 phosphoramidites, and RNA base cyanoethyl phosphoramidites (the passenger portion of the strand). After synthesis, RNA oligonucleotides were deprotected following the manufacturer's protocol (Bioautomation). Deprotected RNA oligonucleotides were purified using high-performance liquid chromatography on a C18 column using 0.1 M triethylammonium acetate and acetonitrile as the solvents. The 5'-dimethoxytrityl (DMT) group was removed from the purified RNA oligonucleotides via treatment with 20% acetic acid at room temperature for 1 h and extracting 3 times with ethyl acetate. The oligonucleotide solution was lyophilized and suspended in DNase/RNase-free water. The oligonucleotide sequences used in this chapter are listed in **Table 2.1**.

Table 2.1. Sequences of RNA oligonucleotides used in this chapter. Observed (obs.) molecular weights (MW) were measured and compared to calculated (calc.) molecular weights. Sp18: spacer 18, SH: thiol modification, DS: dithiol serinol.

Name	Sequence (5' → 3')	Calc. MW (Da)	Obs. MW (Da)
Human Epidermal Growth Factor Receptor 2 *(HER2)* Passenger	GCUCAUCGCUCACAACCAAUU-$(Sp18)_2$-SH	7509	7425
HER2 Guide	UUGGUUGUGAGCGAUGAGCAC	6769	6806
HER2 Hairpin	GCUCAUCGCUCACAACCAAUU-$(Sp18)_2$-DS-$(Sp18)_2$-AAUUGGUUGUGAGCGAUGAGCAC	15912	15964
Nontargeting (Luciferase (*Luc*) Passenger	CGUACGCGGAAUACUUCGAUU-$(Sp18)_2$-SH	7606	7614
Nontargeting (*Luc*) Guide	UCGAAGUAUUCCGCGUACGUG	6689	6729
Nontargeting (*Luc*) Hairpin	CGUACGCGGAAUACUUCGAUU-$(Sp18)_2$-DS-$(Sp18)_2$-AAUCGAAGUAUUCCGCGUACGUG	15928	15888
Vascular Endothelial Growth Factor (*VEGF*) Passenger	ACCUCACCAAAGCCAGCACUU-$(Sp18)_2$-SH	7531	7505
VEGF Guide	GUGCUGGCUUUGGUGAGGUUU	6740	6713
VEGF Hairpin	ACCUCACCAAAGCCAGCACUU-$(Sp18)_2$-DS-$(Sp18)_2$-AAGUGCUGGCUUUGGUGAGGUUU	15904	15876
Noncomplementary 1	GCUCAUCGCUCACAACCAAUU-$(Sp18)_2$-DS-$(Sp18)_2$-GACAAUCCCGACACCCUUAUUAC	15694	15518
Noncomplementary 2 (Hybridized to Noncomplementary 1 for Cocomplementary RNA)	AAUAAGGGUGUCGGGAUUGUC-$(Sp18)_2$-DS-$(Sp18)_2$-AAUUGGUUGUGAGCGAUGAGCAC	16129	16052

Hairpin-like siRNA Characterization. The masses of the hairpin-like siRNAs were measured using matrix-assisted laser desorption/ionization-time of flight (MALDI-TOF) mass spectrometry. Hairpin-like siRNAs were mixed with 2',4'-dihydroxyacetophenone (DHAP) and dried on a MALDI plate. MALDI-TOF was performed using an Autoflex III Smartbeam MALDI-TOF mass spectrometer. Conformation analysis of the hairpin-like siRNAs was performed using native PAGE. The two cocomplementary hairpin-like siRNAs were mixed at an equal molar ratio in duplex buffer (30 mM 4-(2-hydroxyethyl)-1-piperazineethanesulfonic acid (HEPES) (pH 7.3), 100 mM potassium acetate, 2 mM magnesium acetate). The solution was then heated to 95 °C for 2 min and slowly cooled to room temperature to allow for hybridization to occur. RNA samples were analyzed via native polyacrylamide gel electrophoresis (PAGE)

using a 10% gel at 150 V for 45 min. SYBR Gold was used to stain the RNA. The gel was imaged using an Amersham Typhoon biomolecular imager.

SNA Salt-Aging Synthesis. Citrate-capped AuNPs 13 nm in diameter were synthesized by reducing chloroauric acid with sodium citrate in water following the Turkevich-Frens method.[121] To prepare hybridized siRNA-SNAs, 100 μM passenger RNA and 100 μM guide RNA were added to duplex buffer, heated to 95 °C for 2 min, and slowly cooled to room temperature to allow for hybridization. The AuNPs were functionalized with these hybridized siRNAs to form SNAs via a previously described salt-aging procedure.[105] To prepare the hairpin-like siRNA-SNAs, 100 μM hairpin-like siRNA was added to duplex buffer, heated to 95 °C for 2 min, and slowly cooled to room temperature. Hairpin-like siRNA (final concentration = 4 μM) was then added to a solution of 10 nM 13-nm AuNPs, 0.2% Tween-20, and 150 mM NaCl. The solution was incubated overnight. The next day, the salt concentration was gradually increased to 1 M NaCl by adding a concentrated solution of NaCl every 2 h while shaking. The solution was allowed to equilibrize overnight. Unattached oligonucleotides were removed by washing with 1× Dulbecco's phosphate-buffered saline (DPBS) 3 times in Amicon Ultra 100K molecular weight cutoff spin filters (MilliporeSigma). The SNAs were stored at 4 °C for up to 3 months.

SNA Characterization. SNAs and AuNPs were diluted to 1 nM in 1× DPBS and water, respectively, and size was analyzed with dynamic light scattering (DLS) using a Malvern Zetasizer. The SNA concentration was determined by measuring the absorbance spectra of the SNAs using a Cary-5000 spectrophotometer (Agilent). The AuNP's extinction coefficient is not affected by functionalization with oligonucleotides, so AuNP (and, in effect, SNA) concentration was calculated using the absorbance at 520 nm and an extinction coefficient of 2.27×10^8 M^{-1} cm^{-1}.[122] To measure the siRNA duplex loading of hybridized siRNA-SNAs, 3 μL of 100 nM

SNAs were incubated with 100 μL of 9 M urea at 45 °C for 20 min, mixed with 100 μL of 0.01% Tween-20, and centrifuged at maximum speed for 25 min to dissociate the guide strands from the SNAs. The passenger strand-conjugated SNAs formed a pellet while dissociated guide strands were in the supernatant. A portion of the supernatant (25 μL) was added to 75 μL of water and 100 μL of 0.5% Quant-iT OliGreen reagent (Invitrogen) in 1× tris/ethylenediaminetetraacetic acid (EDTA) (TE) buffer. The samples were analyzed in a 96-well plate by measuring OliGreen fluorescence (excitation wavelength (λ_{ex}) = 480 nm, emission wavelength (λ_{em}) = 520 nm) with a BioTek Cytation 5 imaging reader and comparing to a standard curve of guide RNA. siRNA duplex loading of hairpin-like siRNA-SNAs was then calculated by taking the ratio of guide RNA concentration to AuNP concentration. To measure the number of passenger strands on each SNA, the remaining passenger strand-conjugated SNAs were added to 9 M urea to dissolve the gold. The OliGreen assay was repeated with these SNAs to measure passenger RNA concentration. Passenger strand loading on the SNA was then calculated by taking the ratio of passenger RNA concentration to AuNP concentration. To measure the siRNA duplex loading of hairpin-like siRNA-SNAs, 7 μL of 100 nM SNAs were mixed with 7 μL of 40 mM KCN and heated at 55 °C until the gold dissolved. The solution was diluted in 112 μL of 1× DPBS. Then, 25 μL of this solution was mixed with 175 μL of 0.28% Quant-iT OliGreen reagent (Invitrogen) in 1× DPBS. OliGreen fluorescence was measured and compared to a standard curve of hairpin-like siRNA. siRNA duplex loading of hairpin-like siRNA-SNAs was then calculated by taking the ratio of hairpin-like siRNA concentration to AuNP concentration.

Serum Nuclease Resistance of SNAs. The serum nuclease resistance of siRNA-SNAs was measured as previously described.[107] To degrade the siRNA on the SNAs with nucleases, 20 nM SNAs were incubated in 10% fetal bovine serum (FBS) in 1× DPBS at 37 °C. As a negative

control, 20 nM SNAs were incubated in 1× DPBS at 37 °C. At each time point, an 18-μL aliquot was removed and mixed with 30 mM sodium dodecyl sulfate (SDS) to inactivate the nucleases and stop the reaction. The degraded SNAs were then washed 3 times by suspending in 0.01% Tween-20 in 1× DPBS, centrifuging at 21,000 × g for 25 min, and removing the supernatant to remove serum and degraded RNA fragments. The amount of siRNA remaining on the SNA at each time point was measured following the previously described SNA characterization methods. The AuNP concentration of the SNA samples was determined by measuring absorbance at 520 nm using a BioTek Cytation 5 imaging reader.

Cytotoxicity of SNAs. In 96-well cell culture plates with 2,500 SK-OV-3 cells per well, siRNA-SNAs in Opti-MEM were incubated with SK-OV-3 cells in triplicate for 48 h. The wells were washed with 1× DPBS 3 times to remove dead cells and SNAs that remained outside the cells. A mixture of 50 μL 1× DPBS and 50 μL of CellTiter-Glo 2.0 reagent (Promega) was added to the wells, and the luminescence was measured using a BioTek Cytation 5 imaging reader. Luminescent readout from adenosine triphosphate (ATP) concentration was used to indicate live cell count. Cell viability was normalized to cells treated with Opti-MEM only.

Cellular Uptake of SNAs. In 24-well cell culture plates with 50,000 SK-OV-3 cells per well, SK-OV-3 cells were treated with 1 nM SNAs in Opti-MEM for 24 h. At the end of each time point, the cells were washed with 1× DPBS 3 times to remove SNAs that remained outside the cells. The cells were then trypsinized using 150 μL of TrypLE Express (Thermo Fisher). The number of cells in each sample was measured by staining 10 μL of cells with 10 μL of Trypan Blue (Thermo Fisher) and measuring their concentration using an Invitrogen Countess II automated cell counter. Next, 120 μL of cells were dissolved in 50 mL of 2% HCl, 2% HNO_3. The gold concentration in this solution was measured by performing inductively coupled plasma

mass spectrometry (ICP-MS) on the acidified samples. ICP-MS was performed on a computer-controlled (QTEGRA software) Thermo iCapQ ICP-MS (Thermo Fisher Scientific, Waltham, MA, USA) operating in STD mode and equipped with a ESI SC-2DX PrepFAST autosampler (Omaha, NE, USA). Internal standard was added inline using the prepFAST system and consisted of 1 ng/mL of a mixed element solution containing Bi, In, ^{6}Li, Sc, Tb, Y (IV-ICPMS-71D from Inorganic Ventures). Online dilution was also carried out by the prepFAST system and used to generate a calibration curve consisting of 2, 4, 20, 100, and 200 ppb Au. Each sample was acquired using 1 survey run (10 sweeps) and 3 main (peak jumping) runs (40 sweeps). The isotopes selected for analysis were ^{197}Au (for SNA quantification) and ^{89}Y, ^{115}In, ^{159}Tb, and ^{209}Bi (chosen as internal standards for data interpolation and machine stability). Instrument performance was optimized daily through autotuning followed by verification via a performance report (passing manufacturer specifications). The number of SNAs taken up into each cell was calculated by dividing the number of gold nanoparticles per sample by the number of cells per sample. The amount of siRNA taken up into each cell was calculated by multiplying the SNA uptake by the siRNA duplex loading on the SNA.

Quantification of Gene Knockdown by Reverse Transcription Quantitative Polymerase Chain Reaction (RT-qPCR). In 12-well cell culture plates with 25,000 SK-OV-3 cells per well, *HER2*-targeting or nontargeting siRNA or siRNA-SNAs were transfected at a 100 nM siRNA concentration with Lipofectamine RNAiMAX (Thermo Fisher Scientific) using the manufacturer's instructions. After transfection for 24 h, the treatment solution was replaced with McCoy's 5A (modified) medium (Gibco) supplemented with 10% FBS, 1% penicillin-streptomycin, and the cells were incubated for another 24 h. RNA was isolated from the cells using a PureLink RNA Mini Kit (Thermo Fisher Scientific). mRNA levels were measured in

triplicate by RT-qPCR using qScript XLT One-Step RT-qPCR ToughMix (Quanta Biosciences), TaqMan Gene Expression Assays (*HER2*: Hs01001580_m1, *GAPDH*: Hs03929097_g1; Thermo Fisher Scientific), a Bio-Rad C1000 Touch Thermal Cycler, and a Bio-Rad CFX384 Real-time System. C_T values were normalized to the housekeeping gene and untreated cells using the Pfaffl method.[123]

Quantification of Protein Knockdown by In-Cell Western. In 96-well cell culture plates with 20,000 SK-OV-3 cells per well, siRNA-SNAs targeting *HER2* were transfected with Lipofectamine RNAiMAX using the manufacturer's instructions. After transfection for 24 h, the SNA treatment solution was replaced with McCoy's 5A (modified) medium (Gibco) supplemented with 10% FBS, 1% penicillin-streptomycin, and the cells were incubated for the remainder of the treatment period. The medium was replaced twice per week to continuously provide the cells with nutrients. At the end of the treatment period, the wells were washed with 1× DPBS 3 times and fixed in methanol chilled at −20 °C for 15 min. The wells were washed with 0.05% Tween-20 in 1× DPBS 2 times, then 1× DPBS, then incubated with Intercept blocking buffer (LI-COR) for 90 min with shaking. The cells were then incubated with HER2 antibody (29D8) diluted 1:200 in Intercept blocking buffer (Cell Signaling) for 2 h. The wells were washed with 0.1% Tween-20 in 1× DPBS 3 times and incubated with 2 μg/mL IRDye 800CW goat anti-rabbit secondary antibody (LI-COR) and 500 nM CellTag 700 (LI-COR) diluted 1:500 in Intercept blocking buffer for 1 h protected from light, with shaking. The wells were washed with 0.1% Tween-20 in 1× DPBS 3 times and imaged on an Odyssey CLx system (LI-COR). HER2 protein expression was normalized to cell count by normalizing fluorescence at 800 nm to fluorescence at 700 nm.

Calcium-Salting of siRNA-SNAs. To salt siRNA-SNAs with calcium, 70 pmol by siRNA of siRNA-SNAs were mixed with 2.1 μmol of $CaCl_2$ and incubated with shaking at room temperature for 1 h. Calcium-salted siRNA-SNAs were diluted in Opti-MEM and added to a 96-well cell culture plates with 20,000 SK-OV-3 cells per well for protein knockdown studies. Protein knockdown was measured using an in-cell Western assay.

Statistics. All statistical analyses were performed using GraphPad Prism. For comparisons between two groups, means were compared using an unpaired, two-tailed t-test. For comparisons between more than two groups, means were compared using an ordinary one-way analysis of variance (ANOVA) with Tukey's multiple comparison test. *P* values were multiplicity adjusted to account for multiple comparisons. Serum nuclease resistance results were fit with an exponential one-phase decay using a least-squares fit. Cytotoxicity results and in-cell Western protein expression results were fit with a 3-parameter logistic curve using a least-squares fit.

2.3. Results and Discussion

2.3.1. Hairpin-like siRNA Self-Hybridizes to Form a Functional siRNA Duplex

The hairpin-like siRNA molecule consists of a complementary passenger and guide strand joined by PEG spacers and a dithiol serinol group (**Figure 2.4A**). These constructs were synthesized as a single 44-mer RNA oligonucleotide containing the PEG and dithiol serinol groups in the middle using solid phase synthesis via standard protocols. Synthesis of the RNA oligo was confirmed using MALDI-TOF mass spectrometry (**Table 2.1**). The average synthesis yield was 7%, and the hairpin-like RNAs were stored at −20 °C and remained functional after six months.

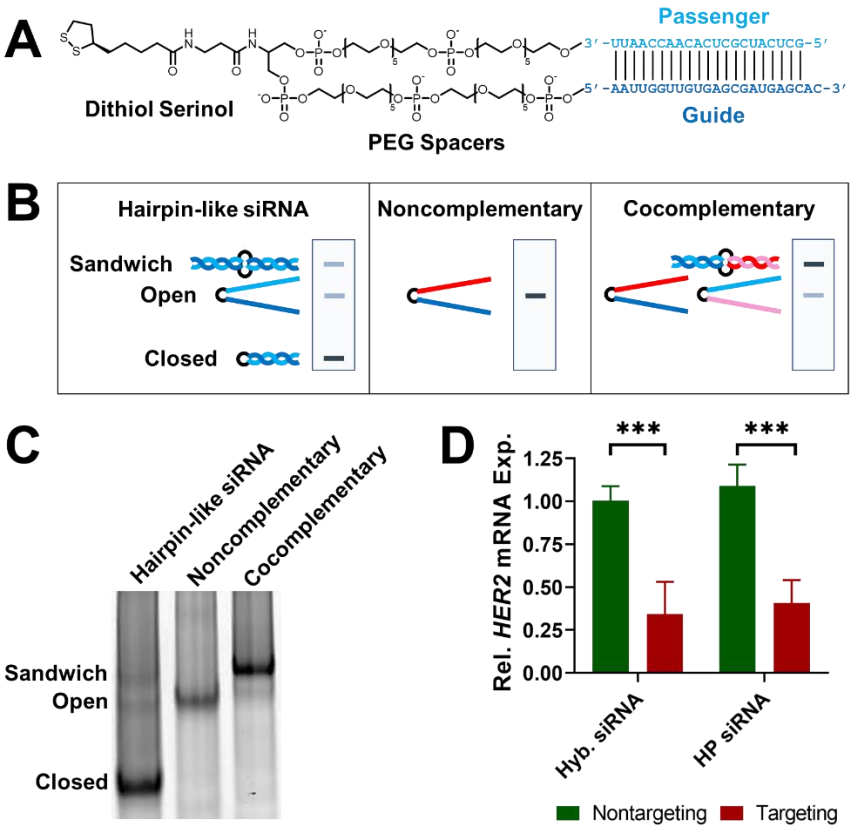

Figure 2.4. Hairpin-like RNAs self-hybridize to function as active siRNA duplexes. (A) Chemical structure of hairpin-like siRNA with passenger strand (light blue) and guide strand (dark blue). The sequence shown is used for targeting *HER2* mRNA. (B) Scheme showing hairpin-like RNA conformations and predicted native PAGE band locations. (C) Native PAGE gel of hairpin-like siRNA, noncomplementary RNA, and cocomplementary RNA. (D) Gene silencing activity of hybridized and hairpin-like siRNA. SK-OV-3 cells were transfected with 100 nM siRNAs. Relative (rel.) gene expression (exp.) was measured 48 h after siRNA administration by RT-qPCR, normalized to transfection agent-only treatment. Error bars are standard deviation (SD) of 3 experimental replicates (***$P \leq 0.001$).

Next, it was confirmed that the passenger and guide strands within the hairpin-like siRNA hybridize at a high efficiency to form the intact siRNA duplex required for gene silencing. In native PAGE analysis, the hairpin-like siRNA strands appear as three bands, one with a much higher intensity than the other two, indicating that the hairpin-like RNA likely exists in three conformations: closed, where the RNA self-hybridized; open, where the RNA did not self-

hybridize; and sandwich, where two of the RNA molecules dimerized due to their complementarity (**Figure 2.4B**). To determine which band corresponded to which conformation, a similar RNA with noncomplementary passenger and guide strands was used; this strand cannot self-hybridize and only exists in the open conformation. This noncomplementary RNA was run through the gel, revealing the location of the band for the open conformation. Then, a second RNA molecule that could not self-hybridize, but that was entirely complementary to the previous noncomplementary RNA was prepared. These two cocomplementary strands form a sandwich conformation and reveal the location of that band. Based on these results, we conclude that the majority (89% intensity according to ImageJ analysis) of the hairpin-like siRNA molecules exist in the closed conformation (**Figure 2.4C**). Thus, the hairpin-like siRNA molecule self-hybridizes at a high efficiency. The hairpin-like RNA was heated to 95 °C and then slowly cooled in duplex buffer to investigate if the percentage of strands in the closed conformation can be increased, but this process did not significantly affect the ratios of the observed conformations (**Figure 2.5**).

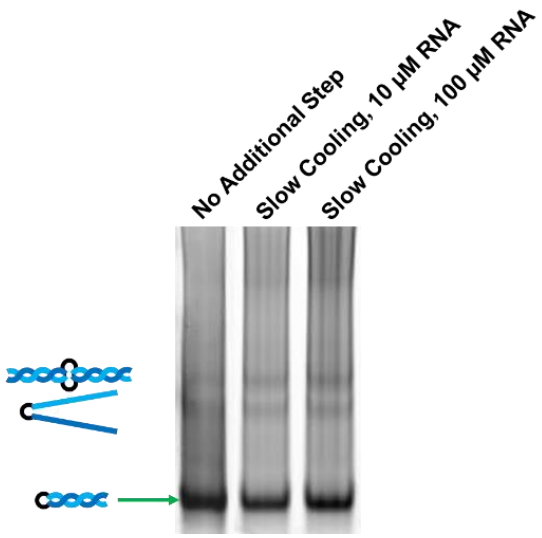

Figure 2.5. Slow cooling does not increase self-hybridization efficiency. Self-complementary hairpin-like siRNA was heated to 95 °C and then slow-cooled to room temperature in duplex buffer at various concentrations. Upon native PAGE analysis, slow-cooling did not significantly increase the fraction of hairpin-like siRNA that existed in a closed conformation.

To investigate if the hairpin-like siRNA functions as an active siRNA duplex, its gene silencing activity was compared to that of standard siRNA that consists of two hybridized strands. As a model system, the human epidermal growth factor receptor 2 (*HER2*) gene was targeted for silencing in SK-OV-3 human ovarian cancer cells since it is a well-established oncogene and the protein it expresses is a common therapeutic target for breast cancer.[124] *HER2*-targeting hairpin-like siRNAs were transfected with Lipofectamine RNAiMAX into SK-OV-3 cells, and gene knockdown was measured by RT-qPCR. *HER2*-targeting hairpin-like siRNAs significantly knocked down the *HER2* gene as compared to a nontargeting control hairpin-like siRNA, and at a similar level to a standard hybridized siRNA of the same sequence (**Figure 2.4D**). Thus, hairpin-like siRNAs self-hybridize and function as active siRNA duplexes.

2.3.2. Hairpin-like Design Enables Higher siRNA Duplex Loading on SNAs than Hybridized Design

HER2-targeting hairpin-like siRNA-SNAs were synthesized by adding hairpin-like siRNA to gold nanoparticles and salt aging them, then washing away unbound oligonucleotides.[83] DLS shows an increase in hydrodynamic diameter when hairpin-like siRNAs are conjugated to the gold nanoparticles, indicating the successful formation of SNAs (bare gold nanoparticle: 10 nm, hyb. siRNA-SNA: 17 nm, HP siRNA-SNA: 23 nm) (**Figure 2.6**). Although the hairpin-like siRNA-SNA is larger than the hybridized siRNA-SNA, the difference in size is minor in the context of these experiments and may be due to a higher density of siRNA duplexes. OliGreen fluorescence quantification revealed 25 siRNA duplexes per *HER2*-targeting hybridized siRNA-SNA particle (14% duplex efficiency) (**Figure 2.7A**). Significantly, the *HER2*-targeting hairpin-like siRNA-SNA has a four-fold higher duplex loading, bearing 103 siRNA duplexes per particle (**Figure 2.7B**). This effect is sequence-independent, as siRNA-

SNAs with other sequences exhibit a similar increase in duplex loading between the hybridized and hairpin-like architectures (**Figure 2.8**). Thus, the hairpin-like architecture allows for a significantly greater loading of siRNA on its surface than the hybridized architecture.

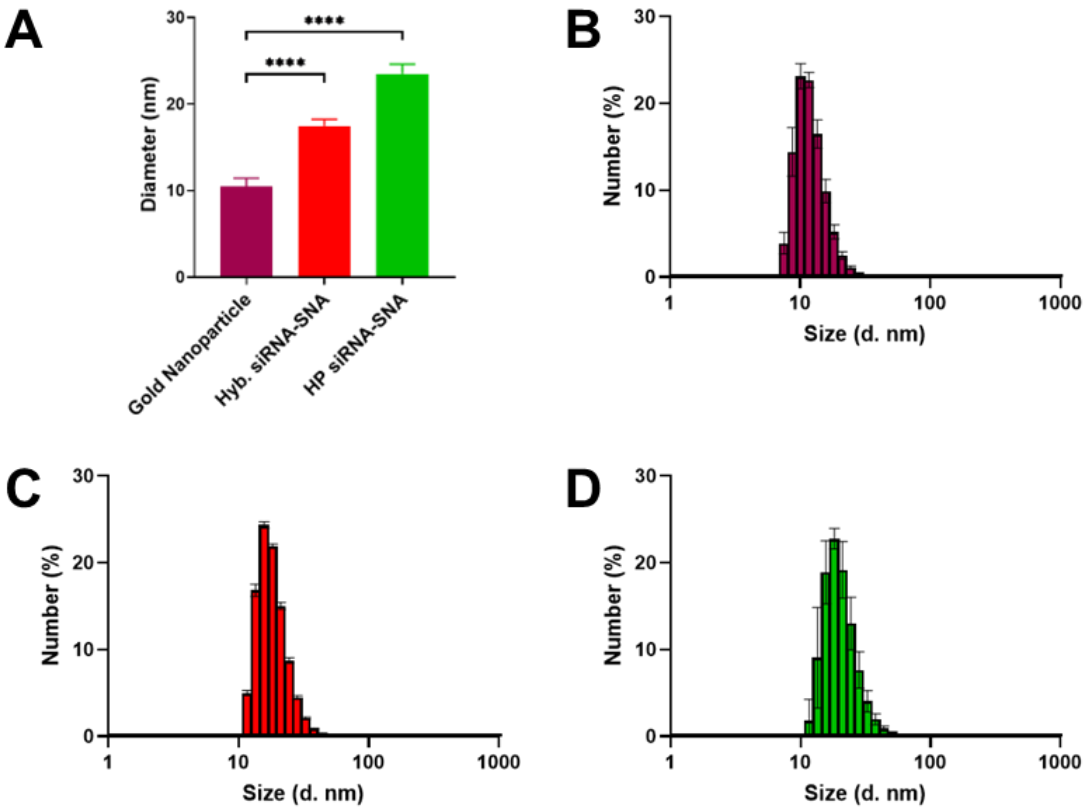

Figure 2.6. DLS analysis shows siRNA-SNA formation. (A) Diameters of bare gold nanoparticles and hybridized and hairpin-like siRNA-SNAs. Diameters shown are number means measured by DLS. Error bars are SD of 10 measurements. (B) DLS number distribution of gold nanoparticles. Error bars are SD of 10 measurements. (C) DLS number distribution of hybridized siRNA-SNAs. Error bars are SD of 10 measurements. (D) DLS number distribution of hairpin-like siRNA-SNAs. Error bars are SD of 10 measurements (****$P \leq 0.0001$).

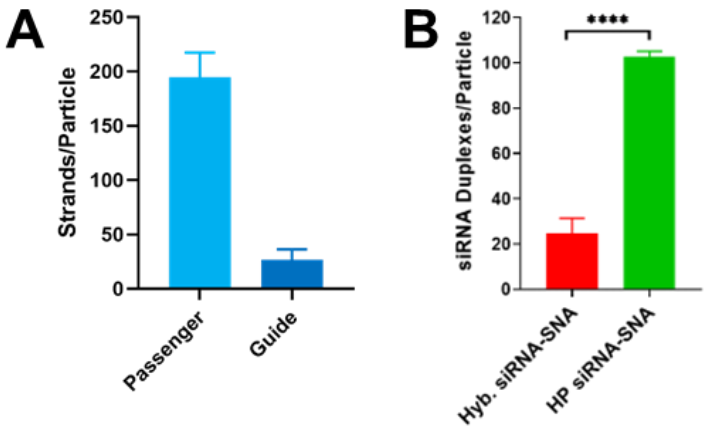

Figure 2.7. Hairpin-like design increases duplex loading of *HER2*-targeting siRNA-SNAs. (A) Passenger and guide strand loading for hybridized siRNA-SNAs. Error bars are SD of 3 batches of SNAs. (B) siRNA duplex loading for each SNA architecture. Error bars are SD of 3 batches of SNAs.

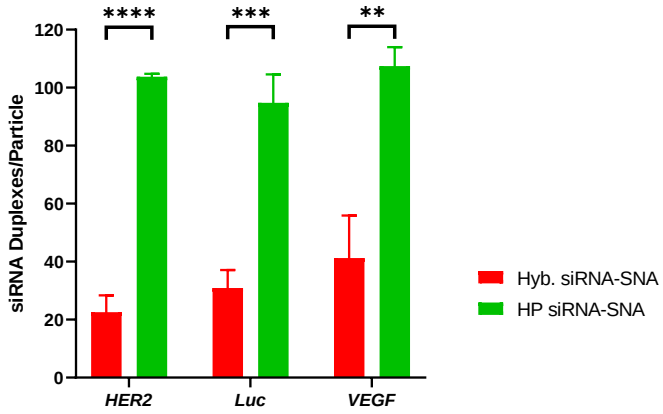

Figure 2.8. Hairpin-like siRNA architecture increases duplex loading on SNAs for a variety of sequences. Hybridized and hairpin-like siRNA-SNAs with sequences targeting *HER2*, *Luc*, and *VEGF* mRNA were synthesized. For all sequences tested, the hairpin-like architecture increased duplex loading. Error bars are SD of 3 batches of SNAs (**$P \leq 0.01$).

2.3.3. Hairpin-like Design Increases Serum Nuclease Resistance and Decreases SNA Cytotoxicity

In general, siRNAs bound to a particle surface in SNA form exhibit higher serum nuclease resistance than free siRNAs due to the negatively charged surface of the SNA, steric congestion, and high local salt concentrations.[102,85,107] siRNA-SNAs have a higher half-life in

serum than linear siRNAs, making them better suited for use as therapeutics. The hairpin-like siRNA-SNA, with its higher duplex density, may provide even greater serum nuclease resistance than the prototypical hybridized siRNA-SNA. The serum stability of hairpin-like and hybridized siRNA-SNAs was compared by incubating them in 10% FBS and measuring the amount of siRNA duplex remaining on the SNA over time (**Figure 2.9**). Hairpin-like siRNA-SNAs were found to have a six-fold longer half-life in serum compared to hybridized siRNA-SNAs (132 min vs. 22 min), indicating that the hairpin-like architecture improves siRNA-SNA resistance to serum nucleases. This enhancement could enable SNAs with the hairpin-like design to deliver a greater amount of intact siRNA to target sites. Interestingly, hairpin-like siRNA-SNAs with a much lower duplex loading (39 duplexes/SNA, comparable to that of the hybridized siRNA-SNAs) had a half-life in serum (17 min) that was closer to that of the hybridized siRNA-SNAs (22 min), indicating that the increased serum nuclease resistance of hairpin-like siRNA-SNAs likely stems from their high siRNA duplex density.

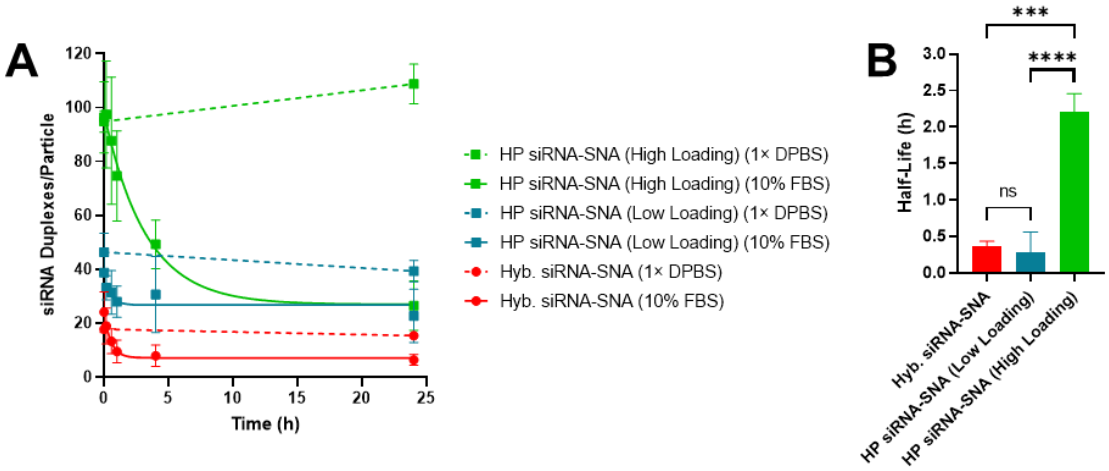

Figure 2.9. Hairpin-like design increases serum stability of siRNA-SNAs in a duplex loading density-dependent manner. (A) Degradation of hairpin-like siRNA-SNAs with high (96 duplexes/SNA) and low (39 duplexes/SNA) loading and hybridized siRNA-SNAs (24 duplexes/SNA) in 1× DPBS and 10% FBS. Error bars are SD of 3 experimental replicates. (B) Half-lives of siRNA-SNAs in 10% FBS, derived from curves in (A). Error bars are SD of 3 experimental replicates (ns $P > 0.05$).

siRNA-SNAs are cytotoxic at high concentrations because the gold accumulates in cells, limiting the maximum dose of siRNA that can be delivered. Since hairpin-like siRNA-SNAs contain more active siRNA duplexes per gold nanoparticle than hybridized siRNA-SNAs, the hairpin-like siRNA-SNAs should be able to deliver greater amounts of siRNA before cytotoxic concentrations of gold are reached. SK-OV-3 cells were treated with increasing concentrations of hybridized and hairpin-like siRNA-SNAs, and cell viability was measured (**Figure 2.10**). Indeed, the median lethal dose (LD_{50}) occurs at a higher siRNA concentration with hairpin-like siRNA-SNAs than with hybridized siRNA-SNAs, indicating that the hairpin-like architecture is less cytotoxic. The increased serum nuclease resistance and decreased cytotoxicity resulting from the hairpin-like design will allow for higher amounts of active siRNA to be delivered by SNAs for therapeutic applications.

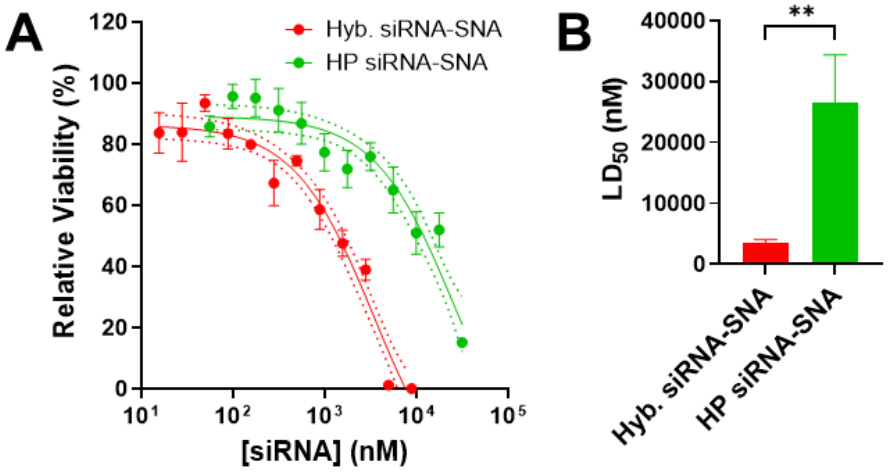

Figure 2.10. Hairpin-like design decreases cytotoxicity of siRNA-SNAs. (A) Cytotoxicity of siRNA-SNAs. Dotted lines are 95% confidence interval (CI). Error bars are SD of 3 biological replicates. (B) LD_{50} of siRNA-SNAs, derived from curves in (A). Error bars are SD of 3 biological replicates.

2.3.4. Hairpin-like siRNA-SNAs Produce a More Durable Gene Silencing Effect than Hybridized siRNA-SNAs

The gene silencing activity of hybridized and hairpin-like siRNA-SNAs was compared to determine if the hairpin-like architecture affects interactions with RNAi proteins. The hairpin-like siRNA-SNAs were observed to enter cells as single-entity agents like their hybridized siRNA-SNA counterparts but delivered higher quantities of siRNA (hyb. siRNA-SNAs: 1.3×10^6 siRNA/cell, HP siRNA-SNAs: 2.5×10^6 siRNA/cell), in agreement with previous results that cellular uptake of SNAs is affected by oligonucleotide density (**Figure 2.11**).[100] To remove the difference in uptake and compare the interactions of siRNA-SNAs with RNAi proteins, *HER2*-targeting siRNA-SNAs were transfected into SK-OV-3 cells such that the same amount of siRNA was delivered for both architectures.[105] Both siRNA-SNAs achieved equal gene knockdown at a 100 nM siRNA concentration, demonstrating that the hairpin-like architecture does not prevent the surface-bound strands from interacting with RNAi proteins and allows for the same gene silencing functionality as the hybridized siRNA-SNA (**Figure 2.12A**).

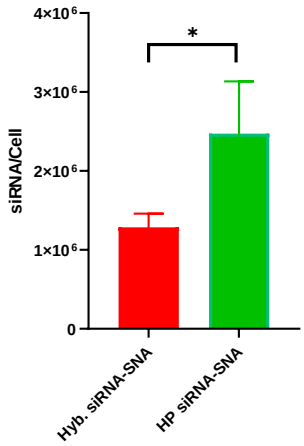

Figure 2.11. Architecture affects cellular uptake. The cellular uptake of siRNA-SNAs with hairpin-like or hybridized designs was compared. Hairpin-like siRNA-SNAs retain the ability to enter cells without the use of transfection reagents and deliver more siRNA into cells than SNAs with the hybridized architecture. Error bars are SD of 3 biological replicates (*$P \leq 0.05$).

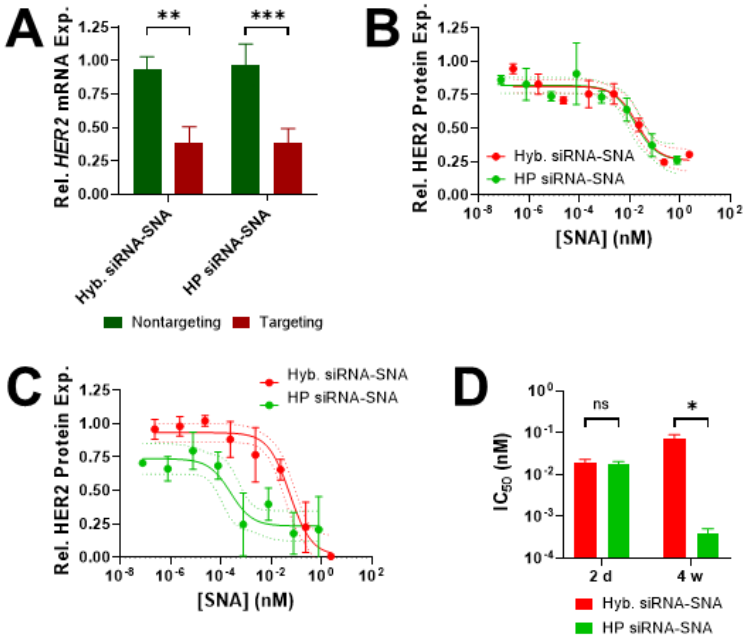

Figure 2.12. Hairpin-like design increases gene silencing durability of siRNA-SNAs. (A) Full gene silencing activity of *HER2*-targeting siRNA-SNAs. SK-OV-3 cells were transfected with 100 nM siRNA equivalent SNAs. Relative gene expression was measured 48 h after SNA administration by RT-qPCR, normalized to transfection agent-only treatment. Error bars are SD of 3 experimental replicates. (B) Knockdown potency of *HER2*-targeting siRNA-SNAs 2 days after SNA administration. SK-OV-3 cells were transfected with a range of SNA concentrations. Protein expression was measured using an in-cell Western assay, normalized to transfection agent-only treatment. Dotted lines are 95% CI. Error bars are SD of 3 biological replicates. (C) Knockdown potency of *HER2*-targeting siRNA-SNAs 4 weeks after SNA administration. Dotted lines are 95% CI. Error bars are SD of 3 biological replicates. (D) Half maximal inhibitory concentration (IC_{50}) of *HER2*-targeting siRNA-SNAs at 2 days and 4 weeks after SNA administration, based on protein expression curves in (B) and (C). Error bars are SD of 3 biological replicates.

Next, the effect of SNA design on gene silencing potency was compared. Specifically, it was investigated whether RNAi machinery recognized both SNAs identically regardless of differences in architecture and loading, or if the higher loading of hairpin-like siRNA-SNAs enabled each SNA to be more potent, or if the denser loading or attachment architecture of hairpin-like siRNA-SNAs inhibited interactions with RNAi machinery. To study differences due

to these interactions, a range of SNA concentrations was transfected into SK-OV-3 cells for 24 h so that at each concentration, the same amount of siRNA of either design was delivered regardless of differences in uptake.[105] HER2 protein expression was measured two days after SNA administration using an in-cell Western assay, since it is higher-throughput than RT-qPCR and correlated the previously measured gene expression with protein expression. The potency of both SNAs was found to be similar in terms of SNA concentration (hybridized siRNA IC_{50}: 0.020 nM, hairpin-like siRNA-SNA IC_{50}: 0.017 nM) (**Figures 2.12B and D**). The dependency of knockdown on SNA concentration, rather than siRNA concentration, is in agreement with previous observations that the SNA is the active entity in gene silencing.[102,105] RNAi proteins recognize both architectures of SNA similarly regardless of attachment architecture or loading, and the hairpin-like attachment strategy does not impair gene silencing activity.

Gene silencing duration is a critical property of siRNA that affects the ability to drive a persistent phenotypic change, the portion of treatment time during which the target protein is below the therapeutic threshold, and the required dosing schedule.[125] The kinetics of siRNA-SNA gene silencing is slower than that of linear siRNA; with siRNA-SNAs, it takes longer to reach maximum knockdown as well as return to pre-treatment gene expression levels.[86,102] Studies have suggested that Dicer-2 cleavage is the rate-limiting step in the SNA gene silencing pathway, resulting in a sustained rate of siRNA removal from SNAs and slower subsequent processing by RNAi machinery.[105] Thus, at early time points, both SNA architectures have a similar gene silencing effect regardless of loading since siRNA release occurs at a similar rate (**Figures 2.12B and 2.13A**). However, because the hairpin-like siRNA-SNAs have a higher siRNA loading than the hybridized siRNA-SNAs, it will take longer for intracellular hairpin-like siRNA-SNAs to be depleted of siRNA so their knockdown should be more persistent than that of

hybridized siRNA-SNAs at later time points (**Figure 2.13B**). Indeed, four weeks after a 24 h SNA treatment, SK-OV-3 cells treated with the hairpin-like siRNA-SNAs had persistent *HER2* gene silencing at lower SNA concentrations, reducing the hairpin-like siRNA-SNA IC_{50} to 0.00038 nM; conversely, cells treated with hybridized siRNA-SNAs had a weakening of the gene silencing effect, with a rise in IC_{50} to 0.070 nM (**Figures 2.12C and D**). This result suggests that the hairpin-like siRNA-SNA allows for the release of siRNA for a longer period than the hybridized siRNA-SNA, lengthening the duration of knockdown. Therefore, not only is the hairpin-like architecture able to deliver more siRNA at low SNA concentrations than the hybridized architecture, it also provides a more persistent gene silencing effect.

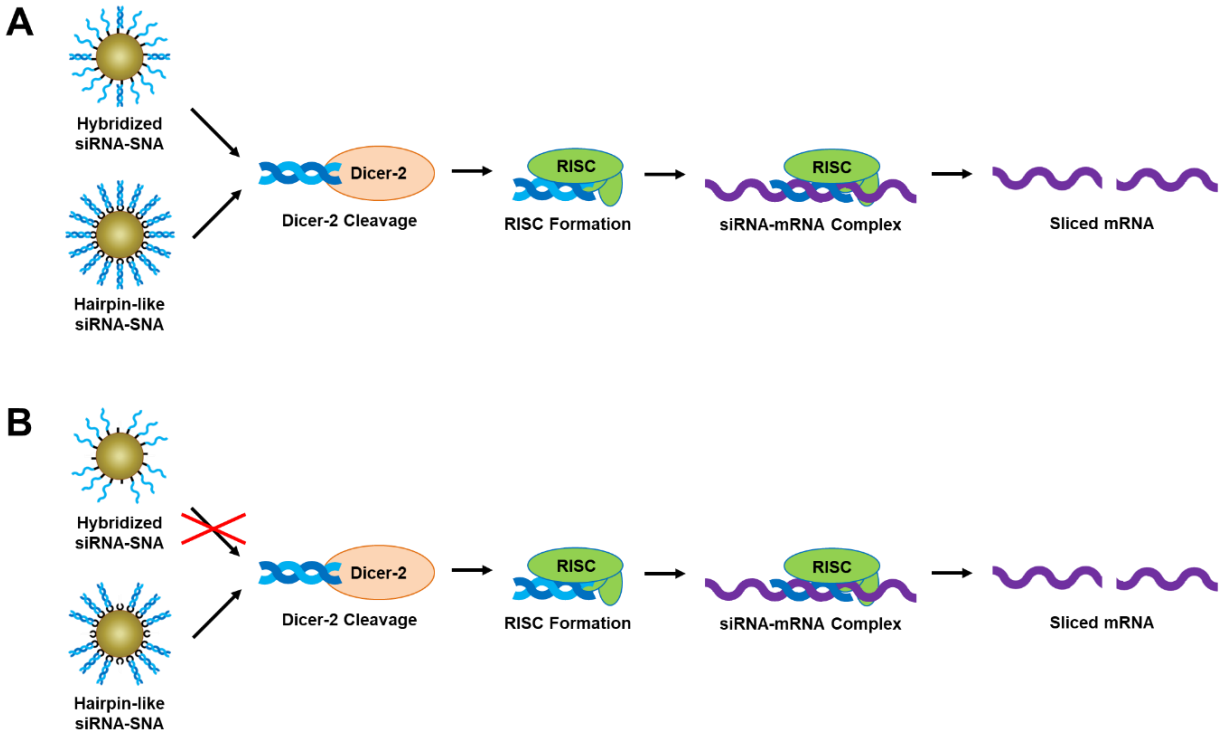

Figure 2.13. RNAi pathway for hybridized and hairpin-like siRNA-SNAs at early and late time points. (A) At early time points, Dicer-2 cleavage releases siRNAs from both architectures of siRNA-SNAs at similar rates, resulting in a similar level of gene silencing. (B) At later time points, hybridized siRNA-SNAs will be depleted of siRNAs first, after which they will no longer sustain a further gene silencing effect. Due to their higher loading, hairpin-like siRNA-SNAs will still have siRNAs remaining that can be cleaved by Dicer-2 and processed to sustain a more durable gene silencing effect.

2.3.5. Calcium-Salting Enhances the Cytosolic Delivery of Hairpin-like siRNA-SNAs

Upon internalization, siRNA-SNAs accumulate in endosomes, while a small fraction of the siRNA-SNAs escape into the cytosol where they engage in gene silencing.[102,111] While siRNA-SNAs towards some targets achieve efficient endosomal escape and gene silencing,[102,86–89] others are restricted by inefficient cytosolic delivery, implying a sequence dependence on endosomal escape. To improve the efficacy of siRNA-SNAs for a broad range of targets, we have investigated a generalizable calcium-salting method for enhancing siRNA-SNA cytosolic delivery. We found that salting PLGA nanoparticle-core siRNA-SNAs with $CaCl_2$ enhances their cytosolic delivery. Ca^{2+} ions associate with the negatively charged phosphate backbone of the siRNAs on the SNAs, and upon endocytosis, these ions promote a proton sponge effect that facilitates efficient endosomal escape of the siRNA-SNAs.[126,127] Calcium-salted PLGA-core siRNA-SNAs achieve efficient cytosolic delivery and gene silencing across multiple sequences and cell types, without inducing any cytotoxicity.

To investigate the applicability of calcium-salting beyond siRNA-SNAs with a PLGA core, we calcium salted hybridized and hairpin-like siRNA-SNAs with a 13-nm gold nanoparticle core. We used siRNA-SNAs with a *HER2* sequence at a concentration at which we did not observe gene silencing without transfection due to inadequate cytosolic delivery. Upon treating SK-OV-3 cells, unsalted siRNA-SNAs resulted in no significant gene silencing while calcium-salted siRNA-SNAs achieved silencing due to enhanced cytosolic delivery enabled by the Ca^{2+} ions (**Figure 2.14**). Thus, the calcium-salting strategy for improving cytosolic delivery is applicable to SNA constructs beyond the PLGA-core siRNA-SNA.

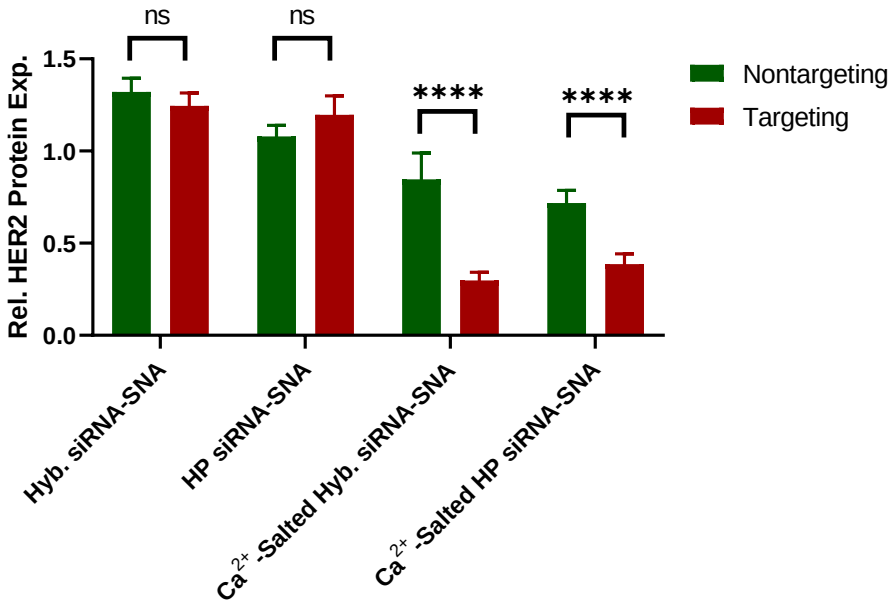

Figure 2.14. Calcium-salting enhances the cytosolic delivery of gold nanoparticle-core siRNA-SNAs. Protein knockdown activity of *HER2*-targeting unsalted and calcium-salted siRNA-SNAs. SK-OV-3 cells were treated with 100 nM siRNA equivalent SNAs. Calcium-salted siRNA-SNAs were at a final Ca^{2+} concentration of 3 mM. Protein expression was measured 48 h after SNA administration by an in-cell Western assay, normalized to untreated cells. Error bars are SD of 3 biological replicates.

Since calcium ions associate with the negatively charged phosphate backbone of the oligonucleotides on the SNA, we hypothesized that a higher amount of calcium ions would associate with an SNA with a higher loading of oligonucleotides. Since hairpin-like siRNA-SNAs have greater loading than hybridized siRNA-SNAs, we expected them to have more calcium ion association, leading to more efficient cytosolic delivery and more potent gene silencing. When comparing the dose-response trends of calcium-salted *HER2*-targeting hairpin-like and hybridized siRNA-SNAs in SK-OV-3 cells, hairpin-like siRNA-SNAs had a lower IC_{50} and therefore greater potency (**Figure 2.15A**). While the difference is not statistically significant, it is still apparent and implies that the hairpin-like design may enhance the cytosolic delivery enabled by calcium-salting.

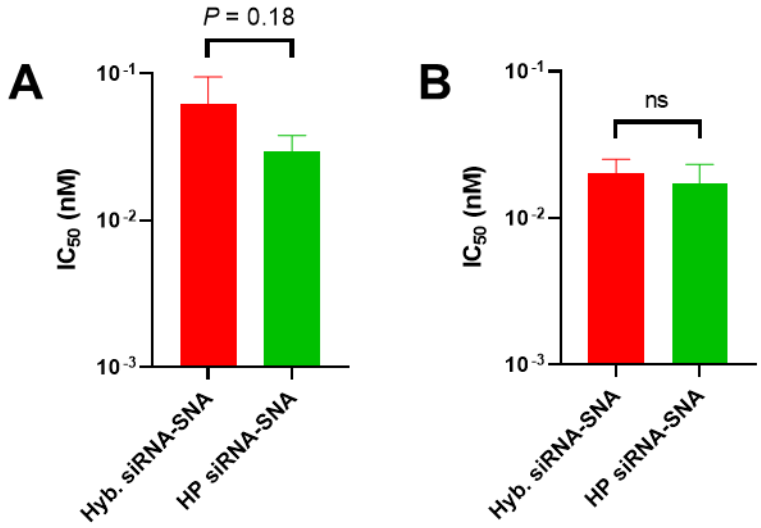

Figure 2.15. Knockdown potency of calcium-salted and RNAiMAX-transfected siRNA-SNAs. (A) IC_{50} of calcium-salted siRNA-SNAs calculated from protein expression curves. Error bars are SD of 3 biological replicates. Error bars are SD of 3 biological replicates. (B) IC_{50} of RNAiMAX-transfected siRNA-SNAs calculated from protein expression curves. Error bars are SD of 3 biological replicates.

To gauge the transfection efficiency of calcium salting, we compared it to the state-of-the-art transfection reagent RNAiMAX. RNAiMAX is a cationic lipid that achieves exceptional transfection efficiency for siRNA and siRNA-SNAs and thus is the gold standard to compare against, but it is cytotoxic and poorly suited for therapeutic use. Calcium-salted siRNA-SNAs had a similar gene silencing potency to RNAiMAX-transfected siRNA-SNAs (**Figure 2.15B**), indicating that calcium-salting achieves cytosolic delivery on the same scale as RNAiMAX without the associated cytotoxicity. Thus, calcium-salting is a highly effective method of enhancing cytosolic delivery for several types of siRNA-SNAs.

2.4. Conclusion

From these data, one can conclude that the incorporation of a hairpin structure into SNA design can lead to marked improvements in SNA performance. Indeed, the novel hairpin-like

architecture improves siRNA-SNA duplex loading, serum nuclease resistance, biocompatibility, cellular uptake, calcium-assisted cytosolic delivery, and gene silencing durability. These factors should work synergistically to enhance the delivery of active siRNA duplexes to target tissues and increase the window for gene silencing. Due to these advantages and the universality of the design, hairpin-like siRNA-SNAs are an important synthetic advance in the development of next-generation siRNA-SNA constructs, potentially driving the development of siRNA therapeutics and significantly expanding their scope of utility.

CHAPTER 3

In Vivo Behavior of Ultrasmall Spherical Nucleic Acids

3.1. Introduction

3.1.1. Prototypical Gold Nanoparticle-Core SNAs

SNAs are defined by the dense, highly oriented arrangement of oligonucleotides around a spherical nanoparticle core.[81,83] This three-dimensional architecture imbues the composite oligonucleotides with properties distinct from their linear analogues, including rapid cellular uptake in high quantity without the need for ancillary transfection agents,[84,90] decreased nuclease susceptibility,[85] and low cytotoxicity.[102,108] Since their discovery, SNAs have made a significant impact in biomedicine,[82,113] with established utility in disease detection,[92,93] cancer immunotherapy,[94,117,128,115,129] and gene regulation.[86–89]

Early work on the SNA platform was based on constructs synthesized from 13-nm gold nanoparticle cores (AuSNAs).[84,92,102] Because the oligonucleotides are covalently conjugated to the gold nanoparticle core, it is easy to both control the loading density and to calculate the drug-to-carrier (i.e., DNA-to-gold) ratios with high precision, allowing for a comprehensive understanding of the structure-function relationships of SNAs in biological settings.[130] High surface loading of oligonucleotides increases the efficiency of SNA cellular uptake, a key consideration when designing systems for intracellular delivery.[100] Furthermore, it has been shown that increasing the oligonucleotide surface density on the SNA not only protects the oligonucleotides from degradation but also reduces overall cellular toxicity without negatively affecting activity.[99,105,131] Clinically, SNAs with a gold nanoparticle core have shown promise as gene regulation agents for glioblastoma multiforme and have exhibited favorable toxicological parameters.[87,103] However, although AuSNAs possess favorable toxicological parameters and clinical safety, long-term retention of the inorganic gold core in off-target organs, particularly the liver, remains a concern, which is an issue rife in nanomedicine.[87,132,133]

3.1.2. Size Affects Nanoparticle Behavior

Size is a key factor that influences nanoparticle retention within the body, as well as blood circulation half-life and tissue distribution following systemic administration.[134] Generally, nanoparticles with hydrodynamic diameters greater than 10 nm exceed the renal filtration threshold and accumulate in the liver and spleen, where they are retained for prolonged periods.[135–138] Conversely, nanoparticles that are smaller than 10 nm ("ultrasmall" nanoparticles) exhibit different behavior from larger nanoparticles.[139] Ultrasmall nanoparticles are cleared through the kidneys, an elimination route that is faster than the hepatic accumulation and slow metabolism of larger nanoparticles.[140–142,139] While this leads to lower accumulation in off-target organs (i.e., decreased off-target toxicity), it also decreases accumulation in the target organ (e.g., tumor).[143] However, the fraction of nanoparticles that *do* reach the target site penetrate the tissue more efficiently.[144] Moreover, cell entry by ultrasmall nanoparticles is highly efficient.[145–147] Thus, for many nanoparticle systems, there is a tradeoff at the ultrasmall scale and it is important to consider if the benefits of faster elimination and lower off-target accumulation outweigh the drawbacks of decreased accumulation at the target site.

3.1.3. SNAs at the Ultrasmall Size Scale

While SNAs have been synthesized from a variety of nanoparticle core types and sizes (**Figure 3.1**),[83,95,148,96,116] ranging from molecularly pure 1-nm buckminsterfullerene C_{60} scaffolds[148] to 300-nm lipid nanoparticles,[114] all *in vivo* analyses have been limited to SNAs with cores exceeding 10 nm in diameter.[87,149,150,114,116] Thus, little is known about the chemical, biological, and *in vivo* behavior of SNAs synthesized from ultrasmall nanoparticle cores. With respect to SNAs in this size regime, it has been found that molecular SNAs, synthesized from T_8 polyoctahedral silsesquioxane (POSS) cores and buckminsterfullerene C_{60} cores are capable of

independently entering cells *in vitro* like their larger SNA counterparts; however, only molecular SNAs synthesized from the C_{60} core exhibit gene silencing activity, defining the lower limit of size and oligonucleotide loading density required for SNA-like behavior.[148] While these molecular SNAs were found to enter cells, their *in vivo* behavior has not been characterized.

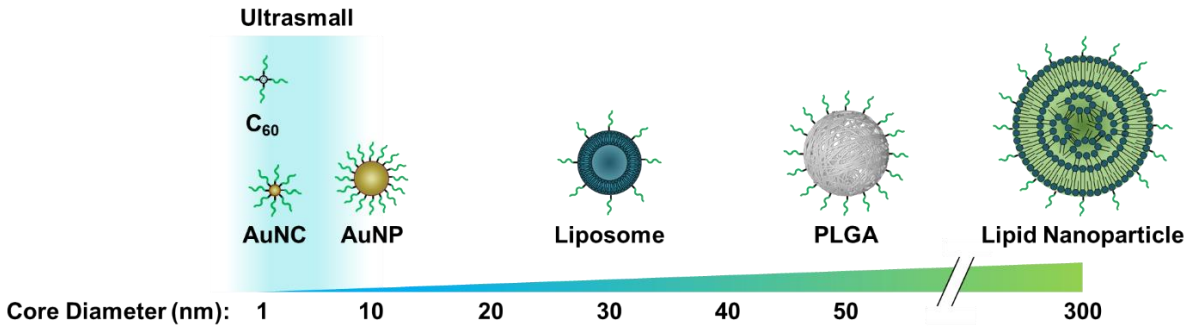

Figure 3.1. SNA core materials and sizes. Cores smaller than 10 nm exist within the ultrasmall size regime. Image is not to scale.

To investigate the effect of an ultrasmall core on SNA *in vivo* properties, we synthesized SNAs from molecularly well-defined 1.4-nm gold nanocluster cores (AuNC-SNAs) and compared their biological behavior to conventional SNAs with 10-nm gold nanoparticle cores (AuNP-SNAs) (**Figure 3.2**). The gold nanocluster was chosen as the SNA core material for these analyses for several reasons. First, having both cores made of gold isolates our study to effects due to differences in size, rather than material. Second, while POSS and C_{60} have a finite and fixed number of attachment sites determined by their chemical structures, the loading density of oligonucleotides onto gold nanoclusters is only limited by the electrostatic and steric interactions from attaching thiolated oligonucleotides to the particle surface, thus overcoming a limitation of molecular SNAs and allowing for a higher surface loading density. Finally, gold can be sensitively traced in cells and tissues. We hypothesized that AuNC-SNAs would possess the

advantageous properties of traditional Au-SNAs (e.g., high cellular uptake, low cytotoxicity) and simultaneously mitigate their biological limitations (e.g., high liver accumulation, inability to be renally cleared, reduced targeting efficiency). Simultaneously, we hypothesized that moving to an ultrasmall size regime would maximize both the oligonucleotide surface density and drug-to-carrier ratio, two important parameters to consider when designing nanoscale therapeutics.[99,100,105,131]

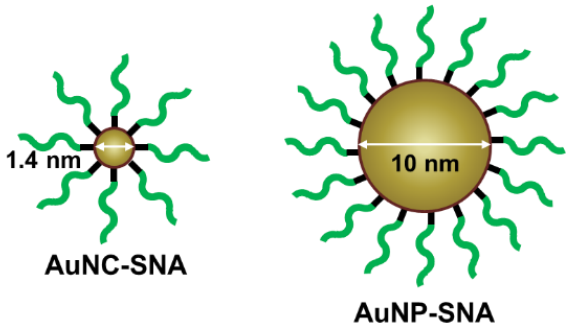

Figure 3.2. Structures of AuNC-SNAs and AuNP-SNAs. AuNC-SNAs consist of a 1.4-nm gold nanocluster core functionalized with oligonucleotides, while AuNP-SNAs consist of a 10-nm gold nanoparticle core functionalized with oligonucleotides. Image is not to scale.

3.2. Materials and Methods

Oligonucleotide Synthesis. DNA oligonucleotides (sequence: 5' TTT-TTT-TTT-TTT-TTT-TTT-TT-(Spacer 18)$_2$-SH 3') were synthesized on a MerMade 12 system (LGC Biosearch Technologies) using 2'-O-triisopropylsilyloxymethyl-protected phosphoramidites (Glen Research). DNA oligonucleotides consisted of DNA base cyanoethyl phosphoramidites (Glen Research), two spacer-18 (18-O-dimethyoxytritylhexaethyleneglycol,1-[(2-cyanoethyl)-(N,N-diisopropyl)] phosphoramidites (Glen Research), and a thiol modification added by using 1-O-dimethoxytrityl-propyl-disulfide,1'-succinyl-lcaa-controlled pore glass beads. After synthesis, DNA oligonucleotides were deprotected following the manufacturer's protocol (Glen Research). Deprotected DNA oligonucleotides were purified by high-performance liquid chromatography

on a C18 column using 0.1 M triethylammonium acetate and acetonitrile as the solvents. The 5'-DMT group was removed from purified DNA oligonucleotides by treating with 20% acetic acid at room temperature for 1 h and extracting 3 times with ethyl acetate. The oligonucleotide solution was lyophilized and suspended in DNase/RNase-free water.

Au_{102}(*p*-mercaptobenzoic acid (*p*-MBA))$_{44}$ Nanocluster Synthesis. Au_{102}(*p*-MBA)$_{44}$ nanoclusters were synthesized following the method developed by Levi-Kalisman et al.[151] Aqueous solutions of 28 mM $HAuCl_4 \cdot 3H2O$, 95 mM p-mercaptobenzoic acid, 300 mM NaOH, methanol, and water were combined into a final mixture of 11.89 mL 3 mM $HAuCl_4$, 9 mM *p*-MBA, 47% (v/v) methanol and mixed in a round bottom flask for 1 h at room temperature. 500 μL 150 mM $NaBH_4$ was added, and the reaction was allowed to continue for 12 h. The product was precipitated by adding 2 M ammonium acetate to 80 mM in the mixture and centrifuging at 6000 rpm for 10 min. The precipitate was air-dried overnight, then re-dissolved in 200 μL water. To purify by fractional precipitation, methanol and 2 M ammonium acetate were added to the solution to a concentration of 0.12 M ammonium acetate, 60% methanol, and the solution was centrifugated at 6000 rpm for 10 min. The supernatant was collected and transferred to a centrifuge tube. Methanol and 2M ammonium acetate were added to a concentration of 0.12 M ammonium acetate, 80% methanol, and the solution was centrifuged at 6000 rpm for 10 min. The precipitate was lyophilized until dry, then re-dissolved in water.

AuNC-SNA Synthesis. Gold nanoclusters were functionalized with thiolated DNA oligonucleotides via salt-aging. 62 nmol DNA was incubated in 100 mM dithiothereitol (DTT, pH 8) for 1 h to reduce the dithiol and purified using Nap-5 exclusion columns (Cytivia). The purified DNA was added to 2 mL 2.6 μM gold nanocluster suspension and incubated with shaking for 30 min at room temperature. 0.05% Tween-20 was added to the solution, which was

then vortexed thoroughly. The salt concentration was gradually increased to 0.5 M by adding NaCl, sonicating, and vortexing every 15 min while shaking, followed by an overnight incubation. Unattached oligonucleotides were removed by washing with 1% Tween-20 2 times, then 1× DPBS 3 times in Amicon Ultra 30K molecular weight cutoff spin filters (MilliporeSigma). SNAs were stored at 4 °C for up to 3 months.

AuNP-SNA Synthesis. 10-nm AuNPs (Ted Pella) were functionalized with thiolated DNA oligonucleotides via salt-aging. 62 nmol DNA was incubated in 100 mM dithiothereitol (DTT, pH 8) for 1 h to reduce the disulfides and purified using Nap-5 exclusion columns (Cytivia). The purified DNA was added to 10 mL 7.7 nM 10-nm AuNP suspension and incubated with shaking for 30 min at room temperature. 0.05% Tween-20 was added to the solution, which was then vortexed thoroughly. The salt concentration was gradually increased to 0.5 M by adding NaCl, sonicating, and vortexing every 15 min while shaking, followed by an overnight incubation. Unattached oligonucleotides were removed by washing with 1% Tween-20 2 times, then 1× DPBS 3 times in Amicon Ultra 50K molecular weight cutoff spin filters (MilliporeSigma). SNAs were stored at 4 °C for up to 3 months.

SNA Characterization. SNA size was measured by diluting in 1 × DPBS and performing DLS using a Zetasizer (Malvern). SNA concentration was determined by measuring the absorbance spectra of the SNAs using a Cary-5000 spectrophotometer (Agilent). AuNC-SNA concentration was calculated using the absorbance at 510 nm and an extinction coefficient of 1.75×10^5 M^{-1} cm^{-1}. AuNP-SNA concentration was calculated using the absorbance at 515 nm and an extinction coefficient of 1.01×10^8 M^{-1} cm^{-1}. To measure DNA loading on SNAs, 2.5 nM SNAs were incubated with 20 nM KCN at 50 °C until the gold dissolved. 25 μL of this solution was added in triplicate to a 96-well plate. A standard curve of DNA in a solution identical to the SNA solution

was prepared. 75 μL water was added to all wells. For SNAs with unlabeled DNA, 100 μL Quanti-iT OliGreen solution (Invitrogen) was added to all wells, and samples were analyzed by measuring OliGreen fluorescence (λ_{ex} = 480 nm) with a BioTek Cytation 5 imaging reader. The fluorescence of the SNA solution was compared to the standard curve to calculate the DNA concentration. DNA loading of SNAs was then calculated by taking the ratio of DNA concentration to gold core concentration. Surface loading density of DNA on SNAs was calculated by dividing the moles of DNA on each SNA by the surface area of the gold core. DNA-to-gold mass ratio was calculated by dividing the mass of DNA on each SNA by the mass of the gold core.

Cellular Uptake of SNAs. In 24-well cell culture plates with 50,000 SK-OV-3 cells per well, SK-OV-3 cells were treated with 250 nM DNA equivalent of AuNC-SNAs and AuNP-SNAs in Opti-MEM for 30 min and 5 h. At the end of their treatment time, the cells were washed with 1× DPBS, 1:10 heparin solution in 1× DPBS, then 1× DPBS to remove any SNAs that remained outside the cells or dead cells. The cells were then trypsinized using 150 μL TrypLE Express (Thermo Fisher). 10 μL cells were stained with 10 μL Trypan Blue (Thermo Fisher) and their concentration was measured using an Invitrogen Countess II automated cell counter. 120 μL cells were dissolved in 50 mL 2% HCl, 2% HNO_3. The gold concentration in this solution was measured by performing ICP-MS. ICP-MS was performed on a computer-controlled (QTEGRA software) Thermo iCapQ ICP-MS (Thermo Fisher Scientific, Waltham, MA, USA) operating in STD mode and equipped with a ESI SC-2DX PrepFAST autosampler (Omaha, NE, USA). Internal standard was added inline using the prepFAST system and consisted of 1 ng/mL of a mixed element solution containing Bi, In, ^{6}Li, Sc, Tb, Y (IV-ICPMS-71D from Inorganic Ventures). Online dilution was also carried out by the prepFAST system and used to generate a

calibration curve consisting of 2, 4, 20, 100, and 200 ppb Au. Each sample was acquired using 1 survey run (10 sweeps) and 3 main (peak jumping) runs (40 sweeps). The isotopes selected for analysis were ^{197}Au (for SNA quantification) and ^{89}Y, ^{115}In, ^{159}Tb, and ^{209}Bi (chosen as internal standards for data interpolation and machine stability). Instrument performance was optimized daily through autotuning followed by verification via a performance report (passing manufacturer specifications). The amount of DNA taken up into each cell was calculated by converting gold atom amount in each sample to gold nanoparticle mole amount (which is equivalent to SNA mole amount), converting moles of SNA to number of SNA particles, multiplying by the number of DNA strands per SNA, and dividing by the number of cells. The amount of SNAs taken up into each cell was calculated by converting gold atom amount in each sample to gold nanoparticle mole amount (which is equivalent to SNA mole amount), converting moles of SNA to number of SNA particles, and dividing by the number of cells. The amount of gold taken up into each cell was calculated by converting gold atom amount in each sample to gold mass and dividing by the number of cells.

Cytotoxicity of SNAs. In 96-well cell culture plates with 5,000 SK-OV-3 cells per well, SNAs in Opti-MEM were incubated with SK-OV-3 cells in triplicate for 48 h. The wells were washed with 1× DPBS 3 times. 50 μL 1× DPBS and 50 μL CellTiter-Glo 2.0 reagent (Promega) were added to the wells and fluorescence was measured using a BioTek Cytation 5 imaging reader. Cell viability was normalized to cells treated with Opti-MEM only.

***In Vivo* Analyses.** All animal procedures were approved by the Northwestern University IACUC. Female mice (Balb/C) were inoculated with 1×10^6 4T1 cells in the right inguinal mammary fat pad via subcutaneous injection. Both blood circulation and biodistribution experiments began at day 7 post-inoculation, when tumors were palpable (n = 3 per group).

Animals were intravenously administered either AuNC-SNAs or AuNP-SNAs (3 nmol with respect to DNA) as a single 100 μL bolus. As a negative control, an additional set of animals were administered saline. To calculate the SNA concentration in blood, blood samples (n = 3 per time point) was collected in a heparinized tube via retro-orbital blood draw and stored on ice before digestion and analysis by ICP-MS (*vide infra*). For the biodistribution analysis at 24 h post-intravenous (IV) injection, animals (n = 3 per group) were humanely euthanized by cardiac perfusion while anesthetized. Tissues (tumor, liver, spleen, kidney, heart, lung) were harvested post-cardiac perfusion with 1× DPBS and stored on ice. For ICP-MS analysis, organs were weighed (wet mass) and lyophilized to facilitate digestion (*vide infra*).

SNA Content in Blood and Organs by ICP-MS. Collected blood and organs were digested with 50% HCl, 50% HNO_3 at 37 °C for three days. The solution was diluted to 2% HCl, 2% HNO_3, and the gold concentration was measured by ICP-MS. ICP-MS was performed on a computer-controlled (QTEGRA software) Thermo iCapQ ICP-MS (Thermo Fisher Scientific, Waltham, MA, USA) operating in STD mode and equipped with a ESI SC-2DX PrepFAST autosampler (Omaha, NE, USA). Internal standard was added inline using the prepFAST system and consisted of 1 ng/mL of a mixed element solution containing Bi, In, ^{6}Li, Sc, Tb, Y (IV-ICPMS-71D from Inorganic Ventures). Online dilution was also carried out by the prepFAST system and used to generate a calibration curve consisting of 2, 4, 20, 100, and 200 ppb Au. Each sample was acquired using 1 survey run (10 sweeps) and 3 main (peak jumping) runs (40 sweeps). The isotopes selected for analysis were ^{197}Au (for SNA quantification) and ^{89}Y, ^{115}In, ^{159}Tb, and ^{209}Bi (chosen as internal standards for data interpolation and machine stability). Instrument performance was optimized daily through autotuning followed by verification via a performance report (passing manufacturer specifications). The amount of DNA in each sample

was calculated by converting gold atom amount in each sample to gold nanoparticle mole amount (which is equivalent to SNA mole amount), converting moles of SNA to number of SNA particles, multiplying by the number of DNA strands per SNA, and dividing by the volume of blood or mass of tissue. The amount of gold in each sample was calculated by converting gold atom amount in each sample to gold mass and dividing by the volume of blood or mass of tissue.

3.3. Results and Discussion

3.3.1. Synthesis and Characterization of AuNC-SNAs

To synthesize AuNC-SNAs, Au_{102}(*p*-MBA)$_{44}$ nanoclusters were first prepared according to established protocols to serve as 1.4-nm AuNC cores.[152] These materials were further functionalized with a 20-thymine thiolated DNA sequence to ensure that the effects observed in downstream studies were due to the overall construct, rather than the oligonucleotide sequence. Successful functionalization of the DNA to AuNCs to afford AuNC-SNAs was confirmed by the increase in hydrodynamic diameter measured by DLS (**Figure 3.3)**. For comparison, larger AuNP-SNAs were synthesized from 10-nm gold nanoparticle cores according to literature protocols and their functionalization was confirmed via DLS.[153,130]

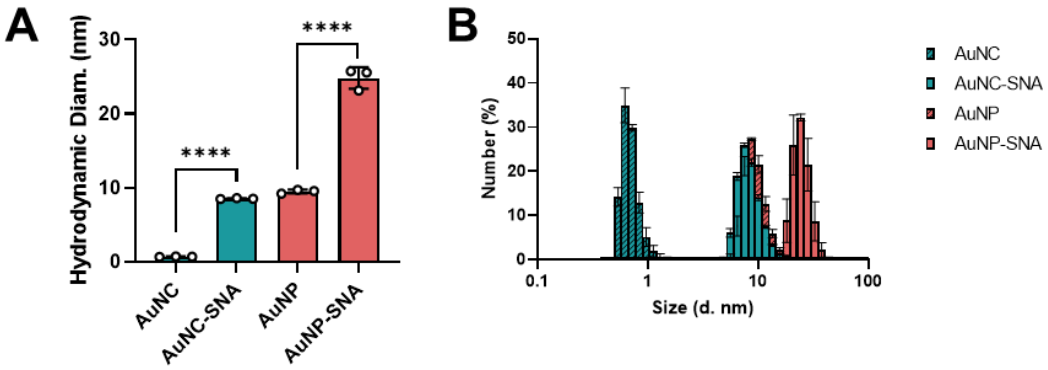

Figure 3.3. DLS analysis shows AuNC-SNA and AuNP-SNA formation. (A) DLS of bare AuNCs, AuNC-SNAs, bare AuNPs, and AuNP-SNAs. Diameters shown are number means measured by DLS. Error bars are SD of 3 measurements. (B) DLS number distribution of bare AuNCs, AuNC-SNAs, bare AuNPs, and AuNP-SNAs. Error bars are SD of 3 measurements.

The extent of DNA loading on both AuNC-SNAs and AuNP-SNAs was then quantified using OliGreen fluorescence assays. As expected, the absolute number of DNA strands per particle was higher for AuNP-SNAs (348 strands/particle) than AuNC-SNAs (11 strands/particle) due to the significantly larger surface area of the AuNP core (**Figure 3.4A**). However, the surface loading density of DNA on AuNC-SNAs was significantly higher as compared to AuNP-SNAs, along with an 11.5-fold higher DNA-to-gold mass ratio (3.21 vs. 0.28, **Figure 3.4B**). Thus, AuNC-SNAs have a higher payload-to-carrier ratio than larger AuNP-SNAs, and each AuNC-SNA can deliver more DNA payload relative to gold material.

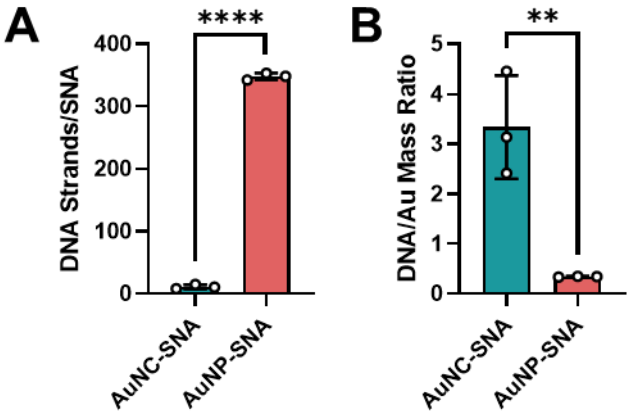

Figure 3.4. DNA loading on AuNC-SNAs and AuNP-SNAs. (A) DNA loading of AuNC-SNAs and AuNP-SNAs, reported on a per-particle basis. Error bars are SD of 3 batches of SNAs. (B) DNA-to-gold mass ratio of AuNC-SNAs and AuNP-SNAs. Error bars are SD of 3 batches of SNAs.

3.3.2. Cellular Interactions of AuNC-SNAs

To determine the cellular uptake of AuNC-SNAs by cells, SK-OV-3 ovarian cancer cells were incubated with AuNC-SNAs at a concentration of 250 nM by DNA and compared to the uptake of AuNP-SNAs at the same DNA concentration. Cellular uptake was measured as a function of gold concentration using ICP-MS, which was used to calculate both nanoparticle and

DNA concentration. After 30 minutes of incubation, we observed that AuNC-SNAs delivered significantly more DNA (**Figure 3.5A**) and particles (**Figure 3.5B**) but significantly less gold (**Figure 3.5C**) per cell than their larger AuNP-SNA counterparts. Thus, AuNC-SNAs are more efficient at delivering DNA into cancer cells than AuNP-SNAs. To investigate the mechanism of AuNC-SNA uptake in comparison to AuNP-SNA uptake, SK-OV-3 cells were pretreated with endocytosis inhibitor fucoidan, then treated with SNAs. AuNC-SNAs and AuNP-SNAs both showed a substantial level of uptake reduction with fucoidan, indicating that AuNC-SNAs enter cells through endocytosis similarly to AuNP-SNAs (**Figure 3.6**).[90]

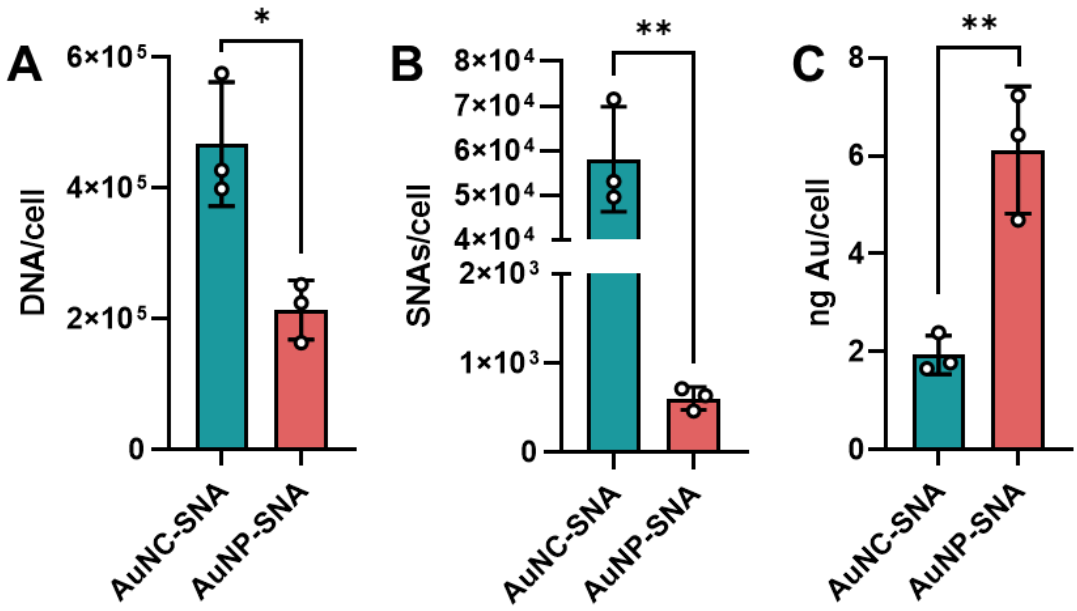

Figure 3.5. AuNC-SNAs deliver more DNA and SNAs and less gold into cells than AuNP-SNAs. SK-OV-3 cells were treated with AuNC-SNAs and AuNP-SNAs at a concentration of 250 nM by DNA for 30 min, and gold content in cells was measured using ICP-MS. (A) Cellular uptake of SNAs by DNA amount. Error bars are SD of 3 biological replicates. (B) Cellular uptake of SNAs by SNA amount. Error bars are SD of 3 biological replicates. (C) Cellular uptake of SNAs by gold amount. Error bars are SD of 3 biological replicates.

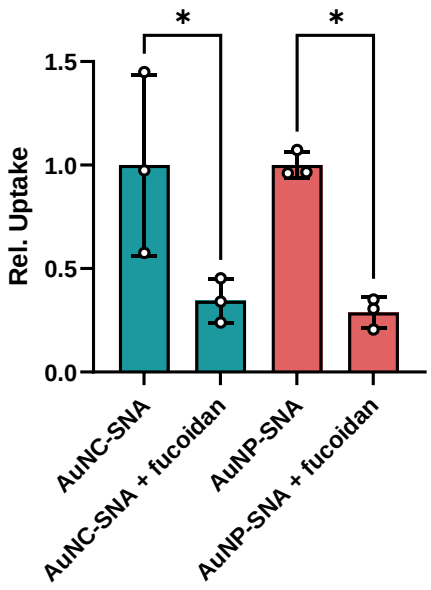

Figure 3.6. AuNC-SNAs and AuNP-SNAs enter cells via endocytosis. SK-OV-3 cells were pretreated with fucoidan, then treated with AuNC-SNAs and AuNP-SNAs at a concentration of 250 nM by DNA for 30 min, and gold content in cells was measured using ICP-MS. Error bars are SD of 3 biological replicates.

It should be noted that the cells were treated with an equivalent 250 nM DNA concentration for both AuNC-SNAs and AuNP-SNAs, and since the AuNC-SNAs have a lower DNA loading per SNA than AuNP-SNAs, a higher concentration of AuNC-SNAs (32 nM by SNA) than AuNP-SNAs (0.71 nM by SNA) was needed to achieve the 250 nM DNA concentration. Thus, it may appear that the greater delivery of SNA particles by the AuNC-SNAs could be attributed to the fact that more AuNC-SNAs were introduced to the cells than AuNP-SNAs (45-fold difference). However, AuNC-SNAs entered cells at a 96-fold greater particle number than AuNP-SNAs. Thus, the difference in SNA particle internalization cannot solely be attributed to the higher number of AuNC-SNAs treated to the cells compared to AuNP-SNAs, but also to more efficient uptake of AuNC-SNAs. AuNC-SNAs have a greater surface loading density than AuNP-SNAs, which has previously been observed to increase cellular uptake.[100] A

possible additional driver of enhanced uptake of AuNC-SNAs is a lower energy requirement to transport the smaller particles into endosomes.[154,155] In addition to superior cellular uptake, AuNC-SNAs matched the *in vitro* biological safety profile of AuNP-SNAs on a per particle basis and exhibited low cytotoxicity (**Figure 3.7**).

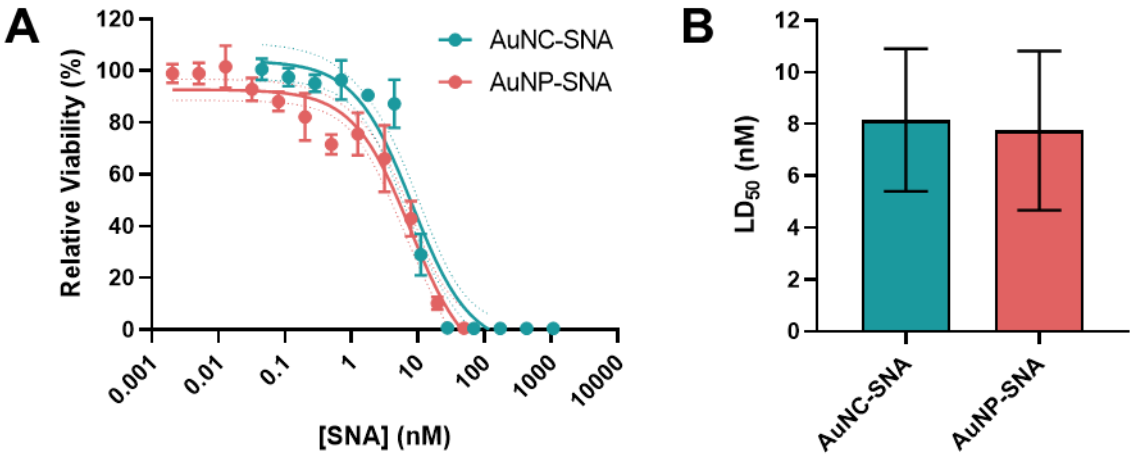

Figure 3.7. Gold-core SNAs exhibit a similar safety profile regardless of size. (A) Cytotoxicity of AuNC-SNAs and AuNP-SNAs in SK-OV-3 cells after a 48 h treatment. Dotted lines are 95% CI. Error bars are SD of 3 biological replicates. (B) LD_{50} values derived from curves in (A). Error bars are SD of 3 biological replicates.

3.3.3. Pharmacokinetic Behavior of AuNC-SNAs

Next, we investigated the *in vivo* biological behavior of AuNC-SNAs as compared to AuNP-SNAs in mice bearing orthotopic 4T1 triple negative breast cancer (TNBC) tumors. Animals were intravenously administered a 3 nmol DNA equivalent of either AuNC-SNAs or AuNP-SNAs. At set timepoints, gold concentration in the blood was measured by ICP-MS and used to calculate the DNA blood concentration as a function of time (**Figure 3.8A**). Remarkably, AuNC-SNAs remained in circulation for significantly prolonged periods relative to AuNP-SNAs, with detectable gold concentrations in the blood at 24 hours post-injection (**Figure 3.8B**). We hypothesized that a driver of the prolonged circulation of AuNC-SNAs was reduced liver

sequestration. Additionally, prolonged circulation of AuNC-SNAs could lead to enhanced tumor accumulation. To investigate, we analyzed the biodistribution of both SNAs in these organs.

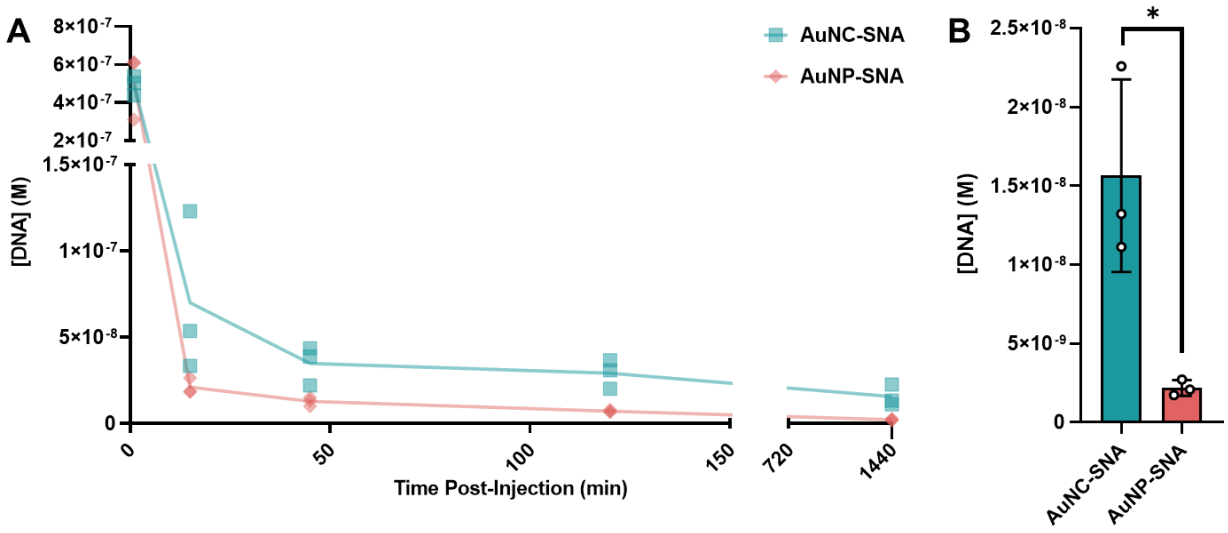

Figure 3.8. AuNC-SNAs circulate longer in blood than AuNP-SNAs. (A) DNA blood concentration as a function of time post-IV injection when delivered as AuNC-SNAs (blue) or AuNP-SNAs (peach). Data points are 3 biological replicates. (B) Final DNA blood concentration at 24 h post-injection. Error bars are SD of 3 biological replicates.

To assess the biodistribution of SNAs with either core size, mice bearing orthotopic 4T1 tumors were administered a 3 nmol DNA equivalent of either AuNC-SNAs or AuNP-SNAs via tail vein IV. At 24 h post-injection, animals were sacrificed and perfused, and tissues were collected and processed for ICP-MS analysis (**Figure 3.9**). As expected, both nanoparticle constructs accumulated in the liver and kidney, in agreement with conventional nanoparticle clearance pathways (**Figure 3.10A**).[135–137] However, the AuNC-SNAs showed significantly lower liver accumulation coupled with increased kidney accumulation as compared to their larger AuNP-SNA counterparts, resulting in a higher kidney-to-liver ratio and revealing a distinct skew towards clearance by the kidney (**Figure 3.10B**). Moreover, AuNC-SNAs delivered a much higher payload to the site of interest (i.e., DNA to tumor) than their larger

counterparts (**Figure 3.10C**). This is in contrast to what has been reported for other ultrasmall nanoparticles,[143,146,156,157] and the greater tumor accumulation of AuNC-SNAs is likely due to a combination of their prolonged blood circulation, greater tumor infiltration,[144] and more efficient entry in tumor cells. Finally, not only do AuNC-SNAs deliver more DNA payload to the tumor than their larger counterparts, but they also deliver significantly less gold to off-target organs (**Figure 3.9B**), owing to their high DNA-to-gold ratios.

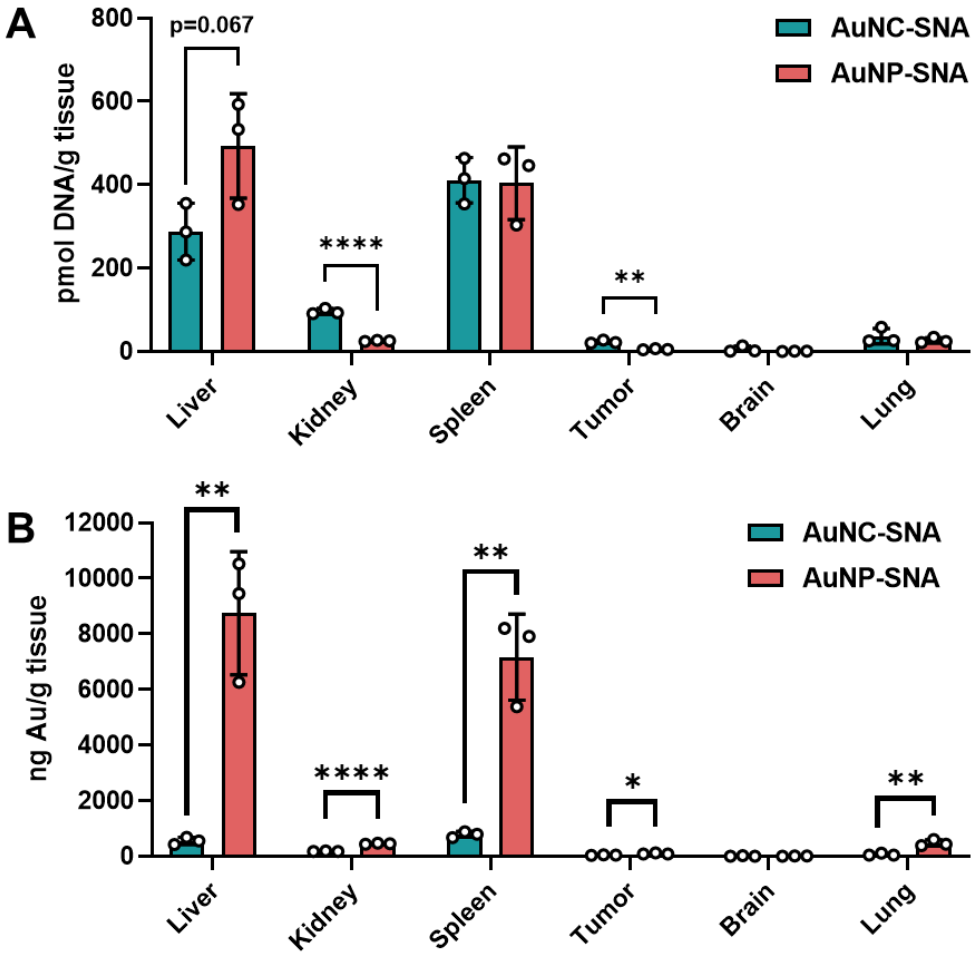

Figure 3.9. Biodistribution of AuNC-SNAs and AuNP-SNAs. Mice with 4T1 tumors were intravenously administered 3 nmol of DNA equivalent of AuNC-SNAs or AuNP-SNAs. Organs were collected at 24 h post-IV injection analyzed for gold content using ICP-MS. (A) Biodistribution of AuNC-SNAs and AuNP-SNAs by DNA. Error bars are SD of 3 biological replicates. (B) Biodistribution of AuNC-SNAs and AuNP-SNAs by gold. Error bars are SD of 3 biological replicates.

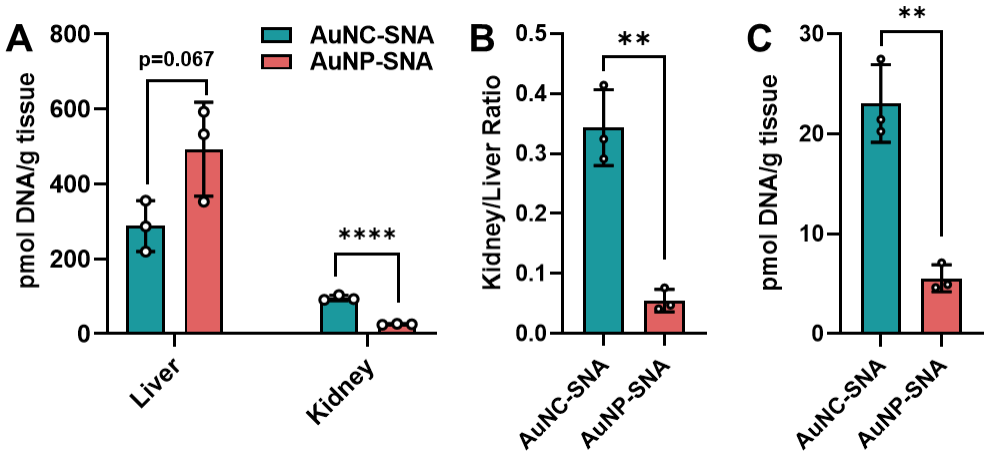

Figure 3.10. SNA accumulation in liver, kidney, and tumor. Mice with 4T1 tumors were intravenously administered 3 nmol of DNA equivalent of AuNC-SNAs or AuNP-SNAs. Organs were collected at 24 h post-IV injection analyzed for gold content using ICP-MS. (A) DNA accumulation from AuNC-SNAs and AuNP-SNAs in the liver and kidney. Error bars are SD of 3 biological replicates. (B) Kidney/liver ratio of DNA accumulation from each SNA. Error bars are SD of 3 biological replicates. (C) Tumor accumulation of DNA from AuNC-SNAs and AuNP-SNAs. Error bars are SD of 3 biological replicates.

3.4. Conclusion

Through these studies, we found that SNA-like biological properties persist down to the sub-10-nanometer length scale *in vivo*, further indicating that the unique properties of SNAs arise from the highly oriented arrangement and surface density of the DNA, rather than the identity of the nanoscale core. Furthermore, AuNC-SNAs possess the favorable characteristics of ultrasmall nanoparticles without their pharmacokinetic drawbacks, providing important insight into the design of maximally effective nanoscale constructs for therapeutic applications. AuNC-SNAs were able to independently enter cells without the use of transfection agents, functioning similarly to larger 10-nm AuNP-SNAs. However, reducing the size of the core led to a significantly increased drug-to-carrier ratio in AuNC-SNAs and the delivery of higher quantities of DNA into cells than AuNP-SNAs. Moreover, AuNC-SNAs exhibited the same advantages of

other ultrasmall nanoparticles (lower off-target organ accumulation, renal clearance) while subverting their disadvantages, instead exhibiting longer circulation in blood and greater tumor accumulation. Thus, we conclude that at the ultrasmall size regime, SNAs possess unique properties that can be leveraged to develop next-generation nanoparticle therapeutics. These findings on the behavior of AuNC-SNAs can be used to inform the design of new types of SNAs and other nanostructures in the ultrasmall regime, such as DNA dendrons.[158]

CHAPTER 4

Next-Generation siRNA-Based Lipid-Core Spherical Nucleic Acids

4.1. Introduction

4.1.1. Prototypical Gold-Core siRNA-SNAs

siRNA is a short, double-stranded RNA molecule that can, in principle, be designed to silence any target gene of interest.[23,25,27] siRNAs have shown tremendous potential as a gene regulation therapeutic, but their widespread clinical use has been restricted by stability and delivery limitations.[40,41,28] For example, siRNAs are rapidly degraded in biological fluids,[35] has unfavorable pharmacokinetics,[36,37] and cannot independently enter cells.[38,39] To overcome these limitations, siRNAs can be radially arranged around a nanoparticle core to form SNAs that impart unique properties distinct from those of linear siRNAs.[81,83] siRNA-SNAs are more resistant to nuclease degradation than linear siRNAs, independently and efficiently enter cells via scavenger receptor-mediated endocytosis, and have longer circulating half-lives that favor delivery to target sites (e.g., tumors).[102,87]

Prototypical siRNA-SNAs consist of thiolated passenger strands attached to a gold nanoparticle core, with guide strands hybridized to the passenger strands.[102] siRNA-SNAs using this architecture have shown therapeutic success in *in vivo* models of impaired wound healing[88] and psoriasis[89] and have progressed to a first-in-human clinical trial for glioblastoma.[87,103] However, this design has several limitations that limit its clinical suitability. First, the hybridized attachment strategy severely limits the number of siRNA duplexes that can be loaded on each SNA. Due to the high charge density near the SNA core, electrostatic repulsion causes the majority of guide strands to dissociate, leaving few siRNA duplexes intact.[105] Recent development of a hairpin-like siRNA attachment strategy that maximizes siRNA duplex loading has solved this problem, albeit it has only been demonstrated on a gold nanoparticle-core siRNA-SNA (siRNA-AuSNA).[131] The second limitation of the prototypical siRNA-SNA design is its

gold nanoparticle core. In particular, gold nanoparticles are known to be cytotoxic at high concentrations,[105,131] poorly eliminated from the body, and non-biodegradable.[110] Thus, there are concerns about their biocompatibility and long-term safety. Conversely, siRNA-SNAs with a core composed of a biocompatible material that is natural, nontoxic, and biodegradable has the potential to overcome many of the limitations of a gold nanoparticle core.

4.1.2. Lipid-Core siRNA-SNAs

Liposomal SNAs (LSNAs) consisting of a liposome core functionalized with DNA have showcased promising potential as a therapeutic platform for the treatment of various cancers and infectious diseases while demonstrating favorable biocompatibility.[94,95,117,128,129,159] Nevertheless, radially orienting siRNA around a liposome core has yet to be performed. Herein, we describe the synthesis and characterization of hairpin-like siRNA-based liposomal SNAs (siRNA-LSNAs) as a proof-of-concept siRNA-SNA platform (**Figure 4.1**). We demonstrate their ability to rapidly enter cells and silence an angiogenesis-promoting gene *in vitro*, with lower cytotoxicity than prototypical gold nanoparticle-core siRNA-SNAs. We then discuss their potential application for treating eye diseases. Finally, we discuss the development of solid lipid nanoparticle (LNP)-core SNAs with enhanced cytosolic delivery of siRNAs. The lipid-based siRNA-SNAs discussed in this work will contribute to the development of next-generation siRNA-SNAs and represent an important step in the advancement of siRNAs toward widespread therapeutic use.

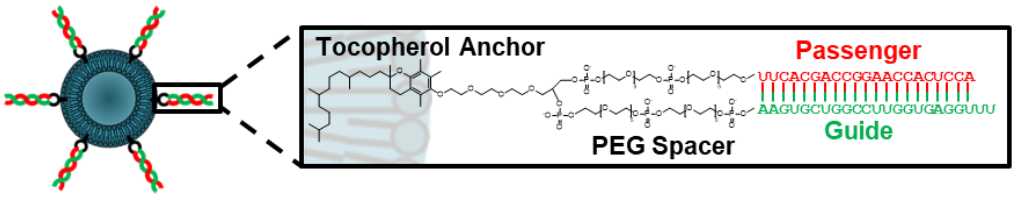

Figure 4.1. Structure of hairpin-like siRNA-LSNAs. Hairpin-like siRNA-LSNAs are composed of a 1,2-dipalmitoyl-sn-glycero-3-phosphocholine (DPPC) core functionalized with hairpin-like siRNAs with a tocopherol anchor.

4.2. Materials and Methods

Oligonucleotide Synthesis. RNA and DNA oligonucleotides were synthesized on a MerMade 12 system (BioAutomation) using 2'-*O*-triisopropylsilyloxymethyl-protected phosphoramidites (ChemGenes). Hairpin-like siRNA consisted of RNA base cyanoethyl phosphoramidites (the guide portion of the strand) (Glen Research), two spacer 18 (18-*O*-dimethyoxytritylhexaethyleneglycol,1-[(2-cyanoethyl)-(*N*,*N*-diisopropyl)] phosphoramidites (Glen Research), a hydrophobic anchor phosphoramidite (the hairpin turn and liposome attachment moiety) (Glen Research), two spacer 18 phosphoramidites, and RNA base cyanoethyl phosphoramidites (the passenger portion of the strand). Tocopherol (single (toc) and double (toc2)) and cholesterol (single (chol) and double (chol2)) phosphoramidites were investigated as the hydrophobic anchor, and a single tocopherol phosphoramidite was selected as the hydrophobic anchor for LSNA synthesis. For AuSNAs, the hairpin-like siRNA contained a dithiol serinol phosphoramidite (Glen Research) in place of the hydrophobic anchor. Hybridized siRNA consisted of separate passenger and guide strands. The passenger strand consisted of RNA base cyanoethyl phosphoramidites, two spacer 18 phosphoramidites, and a tocopherol phosphoramidite as the hydrophobic anchor. The guide strand consisted of RNA base cyanoethyl phosphoramidites. The DNA oligonucleotides that formed the outer shell of the LNP-SNAs consisted of DNA based cyanoethyl phosphoramidites (Glen Research) and a dithiol serinol phosphoramidite. After synthesis, oligonucleotides were deprotected following the manufacturer's protocols (Bioautomation). Deprotected RNA oligonucleotides were purified using high-performance liquid chromatography on a C4 column using 0.1 M triethylammonium acetate and acetonitrile as the solvents. Deprotected DNA oligonucleotides were purified by high-performance liquid chromatography on a C18 column using 0.1 M triethylammonium

acetate and acetonitrile as the solvents. The 5'-DMT group was removed from the purified oligonucleotides via treatment with 20% acetic acid at room temperature for 1 h and extracting 3 times with ethyl acetate. The oligonucleotide solutions were lyophilized and suspended in DNase/RNase-free water. The masses of the oligonucleotides were measured using MALDI-TOF mass spectrometry. Oligonucleotides were mixed with 2',4'-DHAP and dried on a MALDI plate. MALDI-TOF was performed using an Autoflex III Smartbeam MALDI-TOF mass spectrometer. Oligonucleotide concentrations were determined using UV-vis spectroscopy. The oligonucleotide sequences used in this chapter are listed in **Table 4.1**.

Table 4.1. Sequences of oligonucleotides used in this chapter. Uppercase: RNA, lowercase: DNA, red: locked nucleotide, Sp18: spacer 18, toc: tocopherol, chol: cholesterol, NH_2: amine modification, DS: dithiol serinol.

Name	Sequence (5' → 3')
Rat *VEGF* Hairpin Toc	ACCUCACCAAAGCCAGCACAU-$(Sp18)_2$-toc-$(Sp18)_2$-AUGUGCUGGCUUUGGUGAGGUUU
Rat *VEGF* Hairpin Toc2	ACCUCACCAAAGCCAGCACAU-$(Sp18)_2$-$(toc)_2$-$(Sp18)_2$-AUGUGCUGGCUUUGGUGAGGUUU
Rat *VEGF* Hairpin Chol	ACCUCACCAAAGCCAGCACAU-$(Sp18)_2$-chol-$(Sp18)_2$-AUGUGCUGGCUUUGGUGAGGUUU
Rat *VEGF* Hairpin Chol2	ACCUCACCAAAGCCAGCACAU-$(Sp18)_2$-$(chol)_2$-$(Sp18)_2$-AUGUGCUGGCUUUGGUGAGGUUU
Human *VEGF* Hairpin Toc	ACCUCACCAAGGCCAGCACUU-$(Sp18)_2$-toc-$(Sp18)_2$-AAGUGCUGGCCUUGGUGAGGUUU
Human *VEGF* Hairpin Toc Cy5-Labeled	ACCUCACCAAGGCCAGCACUU-$(Sp18)_2$-toc-$(Sp18)_2$-Cy5-AAGUGCUGGCCUUGGUGAGGUUU
Human *VEGF* Passenger Toc	ACCUCACCAAGGCCAGCACUU-$(Sp18)_2$-toc
Human *VEGF* Passenger	ACCUCACCAAGGCCAGCACUU
Human *VEGF* Guide Cy5-Labeled	Cy5-GUGCUGGCCUUGGUGAGGUUU
Nontargeting Hairpin Toc	GGACGAGGACGAGCACUUCUU-$(Sp18)_2$-toc-$(Sp18)_2$-AAGAAGUGCUCGUCCUCGUCCUU
Rat *VEGF* Hairpin DS	ACCUCACCAAAGCCAGCACAU-(Sp18)2-DS-(Sp18)2-AUGUGCUGGCUUUGGUGAGGUUU
Rat *VEGF* Capture Probe	NH_2-$(Sp18)_2$-aaacctcaccaaa
Rat *VEGF* Detector Probe	atgtgctggctt-$(Sp18)_2$-biotin
Luc2 Passenger	GGACGAGGACGAGCACUUCUUtt
Luc2 Guide	GAAGUGCUCGUCCUCGUCCUUtt
Nontargeting Passenger	GCAAGCUGACCCUGAAGUUCAUtt
Nontargeting Guide	GAACUUCAGGGUCAGCUUGCCGtt
LNP-SNA Outer Shell DNA	DS-ttttttttttttttttttt

LSNA Synthesis. A 10 mg thin film of DPPC was prepared by adding 400 μL of 25 mg/mL DPPC in chloroform (Avanti Polar Lipids) to a scintillation vial, evaporating the chloroform under a stream of nitrogen, lyophilizing, then storing under argon at 4 °C. To prepare liposomes, the thin film was rehydrated in 1 mL 1× DPBS, frozen in liquid nitrogen, and sonicated in a 45 °C water bath for 3 h. Liposome size was measured by diluting in 1× DPBS and performing DLS using a Zetasizer (Malvern), while liposome concentration was determined using a phosphatidylcholine (PC) assay kit (Sigma). DPPC liposomes were kept at 45 °C until LSNA synthesis on the same day. siRNAs were duplexed following a previously described hybridization method.[131] To form LSNAs, siRNAs were added to DPPC liposomes at a mole ratio of 30 siRNA duplexes:1 liposome at a final siRNA concentration of 500 nM. Higher siRNA duplex:liposome ratios did not result in any increase in siRNA duplex loading on the LSNA. The siRNA/liposome mixture was vortexed, sonicated 30 s, then incubated with shaking at 45 °C overnight. Unattached oligonucleotides were removed by washing with 1× DPBS 3 times in Amicon Ultra 100K molecular weight cutoff spin filters (MilliporeSigma). The SNAs were stored at 4 °C for up to 1 month.

LSNA Characterization. LSNA formation was confirmed using gel electrophoresis. 50 pmol siRNA equivalent of linear tocopherol-anchor hairpin-like siRNA or hairpin-like siRNA-LSNA was combined with 1 μL of purple gel loading dye (6×) with no SDS (New England Biolabs) and brought up to a volume of 6 μL using 1× DPBS. The samples were run on a 1% agarose gel in 1× tris/borate/EDTA (TBE) on ice at 100 V for 1.5 h. SYBR Gold was used to stain the RNA. The gels were imaged and analyzed using a ChemiDoc MP imaging system (Bio-Rad). LSNA size was measured by diluting in 1× DPBS and performing DLS using a Zetasizer. An OliGreen assay was used to quantify siRNA duplex loading on the hairpin-like siRNA-LSNA. 5 μL of LSNAs

were diluted in 70 μL of 1× DPBS, then mixed with 75 μL of 0.2% Triton X-100 (Sigma) in 1× DPBS to dissociate the liposome core. 25 μL of this mixture was added to 75 μL of 1× DPBS and 100 μL of 0.5% Quanti-iT OliGreen reagent (Invitrogen) in 1× DPBS. The samples were then analyzed in a 96-well black, clear-bottom plate by measuring OliGreen fluorescence (λ_{ex} = 480 nm, λ_{em} = 520 nm) using a BioTek Cytation 5 imaging reader and comparing to a standard curve of hairpin-like siRNA to determine siRNA concentration in the sample. Liposome concentration in the sample was determined using the previously performed PC assay and adjusting the concentration based on the volume before and after synthesis and washing. siRNA duplex loading of the hairpin-like siRNA-LSNA was then calculated by taking the ratio of hairpin-like siRNA concentration to liposome concentration. A PicoGreen assay was used to quantify siRNA duplex loading on the hybridized siRNA-LSNA. 5 μL of LSNAs were combined with 12 μL of RNase A/T1 mix (Thermo) to degrade lone passenger RNA strands, 58 μL of 1× DPBS, and 75 μL of 0.2% Triton X-100 in 1× DPBS to dissociate the liposome core. The mixture was incubated at 37 °C for 10 min to activate the RNase. Next, 25 μL of this mixture was added to 75 μL of 1× DPBS and 100 μL of 0.5% Quanti-iT PicoGreen reagent (Invitrogen) in 1× DPBS. The samples were then analyzed in a 96-well black, clear-bottom plate by measuring PicoGreen fluorescence (λ_{ex} = 480 nm, λ_{em} = 520 nm) using a Cytation 5 imaging multi-mode reader and comparing to a standard curve of hybridized siRNA to determine siRNA concentration in the sample. siRNA duplex loading of the hybridized siRNA-LSNA was then calculated by taking the ratio of hybridized siRNA concentration to liposome concentration.

Flow Cytometry of Human Umbilical Vein Endothelial Cells (HUVECs) to Measure Uptake of LSNAs. HUVECs (ATCC) were grown in Endothelial Cell Growth Medium-2 (EGM-2) (Lonza) containing BulletKit growth factors. For flow cytometry cell uptake studies, HUVECs

were seeded in a 24-well cell culture plate at 40,000 cells/well for 48 h. Cy5-labeled linear siRNAs or hairpin-like siRNA-LSNAs were added to the cells at a concentration of 100 nM siRNA equivalent in EGM-2. At time points of 4 h and 24 h after administration, cells were stained and fixed. Cells were washed with 500 μL of HEPES buffer, then detached using 150 μL Trypsin/EDTA and incubating at 37 °C for 5 min. Cells were transferred to flow cytometry tubes and 200 μL of EGM-2 was added, then the cells were spun down and the supernatant was removed. The cells were resuspended in 100 μL of HEPES buffer and 0.5 μL of blue fluorescent reactive dye (Invitrogen) as a live/dead stain, then incubated for 15 min at room temperature. Next, 600 μL of HEPES buffer was added, then the cells were spun down and the supernatant was removed. The cells were resuspended in 150 μL of fixation buffer (BioLegend) and stored at 4 °C. Flow cytometry was performed using an A3 Symphony flow cytometer (BD Biosciences) with data analysis performed using FlowJo.

Confocal Microscopy of HUVECs to Observe Uptake of LSNAs. HUVECs were seeded in an 8-well slide plate at 40,000 cells/well for 24 h. Cy5-labeled linear siRNA or hairpin-like siRNA-LSNAs were added to the cells at a concentration of 100 nM siRNA equivalent in EGM-2. At 4 h after administration, the cells were washed with 200 μL of 1× DPBS and subsequently fixed with 150 μL of fixation buffer (BioLegend) for 15 min at 4 °C. Cells were then washed with 200 μL of 1× DPBS and subsequently stained for 1 min using 300 nM 4′,6-diamidino-2-phenylindole (DAPI) in 1× DPBS to label cell nuclei. After staining, cells were briefly washed with 200 μL of 1× DPBS and stored in 1× DPBS until imaged. Confocal microscopy was performed using a Zeiss LSM 800 confocal laser scanning microscope.

Cytotoxicity of SNAs. Hairpin-like siRNA-AuSNAs were synthesized and characterized following a previously described method.[131] HUVECs were seeded in a 96-well cell culture plate

at 2,500 cells/well for 24 h. Hairpin-like siRNA-AuSNAs and hairpin-like siRNA-LSNAs in EGM-2 at a range of concentrations were added to the cells for 48 h. The wells were washed with 1× DPBS 3 times to remove dead cells and SNAs that were not internalized by cells. A mixture of 50 μL 1× DPBS and 50 μL of CellTiter-Glo 2.0 reagent (Promega) was added to the wells, and the luminescence was measured using a BioTek Cytation 5 imaging reader. Luminescent readout from ATP concentration was used to indicate live cell count. Cell viability was normalized to cells treated with EGM-2 only.

Tube Formation Assay. Phenol-red free Matrigel basement membrane matrix (Corning) was thawed overnight in the fridge. Next, 75 μL of thawed Matrigel was added to the wells of a pre-cooled 96-well clear cell culture plate on ice using pre-cooled 200 μL pipette tips. The plate was then taken off ice and incubated at room temperature for 10 min, then at 37 °C for 30 min to solidify the Matrigel. For treatments, 30,000 HUVECs were combined with nontargeting hairpin-like siRNA-LSNAs or *VEGF*-targeting hairpin-like siRNA-LSNAs at an siRNA concentration of 250 nM in EGM-2 in a total volume of 75 μL and incubated at 37 °C for 1 h. The treated cells were then added to the Matrigel and kept at 37 °C. Images of cells in Matrigel were captured using an Eclipse Ts2 inverted microscope (Nikon) at 4× magnification at 24 h and 48 h after treatment. Tube formation was analyzed and quantified using ImageJ and the Angiogenesis Analyzer tool.[160]

Biodistribution of Hairpin-like siRNA-AuSNAs in Mouse Eyes. Hairpin-like siRNA-AuSNAs were synthesized at a large scale using the previously described salt-aging method[131] and purified using tangential flow filtration, for a final concentration of 2.4 μM SNAs in 1× DPBS. The biodistribution study was performed on 8–10-week-old male Sprague Dawley rats. Before treatment, rats were anesthetized via an intraperitoneal injection of 10 mg/kg xylazine and 50

mg/kg ketamine. For intravitreal injections, the pupils of both eyes were dilated with 10% phenylephrine and 1% tropicamide, then both eyes were injected with 2 μL of SNAs (0.073 mg of SNAs, 0.48 nmol of siRNA) using a 31-gauge needle 3–4 mm away from the limbus. For subconjunctival injections, both eyes were injected with 20 μL of SNAs (0.73 mg of SNAs, 4.8 nmol of siRNA) using a 31-gauge needle under the conjunctiva. For topical ophthalmic administration, 20 μL of SNAs (0.73 mg of SNAs, 4.8 nmol of siRNA) was administered to both eyes using a precision pipette. The rats were monitored and at 12 h, 1 d, 3 d, or 7 d time points after dosing the rats were euthanized and both eyes and blood samples were collected. The eyes were dissected and the retina, vitreous humor, and sclera were collected. All samples were weighed, then flash frozen and stored at –80 °C until analysis.

Gold Accumulation Analysis of Rat Tissue Samples. Retina, vitreous humor, sclera, and blood samples were digested in HNO_3, HCl, and H_2O_2. The gold concentration in this solution was measured by performing ICP-MS on the acidified samples. ICP-MS was performed on a computer-controlled (QTEGRA software) Thermo iCapQ ICP-MS (Thermo Fisher) operating in STD mode and equipped with a ESI SC-2DX PrepFAST autosampler. Internal standard was added inline using the prepFAST system and consisted of 1 ng/mL of a mixed element solution containing Bi, In, ^{6}Li, Sc, Tb, Y (IV-ICPMS-71D from Inorganic Ventures). Online dilution was also carried out by the prepFAST system and used to generate a calibration curve consisting of 2, 4, 20, 100, and 200 ppb Au. Each sample was acquired using 1 survey run (10 sweeps) and 3 main (peak jumping) runs (40 sweeps). The isotopes selected for analysis were ^{197}Au (for SNA quantification) and ^{89}Y, ^{115}In, ^{159}Tb, and ^{209}Bi (chosen as internal standards for data interpolation and machine stability). Instrument performance was optimized daily through autotuning followed by verification via a performance report (passing manufacturer specifications). The

volume of each tissue sample was calculated by dividing the mass of each sample by the tissue's density.[161–163] The concentration of SNAs in each tissue or blood was calculated by dividing the number of gold nanoparticles in each sample by the initial volume of the tissue or blood sample. The amount of siRNA in the sample was calculated by multiplying the SNA accumulation by the siRNA duplex loading on the SNA.

Hairpin-like siRNA Detection Assay. An aminated capture probe was diluted to 50 nM in coating buffer (10 mM 1-ethyl-3-(3-dimethylaminopropyl)carbodiimide (EDC), 10 mM 1-methylimidazole), then 50 μL was added to the wells of NucleoLink strips (Nunc) that covalently bond to the amine groups, arranged into a plate using a NucleoLink/TopYield frame (Nunc). The NucleoLink strips were sealed with sealing tape (Nunc) and incubated at 50 °C for 18 h. The wells were washed four times by soaking with washing buffer (1× saline-sodium citrate (SSC) buffer (Invitrogen), 0.05% Tween-20 (Sigma)) for 5 min. Nucleic acid detection blocking buffer (Thermo) was pre-heated to 50 °C, then 200 μL was added to each well and incubated at 50 °C for 1 h. The *VEGF*-targeting target hairpin-like siRNA was diluted in NorthernMax prehybridization/hybridization buffer (Thermo Fisher) at a range of concentrations. The biotinylated detection probe was diluted to 1 μM in NorthernMax prehybridization/hybridization buffer, then 30 μL of detection probe was mixed with 30 μL of each target hairpin-like siRNA concentration and heated to 95 °C for 5 min, followed by incubating at 37 °C for 1 h. The NucleoLink strip wells were washed four times by soaking with washing buffer for 5 min. Next, 50 μL of the detection probe/target hairpin-like siRNA mixture was added to the wells and incubated at 37 °C for 1 h. The wells were then washed with washing buffer, three times by soaking at room temperature for 10 min and once by soaking at 50 °C for 10 min. Next, 50 μL of horseradish peroxidase (HRP)-conjugated streptavidin in 10% blocking

buffer was added to the wells and incubated at room temperature for 30 min. The wells were then washed four times with washing buffer. Next, 50 μL of 3,3',5,5'-tetramethylbenzidine (TMB) substrate solution was added to each well and incubated at room temperature for 7 min, followed by adding 50 μL of 0.1 M H_2PO_4 to stop the reaction. Absorbance at 450 nm was measured by a 384 plate reader (SpectraMax) as an indicator of target hairpin-like siRNA detection.

siRNA-LNP-SNA Synthesis. LNPs with encapsulated siRNA were formulated using the ethanol dilution method by combining organic and aqueous components at a volume ratio of 1:3. The organic component contained 15 mM total lipid in ethanol, consisting of mole fractions of 21.5% 1,2-distearoyl-*sn*-glycero-3-phosphocholine (DSPC), 25% cholesterol, 50% D-Lin-MC3-DMA, and 3.5% PEGylated lipid (DSPC-PEG2000-maleimide or 1,2-dioleoyl-*sn*-glycero-3-phosphorethanolamine (DOPC)-PEG2000-maleimide). The aqueous component contained siRNA in 10 nM citrate buffer (pH 4) for a final amine/phosphate (N/P) ratio of 3. The aqueous component was rapidly added to the organic component while shaking using a vortexer. After mixing, LNPs were dialyzed using 3.5K cutoff dialysis membranes to equilibrate buffer overnight. Then, reduced thiolated DNA was added to the LNPs at a mole ratio of 1.1 thiolated DNA:1 maleimide, and the mixture was shaken at room temperature overnight to attach the thiol groups to the maleimides at the ends of the PEGylated lipids.

siRNA-LNP-SNA Characterization. LNP and LNP-SNA size were measured by diluting in 1× DPBS and performing DLS using a Zetasizer. Encapsulation efficiency of siRNA was measured with Quant-iT PicoGreen (Invitrogen) using a previously described method.[116]

siRNA-LNP-SNA Gene Silencing Study. Gene silencing experiments were performed using U-87 MG-Luc2 (ATCC), which stably express luciferase. In a black, clear-bottom 96-well cell culture plate with 12,000 U-87 MG-Luc2 cells per well, LNP-SNAs containing encapsulated

luciferase2 (*Luc2*) or nontargeting siRNA were administered to the cells at a 100 nM siRNA concentration. After 48 h, the wells were washed with 1× DPBS and the luminescence signal was activated using a Bright-Glo Luciferase Assay System (Promega). The luminescence of the cells was measured using a BioTek Cytation 5 imaging reader as an indicator of Luc2 protein expression. Fluorescence was normalized to untreated cells.

Statistics. All statistical analyses were performed using GraphPad Prism. For comparisons between two groups, means were compared using an unpaired, two-tailed t-test. For comparisons between more than two groups, means were compared using an ordinary one-way ANOVA with Tukey's multiple comparison test. P values were multiplicity adjusted to account for multiple comparisons. Cytotoxicity results were fit with a 3-parameter logistic curve using a least-squares fit. The hybridization assay standard curve was fit with a sigmoidal 4-parameter logistic curve using a least-squares fit.

4.3. Results and Discussion

4.3.1. Synthesis and Characterization of Hairpin-like siRNA-LSNAs

Hairpin-like siRNA-LSNAs were synthesized by adding hairpin-like siRNAs with a hydrophobic anchor to a liposome core. To attach the hairpin-like siRNAs to the liposome, a variety of hydrophobic anchors at the turn of the hairpin were investigated, including tocopherol, cholesterol, double tocopherol (two tocopherol phosphoramidites linked together), double cholesterol, and DOPC. To evaluate LSNA formation, linear hairpin-like siRNAs and LSNA formulations were ran through an agarose gel and stained with SYBR Gold to indicate the location of the siRNA. However, only the single tocopherol anchor resulted in successful LSNA formation (**Figure 4.2A**). While free tocopherol hairpin-like siRNAs ran to the bottom of the gel, the much larger LSNAs showed a prominent mobility shift higher in the gel, with excess

unattached siRNA running to the bottom of the gel, similar to previous studies.[95,115] To confirm that the higher band was an LSNA consisting of siRNA attached to a liposome core and not a micelle composed of tocopherol hairpin-like siRNAs, an LSNA containing a rhodamine-labeled lipid was ran through the gel. When analyzing the gel for rhodamine, a band indicating the liposome was present at the same location as the band indicating the siRNA, confirming that the tocopherol anchor hairpin-like siRNAs and liposomes are colocalized in the gel and are indeed an LSNA.

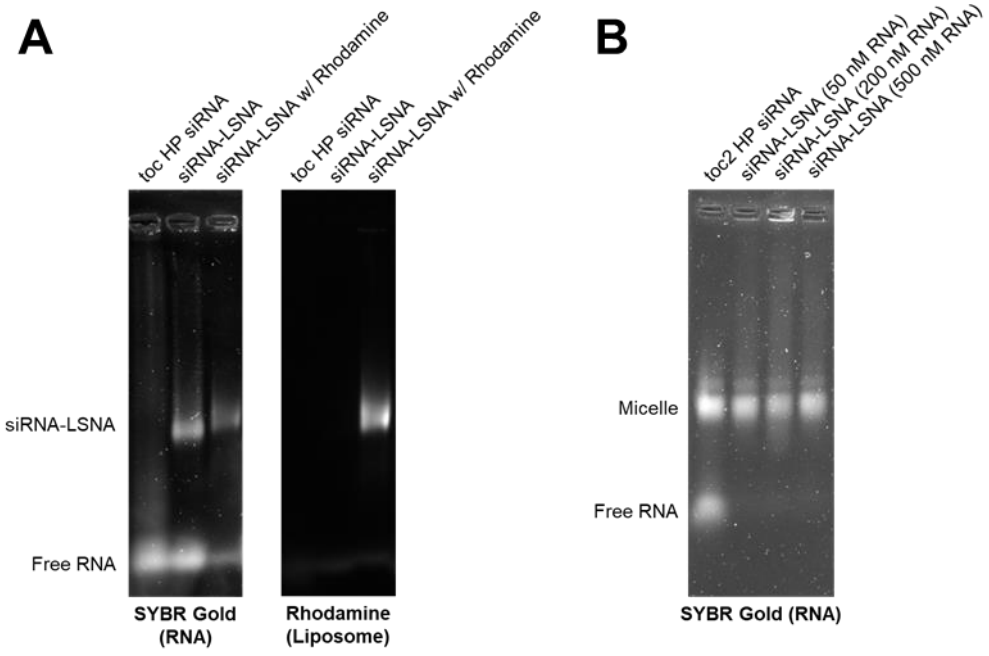

Figure 4.2. Single tocopherol hairpin-like siRNAs form LSNAs while more hydrophobic anchors form micelles. (A) Agarose gel of LSNA formulation with a single tocopherol anchor. (B) Agarose gel of LSNA formulation with a double tocopherol anchor.

While the other anchors are more hydrophobic, which we hypothesized would lead to more stable LSNAs, hairpin-like siRNAs with the more hydrophobic anchors primarily formed micelles instead of LSNAs (**Figure 4.2B**). Dominant micelle formation is likely due to the strong amphiphilicity of these molecules, arising from the high hydrophobicity of the anchor and the

strong hydrophilicity of the 44 RNA nucleotides. While previous findings have demonstrated that more hydrophobic anchors lead to more stable LSNAs, those experiments were done using single-stranded DNA that contained half as many nucleotides as the hairpin-like siRNA.[164] Our results demonstrate that if anchors are too hydrophobic and the nucleic acids are too large (i.e., too hydrophilic), prominent micelle formation can impede the formation of LSNAs. Thus, successful LSNA formation requires an anchor that is sufficiently hydrophobic to stably insert into liposomes but not so hydrophobic to the extent that micelle formation is dominant over LSNA formation. The liposome core was composed of DPPC, since LSNAs with a DPPC core are more stable than LSNAs with cores composed of other lipids.[115]

After synthesis, LSNAs were washed with 1× DPBS using 100K molecular weight cutoff centrifugal filters to remove unattached siRNA. LSNA synthesis was further confirmed via DLS (**Figure 4.3**). As expected, a size increase was observed between bare liposomes and liposomes functionalized with hairpin-like siRNAs, indicating LSNA formation.

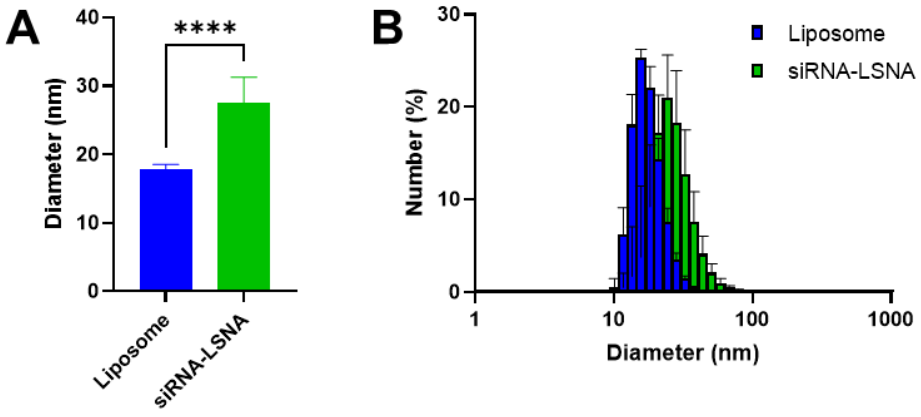

Figure 4.3. DLS analysis shows siRNA-LSNA formation. (A) Diameters of bare liposomes and hairpin-like siRNA-LSNAs. Diameters shown are number means measured by DLS. Error bars are SD of 10 measurements. (B) DLS number distribution of bare liposomes and hairpin-like siRNA-LSNAs. Error bars are SD of 10 measurements.

The amount of siRNA duplexes on the LSNA was quantified using an OliGreen assay (**Figure 4.4**). Hairpin-like siRNA-LSNAs had an average of 29 siRNA duplexes per LSNA, with a surface loading density of 3.7 pmol/cm^2. The loading density of the hairpin-like siRNA-LSNAs was compared with that of LSNAs containing siRNAs attached via the prototypical hybridized architecture. Interestingly, it was found that the hairpin-like architecture enables a significantly higher siRNA duplex loading than the hybridized architecture for siRNA-LSNAs (29 duplexes/particle vs. 11 duplexes/particle, respectively), similar to the increase observed with siRNA-AuSNAs.[131] The hybridized siRNA-LSNAs likely suffer from lower duplex loading due to the high negative charge density from the siRNA near the core causing the majority of guide strands to dissociate from the SNA.[105] The hairpin-like architecture covalently attaches the passenger and guide strand to each other, preventing guide strand dissociation and enabling higher duplex loading on the SNA. This finding demonstrates that the ability of the hairpin-like architecture to increase siRNA duplex loading is not limited to siRNA-AuSNAs, but can be applied to other cores as well. With the advantage of biocompatibility, hairpin-like siRNA-LSNAs are a promising next-generation siRNA-SNA.

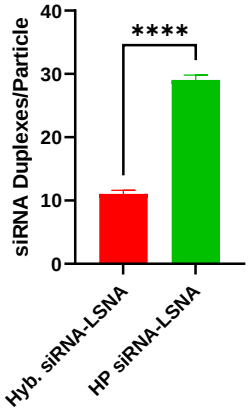

Figure 4.4. Hairpin-like design increases duplex loading of siRNA-LSNAs. siRNA duplex loading on LSNAs using hybridized and hairpin-like architecture. Error bars are SD of 3 measurements.

4.3.2. Hairpin-like siRNA-LSNAs Efficiently Enter Cells

To our knowledge, this is the first demonstration of an siRNA-SNA with a liposome core. Thus, it is necessary to confirm that the hairpin-like siRNA-LSNAs exhibit the important SNA property of independently entering cells. HUVECs were treated with Cy5-labeled linear siRNA and Cy5-labeled hairpin-like siRNA-LSNAs. Flow cytometry analysis revealed that the LSNAs had accumulated in the cells much more efficiently than linear siRNAs at both 4 h and 24 h timepoints (**Figure 4.5A**). This finding was confirmed with confocal microscopy, which showed that LSNAs prominently accumulate in cells while linear siRNAs had no observable entry (**Figure 4.5B**). Thus, hairpin-like siRNA-LSNAs retain the property of independently entering cells.

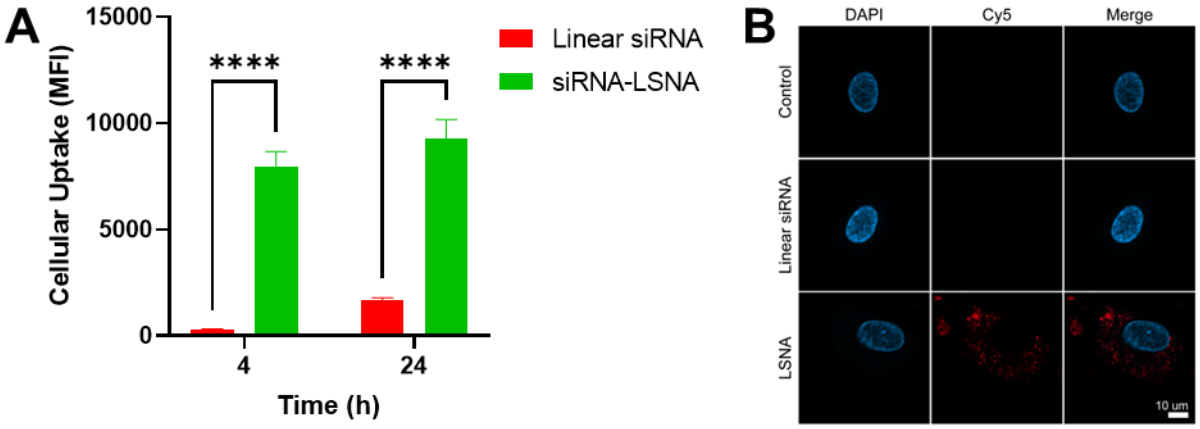

Figure 4.5. Hairpin-like siRNA-LSNAs independently enter cells. (A) Hairpin-like siRNA-LSNAs efficiently enter HUVECs in comparison to linear siRNAs, as measured by flow cytometry. Error bars are SD of 3 biological replicates. (B) Confocal microscopy images of Cy5-labeled linear siRNAs and hairpin-like siRNA-LSNAs internalized in HUVECs (blue: DAPI stain indicating nucleus, red: Cy5 indicating siRNA).

In addition to concerns about their long-term safety, siRNA-AuSNAs are cytotoxic at high concentrations.[105,131] As a test of the biocompatibility of siRNA-LSNAs compared to siRNA-AuSNAs, HUVECs were treated with increasing concentrations of hairpin-like siRNA-

SNAs containing either core for 48 h and assessed for cell viability (**Figure 4.6A**). The LD_{50} of siRNA-LSNAs was higher than that of siRNA-AuSNAs, demonstrating that they are less cytotoxic (**Figure 4.6B**). The lower toxicity of siRNA-LSNAs is an example of their improved biocompatibility compared to siRNA-AuSNAs.

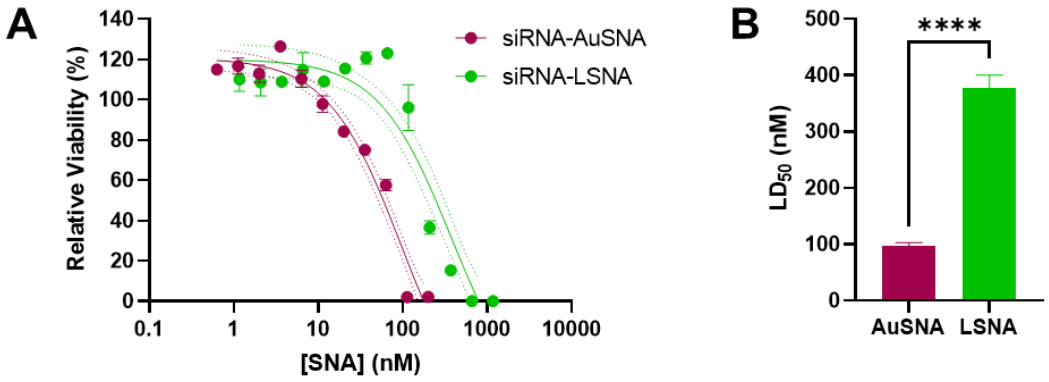

Figure 4.6. Liposome-core siRNA-SNAs are less toxic than gold-core siRNA-SNAs. (A) Cytotoxicity of hairpin-like siRNA-LSNAs and hairpin-like siRNA-AuSNAs. Dotted lines are 95% CI. Error bars are SD of 3 biological replicates. (B) LD50 of hairpin-like siRNA-LSNAs and hairpin-like siRNA-AuSNAs, derived from curves in (A). Error bars are SD of 3 biological replicates.

4.3.3. Hairpin-like siRNA-LSNAs Demonstrate Biological Activity *in Vitro*

The hairpin-like architecture has been previously demonstrated to have no detrimental effect on siRNA gene silencing activity when compared to the hybridized architecture.[131] We sought to investigate the gene silencing activity of hairpin-like siRNA-LSNAs in 2.5-D cell culture using a tube formation assay. Specifically, hairpin-like siRNA-LSNAs were designed to inhibit angiogenesis, as excessive blood vessel formation is a hallmark of eye diseases and cancers, making it an attractive target for silencing.[165,166] The siRNA sequence was designed to target *VEGF*, a key regulator of angiogenesis. As an *in vitro* model of capillary blood vessels, HUVECs were incubated in Matrigel basement membrane matrix with the growth factors

necessary to induce angiogenesis. Under these conditions, HUVECs will form long, branching, interconnected tubes that resemble a network of capillaries. HUVECs with reduced *VEGF* expression will not form tubes, but rather remain as rounded cells.

HUVECs were treated with nontargeting or *VEGF*-targeting hairpin-like siRNA-LSNAs, then embedded in Matrigel. Tube formation was analyzed at 24 h and 48 h after treatment via light microscopy (**Figure 4.7**). Untreated HUVECs and HUVECs treated with nontargeting SNAs showed an extensive network of tubes at both time points, indicating prevalent angiogenesis. However, HUVECs treated with *VEGF*-targeting SNAs showed dramatically reduced tube formation, with nearly complete inhibition of angiogenesis at the 48 h time point, indicating successful *VEGF* silencing.

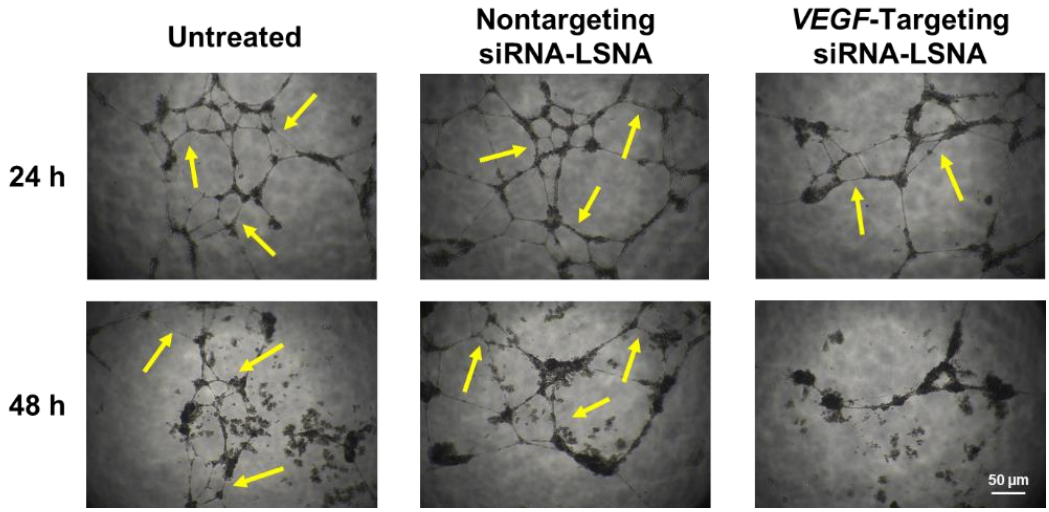

Figure 4.7. *VEGF*-targeting siRNA-LSNAs inhibit angiogenesis *in vitro*. HUVECs were treated with siRNA-LSNAs and images were captured at 24 h and 48 h after treatment using a light microscope. Yellow arrows point to capillary-like tubes.

The degree of tube formation can be quantified via ImageJ's Angiogenesis Analyzer tool, and it was found that treatment with *VEGF*-targeting SNAs reduced tube formation four-fold (**Figure 4.8**). Thus, hairpin-like siRNA-LSNAs demonstrate sequence-specific silencing that

results in an observable phenotypic change. Due to their biocompatibility, transparency, and ability to inhibit angiogenesis, hairpin-like siRNA-LSNAs have particular potential as a treatment for eye diseases such as macular degeneration and diabetic retinopathy as well as cancers.

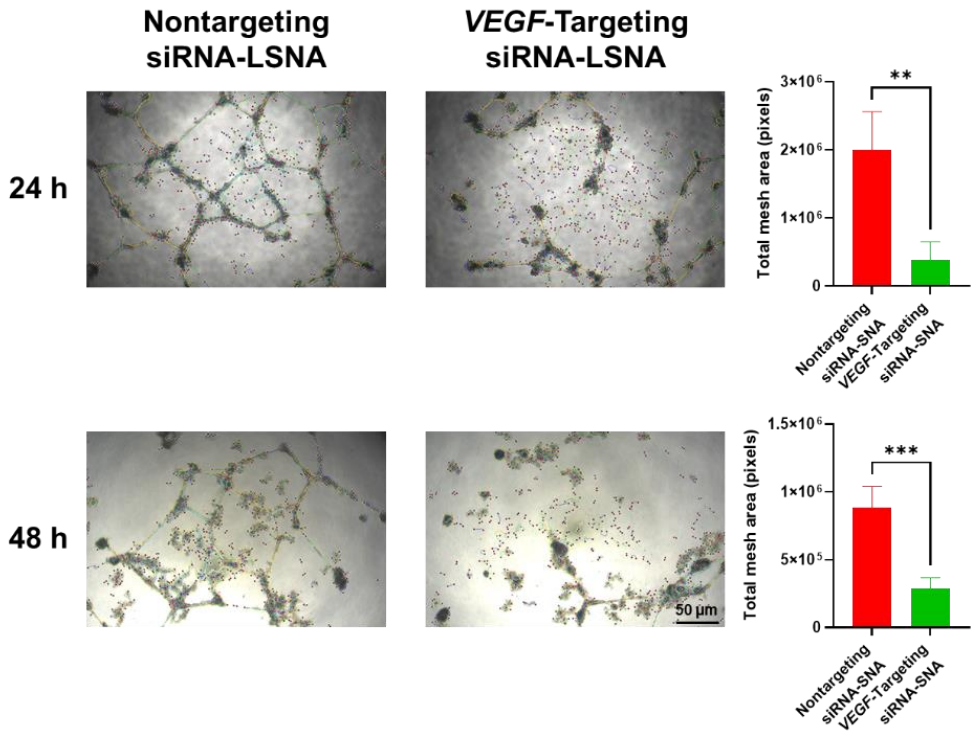

Figure 4.8. Quantification of angiogenesis inhibition by *VEGF*-targeting siRNA-LSNAs. Images were captured at 24 h and 48 h after treatment using a light microscope. Angiogenesis was quantified using ImageJ's Angiogenesis Analyzer tool. Error bars are SD of 4 biological replicates.

4.3.4. SNAs Efficiently Transport Through the Eye

Given the SNA's ability to inhibit angiogenesis and its previously observed favorable transport properties,[86–89] we investigated if SNAs could efficiently transport through the eye to function as a therapeutic for eye diseases. Wet age-related macular degeneration (AMD), diabetic retinopathy, and macular edema are retinal diseases characterized by abnormal choroidal

neovascularization (the aberrant formation and leakage of blood vessels at in the posterior of the eye).[167] The prognosis in patients with advanced disease progression can be blindness. Due to the eye's protective barriers and dearth of active transport mechanisms, current treatment options for the posterior of the eye are primarily limited to repeated intravitreal injections of corticosteroids, anti-angiogenic antibodies, or other drugs using a needle through front of the eye.[168,169] Patient compliance is low (60% for 1 year) for intravitreal injections due to fear, discomfort, and complications.[170] Intravitreal injections are invasive procedures that carry the risks of endophthalmitis, intraocular inflammation, retinal detachment, and hemorrhage, and therefore require monitoring after each injection.[171] *VEGF*-targeting siRNA-SNAs could serve as a promising alternative to currently used eye therapeutics for inhibiting choroidal neovascularization. Nucleic acid drugs in general have shown promise as an ocular nanomedicine featuring efficient delivery and therapeutic activity and a select few have been granted FDA approval.[172,173] The therapeutic effect of each siRNA-SNA dose could be longer lasting than current therapeutics, since mRNA degradation typically yields longer periods of protein reduction than antibody inhibition, the division rate of retinal cells is slow, and the hairpin-like architecture enables longer lasting gene silencing than other siRNA architectures, allowing for less frequent dosing.[174,131] Additionally, the ability of SNAs to transport across difficult-to-cross biological barriers suggests that they may be able to be delivered through less invasive routes than intravitreal administration.[86–89]

We analyzed the delivery of hairpin-like siRNA-SNAs in rat eyes via three routes of administration: intravitreal injection, subconjunctival injection, and topical administration (**Figure 4.9A**). Intravitreal administration consists of inserting a needle through the sclera to deliver the drug. It is the most direct method of delivery to the inside and back of the eye, but it

can have many complications and has low patient compliance due to discomfort. Subconjunctival injection consists of injecting into the subconjunctival tissue below the eye; it is less invasive than an intravitreal injection, but has lower efficiency of delivery into the eye and can be affected by conjunctival circulation. Topical administration consists of applying a drug to the surface of the eye, usually via eye drops. It is easy to perform, can be performed by the patient at home, is noninvasive, and has high patient compliance. However, it suffers from low bioavailability due to the strong barriers of the eye and rapid clearance by tears and blinking.[168,169]

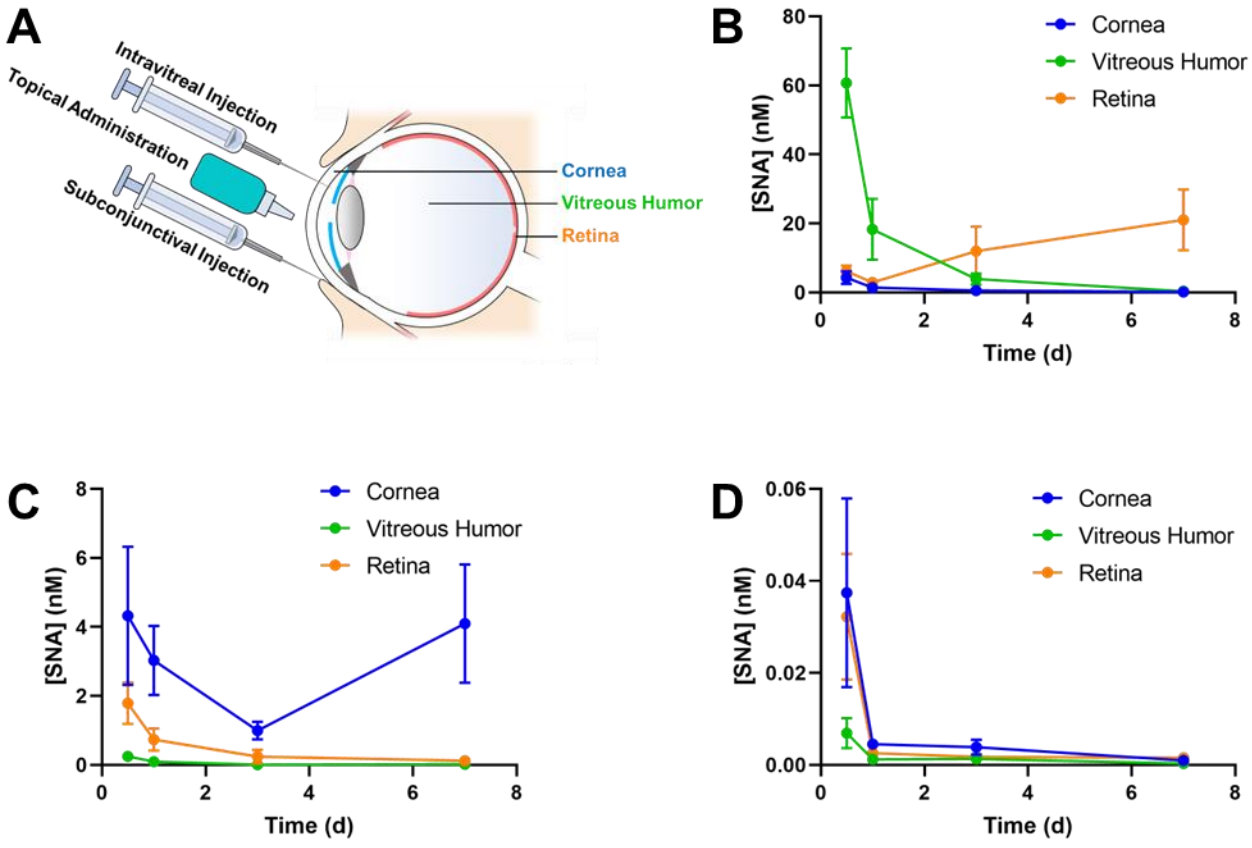

Figure 4.9. Biodistribution of hairpin-like siRNA-SNAs in the eye via different administration routes. (A) Diagram of administration routes and eye components analyzed, and SNA accumulation following (B) intravitreal injection, (C) subconjunctival injection, and (D) topical administration. Error bars are SD of 4–8 biological replicates.

Hairpin-like siRNA-SNAs with a 13-nm gold nanoparticle core were used for this initial pharmacokinetic study since they are easy to detect. Biodistribution analysis of AuSNAs is easy to perform since gold can be sensitively detected in tissue via ICP-MS. SNAs were administered to both eyes of Sprague Dawley rats via intravitreal injection, subconjunctival injection, or topical administration. Rats were then sacrificed at 12 hours, 1 day, 3 days, or 7 days after administration. Eyes were dissected and cornea, retina, vitreous humor, and plasma were collected for SNA biodistribution analysis. The tissues were dissolved in 2% HCl, 2% HNO_3 and gold content was measured via ICP-MS.

As expected, intravitreal injection (**Figure 4.9B**) had the highest delivery to the interior and back of the eye. Upon initial injection most of the SNAs were in the vitreous humor, then transported to the retina over time. Subconjunctival injection (**Figure 4.9C**) mostly resulted in efficient delivery to the cornea, but a therapeutically relevant amount of SNAs still managed to reach the retina (siRNA-SNAs have shown gene silencing activity at SNA concentrations as low as 50 pM).[86] Topical administration (**Figure 4.9D**) did not result in significant delivery to any component of the eye, likely due to washing away by tears and a lack of penetration through the sclera. These results demonstrate that subconjunctival administration of SNAs could be a promising alternative to intravitreal injection for treating retinal diseases such as wet AMD, diabetic retinopathy, and macular edema.[175]

This initial experiment used a hairpin-like siRNA-AuSNA as an easy-to-detect representative for studying SNA transport through the eye, but it is ultimately not suitable as a therapeutic construct for ocular diseases in this form. Gold is not biocompatible, would accumulate in the eye, and is opaque and thus would obstruct vision. An LSNA would be the likely therapeutic construct due to its biocompatibility and transparency. Specifically, the

hairpin-like siRNA-LSNA with a 20 nm DPPC liposome core is ideal for this application due to its stability and small size. However, sensitively detecting hairpin-like siRNA-LSNAs in tissue is challenging.

4.3.5. Hybridization Assay for Detecting Hairpin-like siRNA in Tissue

AuSNAs are easy to detect in tissue, since gold can be measured by ICP-MS, and thus they were useful for the initial study of SNA delivery in the eye. However, liposomes cannot be easily detected in tissues due to the abundance of lipids in cell membranes, so an alternative detection method must be utilized for analyzing LSNA biodistribution. One strategy is to dye-label the siRNA, but this could affect the transport and gene silencing activity of the SNA, and it is also likely that the dye could be removed from the intact siRNA due to degradation and thus not be an accurate indicator of siRNA-LSNA localization. In contrast, hybridization assays are highly sensitive and directly detect the unmodified target oligonucleotide.[176] Thus, we elected to use a hybridization assay to detect unlabeled intact hairpin-like siRNA in the tissue.

We developed a hybridization assay similar in design to an enzyme-linked immunosorbent assay (ELISA). Following RNA extraction from the tissue, the hairpin-like siRNA is hybridized to a capture probe for immobilization and a detection probe for signaling. A unique advantage of the hairpin-like siRNA is that the entire siRNA duplex can be detected using a hybridization assay in this format, since it consists of a single intact RNA strand. Other architectures such as hybridized or doubly-thiolated siRNA consist of two separate strands and thus only a single strand could be detected; there would be no way to specifically detect the therapeutically active siRNA duplex.

There were two important considerations when designing the detector and capture probes for this assay (**Figure 4.10A**). First, the probes cannot be complementary to each other, or else

they will hybridize and produce a signal regardless of the presence of the target hairpin-like siRNA. If the detector probe was complementary to the entirety of one strand of the hairpin (e.g., the passenger strand) and the capture probe was complementary to the entirety of the other strand (e.g., the guide strand), then the probes would be complementary to each other. To avoid this, each probe is only half the length of an siRNA strand and binds to a portion of the hairpin such that the probe sequences are not complementary. The second consideration is that the two strands of the open hairpin must hybridize to the probes more favorably than to each other. Since the two strands of the hairpin-like siRNA are complementary, they can bind to each other, and since the two strands have a greater length of sequence complementarity with each other than with the shorter probes, they will more favorably bind to each other than probes composed of unmodified DNA. To ensure that the hairpin will bind more favorably to the probes than itself, we incorporated several locked nucleic acid (LNA) nucleotides within the probes to increase the melting temperature of the probe-hairpin duplexes. With the final probe designs, the capture probe/hairpin duplex and the detector probe/hairpin duplex both have higher melting temperatures than the self-hybridized hairpin-like siRNA duplex.

For the hybridization detection assay (**Figure 4.10B**), the target hairpin-like siRNA is heated to 95 °C to denature it and make it available to bind to the probes. The biotinylated detector probe is added to the solution, which is cooled to 37 °C to facilitate binding of the detector probe to the hairpin-like siRNA. The hybridized hairpin-like siRNA-detector probe is added to a Nunc NucleoLink plate with aminated capture probes covalently bound to its surface. The mixture is incubated at 37 °C to facilitate binding of the hairpin-like siRNA to the capture probe, then unbound nucleic acids are washed away. Streptavidin-HRP is then added, and the streptavidin binds to the biotin on the detector probe. Finally, TMB is added and reacts with the

HRP to form a diimine. The reaction is halted after 7 min by the addition of dihydrogen phosphate, causing the solution to turn yellow. The optical density at 450 nm is a readout of the amount of target hairpin-like siRNA in the solution (**Figure 4.10C**).

Initial experiments consisting of using the hybridization assay to detect the hairpin-like siRNA in solution revealed a limit of detection of 20 ng/mL (1.28 nM) siRNA. Assuming that LSNAs will have similar a biodistribution profile to AuSNAs, we estimate that subconjunctivally injected LSNAs will accumulate in the retina at a concentration of 2 nM SNA. Since hairpin-like siRNA-LSNAs have a loading density of 29 siRNA/SNA, it can be estimated that around 60 nM siRNA will be accumulated in the retina tissue. This is well above the limit of detection and falls within the dynamic range of the hybridization assay, and any concentrations well above the dynamic range can easily be diluted to fall within it. Thus, this hybridization assay is sensitive enough to detect siRNA biodistribution in eye tissues. Current efforts are focused on optimizing the method for extracting siRNA from tissues with consistent efficiency to accurately quantify the amount of target hairpin-like siRNA in the tissue using this assay. Following the optimization of this hybridization assay, it will be possible to sensitively analyze the biodistribution of hairpin-like siRNA-LSNAs in eye tissues.

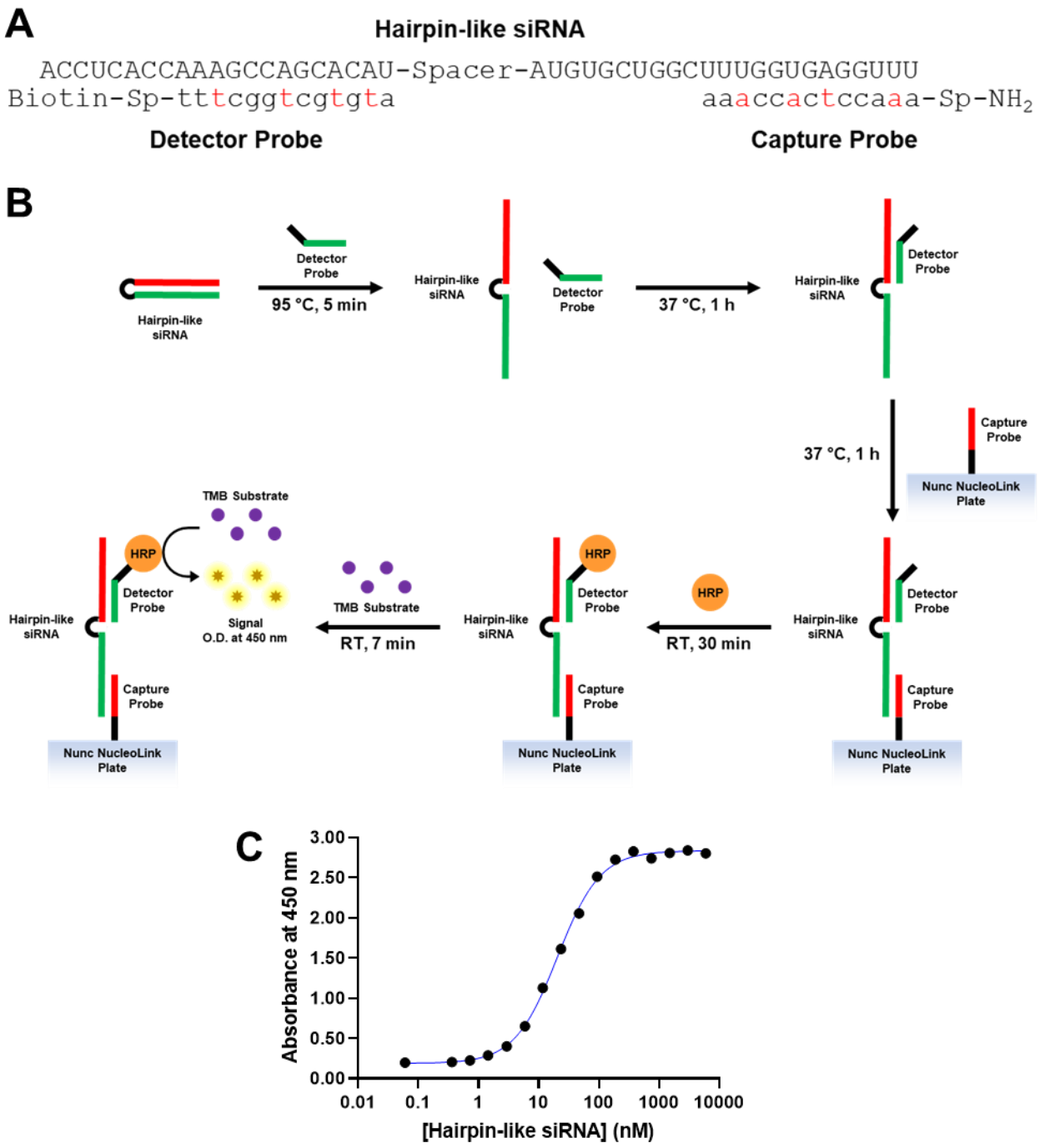

Figure 4.10. Hybridization detection assay. (A) Target hairpin-like siRNA, detector probe, and capture probe designs. Uppercase: RNA, lowercase: DNA, red lowercase: LNA. (B) Hybridization detection assay. (C) Standard curve of detection of target hairpin-like siRNA using hybridization detection assay.

4.3.6. Solid Lipid Nanoparticle-Core siRNA-SNAs Achieve Efficient Gene Silencing

Inefficient cytosolic delivery is a major bottleneck for most nanoparticle-based drugs that rely on endocytosis to enter cells, including siRNA-SNAs. While some siRNA-SNAs efficiently enter the cytosol to induce gene silencing, including the *VEGF*-targeting hairpin-like siRNA-LSNA developed in this chapter, others remain trapped in the endosome, indicating a sequence dependency on endosomal escape. Thus, while *VEGF*-targeting hairpin-like siRNA-LSNAs are well-suited for treating eye diseases characterized by excessive blood vessel formation, a structural change to the SNA that significantly improves its cytosolic delivery would greatly benefit its application to other disease targets.

To improve cytosolic delivery, a lipid-based core different from hollow liposomes has been developed. SNAs composed of a solid LNP core with encapsulated therapeutic nucleic acids and an outer shell of radially arranged DNA demonstrate efficient cytosolic delivery of the encapsulated cargo (**Figure 4.11**).[116] The LNP core contains ionizable lipids that become positively charged at endosomal pH and promote cytosolic delivery of the encapsulated cargo, such that LNP-core SNAs (LNP-SNAs) containing encapsulated siRNA reduce the siRNA concentration necessary to silence mRNA by two orders of magnitude in comparison with hollow liposome-core siRNA-SNAs. Additionally, the outer shell of DNA on LNP-SNAs provides several advantages in comparison to bare LNPs: LNP-SNAs have more efficient cellular uptake than bare LNPs leading to more potent gene silencing, and LNP-SNAs can accumulate in organs such as the spleen while bare LNPs are often limited to liver accumulation.[34]

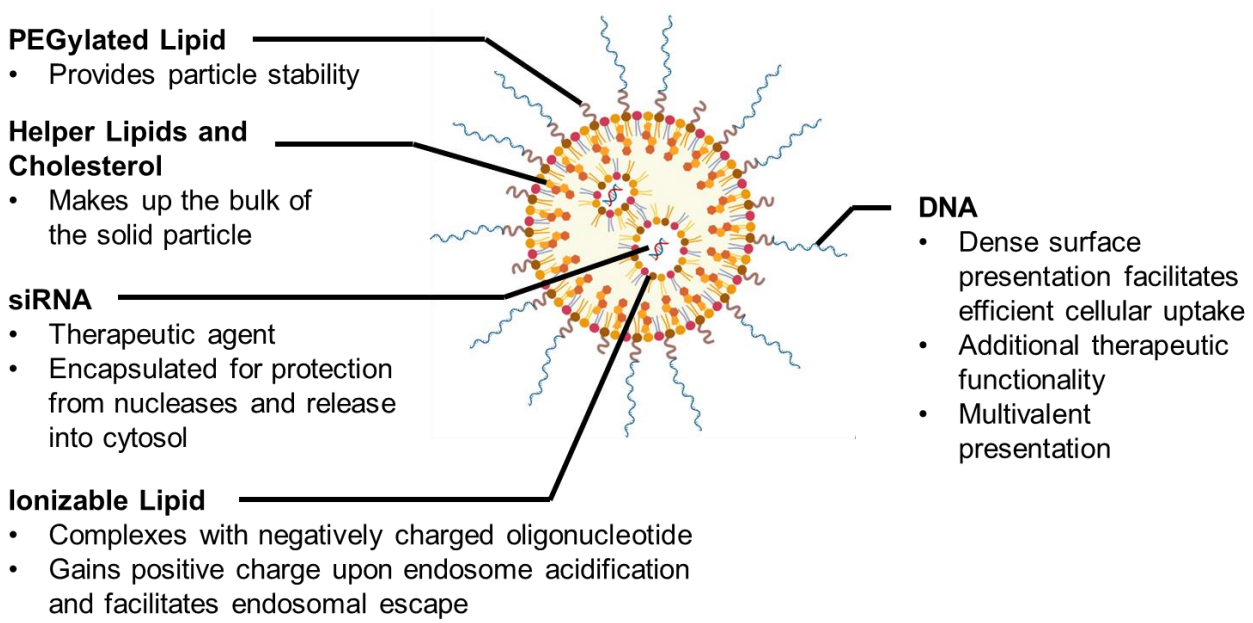

Figure 4.11. Structure of LNP-SNAs. LNP-SNAs consist of an LNP core with encapsulated nucleic acids and an outer shell of nucleic acids. LNP-SNA image created by Alex Anderson.

With the goal of further developing LNP-SNAs as a next-generation SNA that can efficiently delivery siRNA, we explored several compositions and compared their gene silencing activity (**Figure 4.12**). LNP-SNAs with DSPC and DOPC as the PEGylated lipid both achieved greater silencing than bare LNPs containing the same PEGylated lipids, likely due to the greater internalization enabled by the nucleic acid shell. Additionally, LNP-SNAs with DOPC had greater gene silencing activity than LNP-SNAs with DSPC. This is likely due to the fact that DOPC has a lower melting temperature than DSPC (–17 °C vs. 55 °C, respectively), reducing the stability of the LNP and enhancing the release of siRNA into the cytosol. Thus, the structure of the LNP-SNA has a strong effect on its performance. Ongoing work is focused on exploring additional structures and imparting the outer nucleic acids with therapeutic functionality to create a multifunctional LNP-SNA.

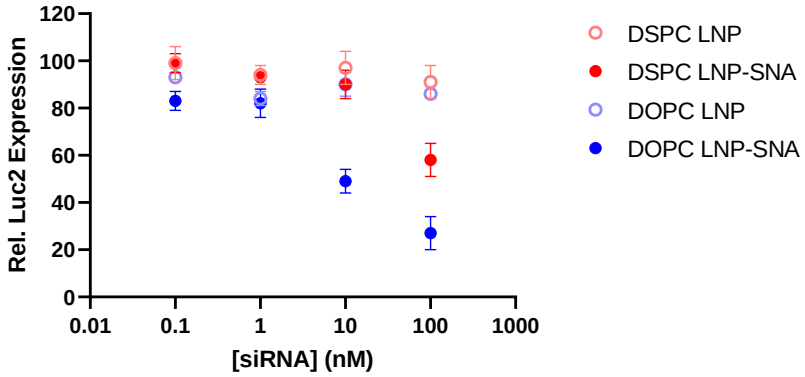

Figure 4.12. Gene silencing activity of LNP-SNAs and bare LNPs containing different PEGylated lipids. LNP-SNAs with DOPC outperformed LNP-SNAs with DSPC, and both LNP-SNAs outperformed bare LNPs. Error bars are SD of 3 biological replicates.

4.4. Conclusion

These results demonstrate the benefits of utilizing lipid-based cores in the development of next-generation siRNA-SNAs. Hairpin-like siRNA-LSNAs are more biocompatible than siRNA-AuSNAs and feature efficient cellular uptake and effective gene silencing, while LNP-SNAs display enhanced cytosolic delivery of siRNA. Structures such as the hairpin-like attachment architecture, hydrophobic tocopherol anchor, stable DPPC liposome core, and biocompatible lipid core materials were utilized to form these next-generation siRNA-SNAs, demonstrating that a toolkit of structural features can be combined for a synergistic benefit. The antiangiogenic next-generation siRNA-SNAs introduced in this chapter could potentially serve as promising therapeutics for eye diseases and cancers. The development of next-generation siRNA-SNAs is an important step in the progress of siRNAs toward widespread clinical use.

CHAPTER 5

Summary and Future Work

5.1. Summary

Nucleic acid therapeutics have the potential to radically change the strategy for treating diseases by offering intentionally designed, specific drugs for a broad range of conditions. Nucleic acids can be precisely designed to interact with disease-associated genes and alter, silence, or eliminate them. siRNAs are an especially promising nucleic acid therapeutic, since they can potently and specifically silence any gene of interest and thus can be designed to silence a wide range of disease-associated overexpressed genes. However, stability and delivery limitations have prevented siRNAs from reaching widespread clinical use.

siRNA-SNAs have beneficial properties that overcome these limitations: they exhibit resistance to nuclease degradation, have favorable pharmacokinetics, and independently enter cells. However, the biological properties of prototypical siRNA-SNAs are restricted by their structure. siRNA-SNAs composed of a ~13-nm gold nanoparticle core functionalized with hybridized siRNA are limited in structural stability, nuclease resistance, biocompatibility, pharmacokinetics, cellular uptake, cytosolic delivery, and ultimately therapeutic activity. We aimed to improve these biological properties by modifying the siRNA-SNA structure. By changing the siRNA-SNA attachment strategy, size, and core composition, we were able to markedly improve each of its biological properties and its overall therapeutic suitability.

First, we developed a hairpin-like architecture to attach siRNA to the nanoparticle core to prevent the guide strand dissociation that occurs with the prototypical hybridized attachment architecture. By attaching both strands of the siRNA with a covalent bond, the hairpin-like design significantly improves the structural stability of the siRNA-SNA and leads to a fourfold increase in siRNA duplex loading. This in turn enhances serum nuclease resistance, biocompatibility, cellular uptake, calcium-associated cytosolic delivery, and gene silencing

durability of the siRNA-SNA. By simply altering the architecture through which the siRNA is attached to a 13-nm gold nanoparticle core and observing the changes in SNA behavior, this work demonstrates how a small structural change can significantly alter the siRNA-SNA's therapeutic suitability. Interestingly, this work also demonstrates that there is an order to biological properties: by focusing on improving the "upstream" property of structural stability, the hairpin-like architecture ended up significantly improving many "downstream" properties, including therapeutic activity. This perspective can be utilized by other researchers when developing therapeutic constructs to decide which properties to prioritize for the greatest improvement in efficacy.

Next, we investigated the effect of size on SNA behavior. We compared the *in vitro* and *in vivo* behavior of SNAs containing either a 10-nm AuNP core or an ultrasmall 1.4-nm AuNC core and found substantial differences. The AuNC-SNA exhibited a greater drug-to-carrier ratio, enhanced cellular uptake, extended circulation in blood, possible renal clearance, and increased tumor accumulation compared to the larger AuNP-SNA. The AuNC-SNA demonstrates advantageous biological properties that can be harnessed at the ultrasmall scale.

Finally, we developed lipid-core next-generation siRNA-SNAs to serve as more biocompatible constructs than gold-core siRNA-SNAs. By utilizing highly stable hairpin-like siRNAs and DPPC liposomes, we constructed hairpin-like siRNA-LSNAs that exhibit efficient cellular uptake, biocompatibility, and antiangiogenic gene silencing. We explored their application as an ocular nanomedicine by observing efficient transport of SNAs through the eye by multiple administration routes and developing a method of directly detecting hairpin-like siRNA in tissue. We also investigated LNP-SNAs as method of enhancing cytosolic delivery of siRNA and found that they achieved more potent gene silencing than bare LNPs. The lipid-based

next-generation siRNA-SNAs that we have developed are well suited for *in vivo* applications and will advance siRNA toward therapeutic use.

Overall, this work demonstrates the power of structural control by showing how advances to the siRNA-SNA structure can substantially improve its biological properties and ultimately its therapeutic suitability. These improvements to the prototypical siRNA-SNA structure have unlocked its potential as a compelling therapeutic candidate. Combined, these structural features form a toolkit that can be harnessed when developing next-generation siRNA-SNAs for therapeutic applications. Each of the structural features described in this work can be utilized to enhance siRNA-SNAs for specific therapeutic contexts, depending on which biological properties are most critical to meet the needs of the application. Additionally, while this dissertation primarily focuses on improving siRNA-SNAs, many of the structure-function relationships described herein will apply to SNAs composed of other oligonucleotides as well. These improvements, as well as future ones yet to be characterized, will be essential in the development of next-generation SNAs, an important step in progressing siRNAs to widespread clinical use.

5.2. Future Work

5.2.1. Mechanistic Insights and Applications of Ultrasmall SNAs

In Chapter 3, we observed that ultrasmall SNAs have greater cellular uptake, longer circulation in blood, possible renal clearance, and greater tumor accumulation than larger gold nanoparticle-core SNAs. While these observations are useful, we would benefit from a more thorough mechanistic understanding of why the decrease in SNA size leads to these changes in properties. This fuller understanding will be helpful for designing and optimizing SNA size for specific applications. We reasoned that AuNC-SNAs had greater cellular uptake than AuNP-

SNAs because they have a greater oligonucleotide surface density, which has been previously shown to enhance cellular uptake.[100] The mechanism behind this phenomenon is not well understood, but it is likely due to altered interactions with scavenger receptors. Measuring the binding strength of SNAs of different sizes and surface densities to scavenger receptors would provide a better understanding of the driver of the observed enhanced cellular uptake. We hypothesized that AuNC-SNAs had longer circulation in blood due to evasion of mononuclear phagocyte system (MPS) cells, but we will further investigate this by comparing the interactions and uptake of SNAs of different sizes with MPS cells *in vitro*. To more thoroughly investigate the renal clearance of the AuNC-SNAs, an analysis of the mice's urine will reveal the magnitude and kinetics of renal clearance. Finally, to gain a greater understanding of the tumor accumulation of AuNC-SNAs, more sensitive imaging techniques can be used to observe SNA infiltration into the tumor tissue.

There are several applications of ultrasmall SNAs that could take advantage of its properties. Ultrasmall SNAs containing siRNA or immunostimulatory DNA could function well as cancer therapeutics due to their extended circulation time, enhanced tumor accumulation, efficient cellular uptake, and renal clearance. Ultrasmall SNAs containing aptamers could be designed as a diagnostic sensor; for example, after injection of aptamer ultrasmall SNAs, they will bind to their target in the bloodstream and display a colorimetric signal, then be renally cleared, and the color of the patient's urine will indicate detection of the target.

5.2.2. Applications of Next-Generation siRNA-SNAs

In Chapter 4, we developed hairpin-like siRNA-LSNAs as a treatment for ocular diseases such as wet AMD. We demonstrated that hairpin-like siRNA-AuSNAs efficiently transport through the eye via intravitreal injection and the less invasive subconjunctival injection. We also

developed a hybridization assay for directly detecting hairpin-like siRNA in tissue. Once the siRNA tissue extraction method is optimized, the next experiment will be to observe the biodistribution of hairpin-like siRNA-LSNAs and confirm that we observe the same efficient transport that we saw with hairpin-like siRNA-AuSNAs. The next experiment will be to evaluate the therapeutic efficacy of siRNA-SNAs in a rat model of wet AMD. A laser will be fired into the eyes of Sprague Dawley rats to induce choroidal neovascularization as a model of wet AMD.[177] The rats will then be treated with *VEGF*-targeting hairpin-like siRNA-LSNAs, nontargeting hairpin-like siRNA-LSNAs, or a saline solution via intravitreal injection or subconjunctival injection. At several time points, eyes will be collected and neovascularization will be analyzed using anti-cluster of differentiation 31 (CD31) staining. If *VEGF*-targeting hairpin-like siRNA-LSNAs inhibit neovascularization, they achieve gene silencing in rat eyes and demonstrate further potential as a gene regulatory therapeutic for eye diseases. Furthermore, if the subconjunctivally injected SNAs demonstrate therapeutic success, the siRNA-SNA will show strong potential as a less invasive treatment than current drugs for retinal diseases. In additional to ocular applications, hairpin-like siRNA-SNAs demonstrate promise as a systemically delivered drug for treating cancer due to their increased serum nuclease resistance, enhanced cellular uptake, and durable gene silencing effect. Due to the ability of SNAs to cross the blood-brain barrier, hairpin-like siRNA-SNAs could be uniquely suited as a treatment for brain cancers.

5.2.3. Other Structures for Hairpin-like siRNAs

In Chapters 2 and 4, we attached hairpin-like siRNAs to gold cores and liposome cores, respectively. However, other cores and structures feature additional advantages that can be combined with hairpin-like siRNAs. Since the attachment moiety at the hairpin turn can be

modified, the hairpin-like siRNA can be attached to a variety of different materials. As an example, hairpin-like siRNAs can be attached to a PLGA nanoparticle core using click chemistry.[96] PLGA nanoparticles can encapsulate hydrophobic drugs that can be released upon degradation of the nanoparticle. Thus, PLGA-core hairpin-like siRNA-SNAs could be used to co-deliver siRNAs and hydrophobic drugs as a combination therapeutic. Hairpin-like siRNAs could also be attached to the cysteine or lysine groups on a therapeutically relevant enzyme to form a protein-core siRNA-SNA as another combination therapeutic.[97,178] Finally, hairpin-like siRNAs could be attached to DNA dendrons as a smaller, molecularly pure alternative to SNAs while still achieving high structural stability, nuclease resistance, and efficient intracellular delivery.[158]

5.2.4. Multifunctional Lipid Nanoparticle-Core Spherical Nucleic Acids

LNP-SNAs have enabled the efficient cytosolic delivery of encapsulated nucleic acids while benefiting from increased cellular internalization driven by the outer coating of DNA on the LNP.[116] The prototypical LNP-SNA consists of an LNP core with encapsulated therapeutic nucleic acids, while the outside is functionalized with DNA with the sole purpose of increasing cellular uptake. There is an opportunity to impart the outer oligonucleotides with additional therapeutic functionality for a multifunctional LNP-SNA. As a demonstration of this concept, we are developing LNP-SNAs as siRNA-enhanced cancer vaccines that contain encapsulated signal transducer and activator of transcription 3 (*STAT3*)-targeting siRNA, while the outside of the LNP is functionalized with toll-like receptor 9 (TLR9) agonist immunostimulatory DNA and tumor peptide antigens. When the LNP-SNAs enter antigen-presenting cells, the TLR9 agonist DNA functions as an adjuvant that will engage with TLR9 in the endosome to activate the immune system, while the tumor peptide antigen will be processed and presented by the antigen-

presenting cells to T cells for an adaptive immune response to the tumor.[94] The encapsulated *STAT3* siRNA will be released from the endosome and silence the immunosuppressive *STAT3* gene, lifting the brakes on immune activation and allowing the cancer vaccine to have a stronger effect.[179,180] The location of each component on the LNP-SNA plays to its strengths: the siRNA is encapsulated within the LNP for protection from nucleases and enhanced cytosolic delivery,[54] the TLR9 agonist DNA is on the outside of the LNP to promote efficient cellular uptake and multivalent engagement with TLR9,[94] and the tumor peptide antigen is hybridized to the TLR9 agonist DNA for maximal immune activation.[117] By utilizing structural control and rational design, multifunctional LNP-SNAs have the potential to serve as powerful next-generation nucleic acid therapeutics.

References

(1) Govardhanagiri, S.; Bethi, S.; Nagaraju, G. P. Chapter 8 - Small Molecules and Pancreatic Cancer Trials and Troubles. In *Breaking Tolerance to Pancreatic Cancer Unresponsiveness to Chemotherapy*; Nagaraju, G. P., Ed.; Cancer Sensitizing Agents for Chemotherapy; Academic Press, 2019; Vol. 5, pp 117–131. https://doi.org/10.1016/B978-0-12-817661-0.00008-1.

(2) Stocks, M. Chapter 3 - The Small Molecule Drug Discovery Process – from Target Selection to Candidate Selection. In *Introduction to Biological and Small Molecule Drug Research and Development*; Ganellin, R., Roberts, S., Jefferis, R., Eds.; Elsevier: Oxford, 2013; pp 81–126. https://doi.org/10.1016/B978-0-12-397176-0.00003-0.

(3) Hingorani, A. D.; Kuan, V.; Finan, C.; Kruger, F. A.; Gaulton, A.; Chopade, S.; Sofat, R.; MacAllister, R. J.; Overington, J. P.; Hemingway, H.; Denaxas, S.; Prieto, D.; Casas, J. P. Improving the Odds of Drug Development Success through Human Genomics: Modelling Study. *Sci Rep* **2019**, *9* (1), 18911. https://doi.org/10.1038/s41598-019-54849-w.

(4) Lo, B.; Field, M. J.; Institute of Medicine (US) Committee on Conflict of Interest in Medical Research, E. *The Pathway from Idea to Regulatory Approval: Examples for Drug Development*; National Academies Press (US), 2009.

(5) Van Vleet, T. R.; Liguori, M. J.; Lynch, I., James J.; Rao, M.; Warder, S. Screening Strategies and Methods for Better Off-Target Liability Prediction and Identification of Small-Molecule Pharmaceuticals. *SLAS Discovery* **2019**, *24* (1), 1–24. https://doi.org/10.1177/2472555218799713.

(6) Dandapani, S.; Marcaurelle, L. A. Grand Challenge Commentary: Accessing New Chemical Space for "Undruggable" Targets. *Nat Chem Biol* **2010**, *6* (12), 861–863. https://doi.org/10.1038/nchembio.479.

(7) Makurvet, F. D. Biologics vs. Small Molecules: Drug Costs and Patient Access. *Medicine in Drug Discovery* **2021**, *9*, 100075. https://doi.org/10.1016/j.medidd.2020.100075.

(8) Beall, R. F.; Hwang, T. J.; Kesselheim, A. S. Pre-Market Development Times for Biologic versus Small-Molecule Drugs. *Nat Biotechnol* **2019**, *37* (7), 708–711. https://doi.org/10.1038/s41587-019-0175-2.

(9) Morrow, T.; Felcone, L. H. Defining the Difference: What Makes Biologics Unique. *Biotechnol Healthc* **2004**, *1* (4), 24–29.

(10) Ngo, H. X.; Garneau-Tsodikova, S. What Are the Drugs of the Future? *Medchemcomm* **2018**, *9* (5), 757–758. https://doi.org/10.1039/c8md90019a.

(11) Breaker, R. R.; Joyce, G. F. The Expanding View of RNA and DNA Function. *Chem Biol* **2014**, *21* (9), 1059–1065. https://doi.org/10.1016/j.chembiol.2014.07.008.

(12) Sridharan, K.; Gogtay, N. J. Therapeutic Nucleic Acids: Current Clinical Status. *Br J Clin Pharmacol* **2016**, *82* (3), 659–672. https://doi.org/10.1111/bcp.12987.

(13) Hopkins, A. L.; Groom, C. R. The Druggable Genome. *Nature Reviews Drug Discovery* **2002**, *1* (9), 727. https://doi.org/10.1038/nrd892.

(14) Lee, T. I.; Young, R. A. Transcriptional Regulation and Its Misregulation in Disease. *Cell* **2013**, *152* (6), 1237–1251. https://doi.org/10.1016/j.cell.2013.02.014.

(15) Kulkarni, J. A.; Witzigmann, D.; Thomson, S. B.; Chen, S.; Leavitt, B. R.; Cullis, P. R.; van der Meel, R. The Current Landscape of Nucleic Acid Therapeutics. *Nat. Nanotechnol.* **2021**, *16* (6), 630–643. https://doi.org/10.1038/s41565-021-00898-0.

(16) Chan, J. H.; Lim, S.; Wong, W. F. Antisense Oligonucleotides: From Design to Therapeutic Application. *Clinical and Experimental Pharmacology and Physiology* **2006**, *33* (5–6), 533–540. https://doi.org/10.1111/j.1440-1681.2006.04403.x.

(17) Hu, B.; Zhong, L.; Weng, Y.; Peng, L.; Huang, Y.; Zhao, Y.; Liang, X.-J. Therapeutic siRNA: State of the Art. *Sig Transduct Target Ther* **2020**, *5* (1), 1–25. https://doi.org/10.1038/s41392-020-0207-x.

(18) Diener, C.; Keller, A.; Meese, E. Emerging Concepts of miRNA Therapeutics: From Cells to Clinic. *Trends in Genetics* **2022**, *38* (6), 613–626. https://doi.org/10.1016/j.tig.2022.02.006.

(19) Sheridan, C. CRISPR Therapeutics Push into Human Testing. *Nature Biotechnology* **2017**, *35* (1), 3–5. https://doi.org/10.1038/nbt0117-3.

(20) Jani, M. S.; Veetil, A. T.; Krishnan, Y. Precision Immunomodulation with Synthetic Nucleic Acid Technologies. *Nat Rev Mater* **2019**, *4* (6), 451–458. https://doi.org/10.1038/s41578-019-0105-4.

(21) Nimjee, S. M.; White, R. R.; Becker, R. C.; Sullenger, B. A. Aptamers as Therapeutics. *Annu Rev Pharmacol Toxicol* **2017**, *57*, 61–79. https://doi.org/10.1146/annurev-pharmtox-010716-104558.

(22) Elbashir, S. M.; Harborth, J.; Lendeckel, W.; Yalcin, A.; Weber, K.; Tuschl, T. Duplexes of 21-Nucleotide RNAs Mediate RNA Interference in Cultured Mammalian Cells. *Nature* **2001**, *411* (6836), 494. https://doi.org/10.1038/35078107.

(23) Fire, A.; Xu, S.; Montgomery, M. K.; Kostas, S. A.; Driver, S. E.; Mello, C. C. Potent and Specific Genetic Interference by Double-Stranded RNA in *Caenorhabditis Elegans*. *Nature* **1998**, *391* (6669), 806. https://doi.org/10.1038/35888.

(24) McCaffrey, A. P.; Meuse, L.; Pham, T.-T. T.; Conklin, D. S.; Hannon, G. J.; Kay, M. A. RNA Interference in Adult Mice. *Nature* **2002**, *418* (6893), 38–39. https://doi.org/10.1038/418038a.

(25) Sørensen, D. R.; Leirdal, M.; Sioud, M. Gene Silencing by Systemic Delivery of Synthetic siRNAs in Adult Mice. *Journal of Molecular Biology* **2003**, *327* (4), 761–766. https://doi.org/10.1016/S0022-2836(03)00181-5.

(26) Reynolds, A.; Leake, D.; Boese, Q.; Scaringe, S.; Marshall, W. S.; Khvorova, A. Rational siRNA Design for RNA Interference. *Nature Biotechnology* **2004**, *22* (3), 326–330. https://doi.org/10.1038/nbt936.

(27) Dorsett, Y.; Tuschl, T. siRNAs: Applications in Functional Genomics and Potential as Therapeutics. *Nature Reviews Drug Discovery* **2004**, *3* (4), 318–329. https://doi.org/10.1038/nrd1345.

(28) Setten, R. L.; Rossi, J. J.; Han, S. The Current State and Future Directions of RNAi-Based Therapeutics. *Nature Reviews Drug Discovery* **2019**, *18* (6), 421. https://doi.org/10.1038/s41573-019-0017-4.

(29) Bertrand, J.-R.; Pottier, M.; Vekris, A.; Opolon, P.; Maksimenko, A.; Malvy, C. Comparison of Antisense Oligonucleotides and siRNAs in Cell Culture and *in Vivo*. *Biochem Biophys Res Commun* **2002**, *296* (4), 1000–1004. https://doi.org/10.1016/s0006-291x(02)02013-2.

(30) Watts, J. K.; Corey, D. R. Gene Silencing by siRNAs and Antisense Oligonucleotides in the Laboratory and the Clinic. *J Pathol* **2012**, *226* (2), 365–379. https://doi.org/10.1002/path.2993.

(31) Bernards, R. Exploring the Uses of RNAi—Gene Knockdown and the Nobel Prize. *New England Journal of Medicine* **2006**, *355* (23), 2391–2393.

(32) Adams, D.; Gonzalez-Duarte, A.; O'Riordan, W. D.; Yang, C.-C.; Ueda, M.; Kristen, A. V.; Tournev, I.; Schmidt, H. H.; Coelho, T.; Berk, J. L.; Lin, K.-P.; Vita, G.; Attarian, S.; Planté-Bordeneuve, V.; Mezei, M. M.; Campistol, J. M.; Buades, J.; Brannagan, T. H.; Kim, B. J.; Oh, J.; Parman, Y.; Sekijima, Y.; Hawkins, P. N.; Solomon, S. D.; Polydefkis, M.; Dyck, P. J.; Gandhi, P. J.; Goyal, S.; Chen, J.; Strahs, A. L.; Nochur, S. V.; Sweetser, M. T.; Garg, P. P.; Vaishnaw, A. K.; Gollob, J. A.; Suhr, O. B. Patisiran, an RNAi Therapeutic, for Hereditary Transthyretin Amyloidosis. *New England Journal of Medicine* **2018**, *379* (1), 11–21. https://doi.org/10.1056/NEJMoa1716153.

(33) Hoy, S. M. Patisiran: First Global Approval. *Drugs* **2018**, *78* (15), 1625–1631. https://doi.org/10.1007/s40265-018-0983-6.

(34) Zhang, M. M.; Bahal, R.; Rasmussen, T. P.; Manautou, J. E.; Zhong, X. The Growth of siRNA-Based Therapeutics: Updated Clinical Studies. *Biochemical Pharmacology* **2021**, *189*, 114432. https://doi.org/10.1016/j.bcp.2021.114432.

(35) Behlke, M. A. Progress towards *in Vivo* Use of siRNAs. *Molecular Therapy* **2006**, *13* (4), 644–670. https://doi.org/10.1016/j.ymthe.2006.01.001.

(36) Park, J.; Park, J.; Pei, Y.; Xu, J.; Yeo, Y. Pharmacokinetics and Biodistribution of Recently-Developed siRNA Nanomedicines. *Advanced Drug Delivery Reviews* **2016**, *104*, 93–109. https://doi.org/10.1016/j.addr.2015.12.004.

(37) Guo, P.; Coban, O.; Snead, N. M.; Trebley, J.; Hoeprich, S.; Guo, S.; Shu, Y. Engineering RNA for Targeted siRNA Delivery and Medical Application. *Adv Drug Deliv Rev* **2010**, *62* (6), 650–666. https://doi.org/10.1016/j.addr.2010.03.008.

(38) Whitehead, K. A.; Langer, R.; Anderson, D. G. Knocking down Barriers: Advances in siRNA Delivery. *Nat Rev Drug Discov* **2009**, *8* (2), 129–138. https://doi.org/10.1038/nrd2742.

(39) Wang, J.; Lu, Z.; Wientjes, M. G.; Au, J. L.-S. Delivery of siRNA Therapeutics: Barriers and Carriers. *AAPS J* **2010**, *12* (4), 492–503. https://doi.org/10.1208/s12248-010-9210-4.

(40) Aagaard, L.; Rossi, J. J. RNAi Therapeutics: Principles, Prospects and Challenges. *Adv Drug Deliv Rev* **2007**, *59* (2–3), 75–86. https://doi.org/10.1016/j.addr.2007.03.005.

(41) Gavrilov, K.; Saltzman, W. M. Therapeutic siRNA: Principles, Challenges, and Strategies. *Yale J Biol Med* **2012**, *85* (2), 187–200.

(42) Choung, S.; Kim, Y. J.; Kim, S.; Park, H.-O.; Choi, Y.-C. Chemical Modification of siRNAs to Improve Serum Stability without Loss of Efficacy. *Biochem Biophys Res Commun* **2006**, *342* (3), 919–927. https://doi.org/10.1016/j.bbrc.2006.02.049.

(43) Corey, D. R. Chemical Modification: The Key to Clinical Application of RNA Interference? *J Clin Invest* **2007**, *117* (12), 3615–3622. https://doi.org/10.1172/JCI33483.

(44) Ku, S. H.; Jo, S. D.; Lee, Y. K.; Kim, K.; Kim, S. H. Chemical and Structural Modifications of RNAi Therapeutics. *Advanced Drug Delivery Reviews* **2016**, *104*, 16–28. https://doi.org/10.1016/j.addr.2015.10.015.

(45) Bramsen, J. B.; Laursen, M. B.; Nielsen, A. F.; Hansen, T. B.; Bus, C.; Langkjær, N.; Babu, B. R.; Højland, T.; Abramov, M.; Van Aerschot, A.; Odadzic, D.; Smicius, R.; Haas, J.; Andree, C.; Barman, J.; Wenska, M.; Srivastava, P.; Zhou, C.; Honcharenko, D.; Hess, S.; Müller, E.; Bobkov, G. V.; Mikhailov, S. N.; Fava, E.; Meyer, T. F.; Chattopadhyaya, J.; Zerial, M.; Engels, J. W.; Herdewijn, P.; Wengel, J.; Kjems, J. A Large-Scale Chemical Modification Screen Identifies Design Rules to Generate siRNAs

with High Activity, High Stability and Low Toxicity. *Nucleic Acids Res* **2009**, *37* (9), 2867–2881. https://doi.org/10.1093/nar/gkp106.

(46) Gao, Y.; Liu, X.-L.; Li, X.-R. Research Progress on siRNA Delivery with Nonviral Carriers. *Int J Nanomedicine* **2011**, *6*, 1017–1025. https://doi.org/10.2147/IJN.S17040.

(47) Gary, D. J.; Puri, N.; Won, Y.-Y. Polymer-Based siRNA Delivery: Perspectives on the Fundamental and Phenomenological Distinctions from Polymer-Based DNA Delivery. *Journal of Controlled Release* **2007**, *121* (1), 64–73. https://doi.org/10.1016/j.jconrel.2007.05.021.

(48) Biswas, S.; Torchilin, V. P. Dendrimers for siRNA Delivery. *Pharmaceuticals* **2013**, *6* (2), 161–183. https://doi.org/10.3390/ph6020161.

(49) Kim, B.; Park, J.-H.; Sailor, M. J. Rekindling RNAi Therapy: Materials Design Requirements for *in Vivo* siRNA Delivery. *Advanced Materials* **2019**, *31* (49), 1903637. https://doi.org/10.1002/adma.201903637.

(50) Li, W.; Szoka, F. C. Lipid-Based Nanoparticles for Nucleic Acid Delivery. *Pharm Res* **2007**, *24* (3), 438–449. https://doi.org/10.1007/s11095-006-9180-5.

(51) Wasungu, L.; Hoekstra, D. Cationic Lipids, Lipoplexes and Intracellular Delivery of Genes. *Journal of Controlled Release* **2006**, *116* (2), 255–264. https://doi.org/10.1016/j.jconrel.2006.06.024.

(52) Lv, H.; Zhang, S.; Wang, B.; Cui, S.; Yan, J. Toxicity of Cationic Lipids and Cationic Polymers in Gene Delivery. *Journal of Controlled Release* **2006**, *114* (1), 100–109. https://doi.org/10.1016/j.jconrel.2006.04.014.

(53) Harris, T. J.; Green, J. J.; Fung, P. W.; Langer, R.; Anderson, D. G.; Bhatia, S. N. Tissue-Specific Gene Delivery via Nanoparticle Coating. *Biomaterials* **2010**, *31* (5), 998–1006. https://doi.org/10.1016/j.biomaterials.2009.10.012.

(54) Kulkarni, J. A.; Witzigmann, D.; Chen, S.; Cullis, P. R.; van der Meel, R. Lipid Nanoparticle Technology for Clinical Translation of siRNA Therapeutics. *Acc. Chem. Res.* **2019**, *52* (9), 2435–2444. https://doi.org/10.1021/acs.accounts.9b00368.

(55) Dowdy, S. F. Overcoming Cellular Barriers for RNA Therapeutics. *Nat Biotechnol* **2017**, *35* (3), 222–229. https://doi.org/10.1038/nbt.3802.

(56) Chernikov, I. V.; Vlassov, V. V.; Chernolovskaya, E. L. Current Development of siRNA Bioconjugates: From Research to the Clinic. *Front Pharmacol* **2019**, *10*, 444. https://doi.org/10.3389/fphar.2019.00444.

(57) Springer, A. D.; Dowdy, S. F. GalNAc-siRNA Conjugates: Leading the Way for Delivery of RNAi Therapeutics. *Nucleic Acid Ther* **2018**, *28* (3), 109–118. https://doi.org/10.1089/nat.2018.0736.

(58) Sardh, E.; Harper, P.; Balwani, M.; Stein, P.; Rees, D.; Bissell, D. M.; Desnick, R.; Parker, C.; Phillips, J.; Bonkovsky, H. L.; Vassiliou, D.; Penz, C.; Chan-Daniels, A.; He, Q.; Querbes, W.; Fitzgerald, K.; Kim, J. B.; Garg, P.; Vaishnaw, A.; Simon, A. R.; Anderson, K. E. Phase 1 Trial of an RNA Interference Therapy for Acute Intermittent Porphyria. *New England Journal of Medicine* **2019**, *380* (6), 549–558. https://doi.org/10.1056/NEJMoa1807838.

(59) Gonzalez-Aseguinolaza, G. Givosiran — Running RNA Interference to Fight Porphyria Attacks. *New England Journal of Medicine* **2020**, *382* (24), 2366–2367. https://doi.org/10.1056/NEJMe2010986.

(60) Sun, Y.; Zhao, Y.; Zhao, X.; Lee, R. J.; Teng, L.; Zhou, C. Enhancing the Therapeutic Delivery of Oligonucleotides by Chemical Modification and Nanoparticle Encapsulation. *Molecules* **2017**, *22* (10), E1724. https://doi.org/10.3390/molecules22101724.

(61) Zhang, X.; Goel, V.; Robbie, G. J. Pharmacokinetics of Patisiran, the First Approved RNA Interference Therapy in Patients With Hereditary Transthyretin-Mediated Amyloidosis. *The Journal of Clinical Pharmacology* **2020**, *60* (5), 573–585. https://doi.org/10.1002/jcph.1553.

(62) Scott, L. J. Givosiran: First Approval. *Drugs* **2020**, *80* (3), 335–339. https://doi.org/10.1007/s40265-020-01269-0.

(63) Balwani, M.; Sardh, E.; Ventura, P.; Peiró, P. A.; Rees, D. C.; Stölzel, U.; Bissell, D. M.; Bonkovsky, H. L.; Windyga, J.; Anderson, K. E.; Parker, C.; Silver, S. M.; Keel, S. B.; Wang, J.-D.; Stein, P. E.; Harper, P.; Vassiliou, D.; Wang, B.; Phillips, J.; Ivanova, A.; Langendonk, J. G.; Kauppinen, R.; Minder, E.; Horie, Y.; Penz, C.; Chen, J.; Liu, S.; Ko, J. J.; Sweetser, M. T.; Garg, P.; Vaishnaw, A.; Kim, J. B.; Simon, A. R.; Gouya, L. Phase 3 Trial of RNAi Therapeutic Givosiran for Acute Intermittent Porphyria. *New England Journal of Medicine* **2020**, *382* (24), 2289–2301. https://doi.org/10.1056/NEJMoa1913147.

(64) Scott, L. J.; Keam, S. J. Lumasiran: First Approval. *Drugs* **2021**, *81* (2), 277–282. https://doi.org/10.1007/s40265-020-01463-0.

(65) Garrelfs, S. F.; Frishberg, Y.; Hulton, S. A.; Koren, M. J.; O'Riordan, W. D.; Cochat, P.; Deschênes, G.; Shasha-Lavsky, H.; Saland, J. M.; van't Hoff, W. G.; Fuster, D. G.; Magen, D.; Moochhala, S. H.; Schalk, G.; Simkova, E.; Groothoff, J. W.; Sas, D. J.; Meliambro, K. A.; Lu, J.; Sweetser, M. T.; Garg, P. P.; Vaishnaw, A. K.; Gansner, J. M.;

McGregor, T. L.; Lieske, J. C. Lumasiran, an RNAi Therapeutic for Primary Hyperoxaluria Type 1. *New England Journal of Medicine* **2021**, *384* (13), 1216–1226. https://doi.org/10.1056/NEJMoa2021712.

(66) Garrelfs, S.; Frishberg, Y.; Hulton, S.; Koren, M.; O'Riordan, W.; Cochat, P.; Deschenes, G.; Shasha-Lavsky, H.; Saland, J.; Van't Hoff, W.; Fuster, D. G.; Magen, D.; Moochhala, S.; Schalk, G.; Simkova, E.; Groothoff, J.; Sas, D.; Meliambro, K.; Lu, J.; Garg, P.; Gansner, J.; McGregor, T.; Lieske, J. LB002ILLUMINATE-A, A Phase 3 Study of Lumasiran, an Investigational RNAi Therapeutic, in Children and Adults with Primary Hyperoxaluria Type 1 (PH1). *Nephrology Dialysis Transplantation* **2020**, *35* (Supplement_3), gfaa146.LB002. https://doi.org/10.1093/ndt/gfaa146.LB002.

(67) Frishberg, Y.; Deschênes, G.; Groothoff, J. W.; Hulton, S.-A.; Magen, D.; Harambat, J.; Hoff, W. G. van't; Lorch, U.; Milliner, D. S.; Lieske, J. C.; Haslett, P.; Garg, P. P.; Vaishnaw, A. K.; Talamudupula, S.; Lu, J.; Habtemariam, B. A.; Erbe, D. V.; McGregor, T. L.; Cochat, P.; Collaborators, O. B. of the S. Phase 1/2 Study of Lumasiran for Treatment of Primary Hyperoxaluria Type 1: A Placebo-Controlled Randomized Clinical Trial. *CJASN* **2021**, *16* (7), 1025–1036. https://doi.org/10.2215/CJN.14730920.

(68) Lamb, Y. N. Inclisiran: First Approval. *Drugs* **2021**, *81* (3), 389–395. https://doi.org/10.1007/s40265-021-01473-6.

(69) Raal, F. J.; Kallend, D.; Ray, K. K.; Turner, T.; Koenig, W.; Wright, R. S.; Wijngaard, P. L. J.; Curcio, D.; Jaros, M. J.; Leiter, L. A.; Kastelein, J. J. P. Inclisiran for the Treatment of Heterozygous Familial Hypercholesterolemia. *New England Journal of Medicine* **2020**, *382* (16), 1520–1530. https://doi.org/10.1056/NEJMoa1913805.

(70) German, C. A.; Shapiro, M. D. Small Interfering RNA Therapeutic Inclisiran: A New Approach to Targeting PCSK9. *BioDrugs* **2020**, *34* (1), 1–9. https://doi.org/10.1007/s40259-019-00399-6.

(71) Ray, K. K.; Landmesser, U.; Leiter, L. A.; Kallend, D.; Dufour, R.; Karakas, M.; Hall, T.; Troquay, R. P. T.; Turner, T.; Visseren, F. L. J.; Wijngaard, P.; Wright, R. S.; Kastelein, J. J. P. Inclisiran in Patients at High Cardiovascular Risk with Elevated LDL Cholesterol. *New England Journal of Medicine* **2017**, *376* (15), 1430–1440. https://doi.org/10.1056/NEJMoa1615758.

(72) Ray, K. K.; Wright, R. S.; Kallend, D.; Koenig, W.; Leiter, L. A.; Raal, F. J.; Bisch, J. A.; Richardson, T.; Jaros, M.; Wijngaard, P. L. J.; Kastelein, J. J. P. Two Phase 3 Trials of Inclisiran in Patients with Elevated LDL Cholesterol. *New England Journal of Medicine* **2020**, *382* (16), 1507–1519. https://doi.org/10.1056/NEJMoa1912387.

(73) Bamji, A. N. Do PCSK9 Inhibitors Do Anything More than Reduce LDL Cholesterol? *BMJ* **2020**, *368*, m1159. https://doi.org/10.1136/bmj.m1159.

(74) Asbeutah, A. A. A.; Asbeutah, S. A.; Abu-Assi, M. A. A Meta-Analysis of Cardiovascular Outcomes in Patients With Hypercholesterolemia Treated With Inclisiran. *Am J Cardiol* **2020**, *128*, 218–219. https://doi.org/10.1016/j.amjcard.2020.05.024.

(75) Santulli, G.; Jankauskas, S. S.; Gambardella, J. Inclisiran: A New Milestone on the PCSK9 Road to Tackle Cardiovascular Risk. *Eur Heart J Cardiovasc Pharmacother* **2021**, *7* (3), e11–e12. https://doi.org/10.1093/ehjcvp/pvab014.

(76) Keam, S. J. Vutrisiran: First Approval. *Drugs* **2022**. https://doi.org/10.1007/s40265-022-01765-5.

(77) Adams, D.; Tournev, I. L.; Taylor, M. S.; Coelho, T.; Planté-Bordeneuve, V.; Berk, J. L.; González-Duarte, A.; Gillmore, J. D.; Low, S.-C.; Sekijima, Y.; Obici, L.; Chen, C.; Badri, P.; Arum, S. M.; Vest, J.; Polydefkis, M. Efficacy and Safety of Vutrisiran for Patients with Hereditary Transthyretin-Mediated Amyloidosis with Polyneuropathy: A Randomized Clinical Trial. *Amyloid* **2022**, *0* (0), 1–9. https://doi.org/10.1080/13506129.2022.2091985.

(78) Habtemariam, B. A.; Karsten, V.; Attarwala, H.; Goel, V.; Melch, M.; Clausen, V. A.; Garg, P.; Vaishnaw, A. K.; Sweetser, M. T.; Robbie, G. J.; Vest, J. Single-Dose Pharmacokinetics and Pharmacodynamics of Transthyretin Targeting N-Acetylgalactosamine–Small Interfering Ribonucleic Acid Conjugate, Vutrisiran, in Healthy Subjects. *Clinical Pharmacology & Therapeutics* **2021**, *109* (2), 372–382. https://doi.org/10.1002/cpt.1974.

(79) Gonzalez, -Duarte Alejandra; Adams, D.; Tournev, I.; Taylor, M.; Coelho, T.; Plante, -Bordeneuve Violaine; Berk, J.; Gillmore, J. D.; Low, S.-C.; Sekijima, Y.; Obici, L.; Chen, C.; Badri, P.; Arum, S.; Vest, J.; Polydefkis, M. Helios-a: Results from the Phase 3 Study of Vutrisiran in Patients with Hereditary Transthyretin-Mediated Amyloidosis with Polyneuropathy. *Journal of the American College of Cardiology* **2022**, *79* (9_Supplement), 302–302. https://doi.org/10.1016/S0735-1097(22)01293-1.

(80) Mullard, A. FDA Approves Fifth RNAi Drug — Alnylam's Next-Gen HATTR Treatment. *Nature Reviews Drug Discovery* **2022**, *21* (8), 548–549. https://doi.org/10.1038/d41573-022-00118-x.

(81) Cutler, J. I.; Auyeung, E.; Mirkin, C. A. Spherical Nucleic Acids. *J. Am. Chem. Soc.* **2012**, *134* (3), 1376–1391. https://doi.org/10.1021/ja209351u.

(82) Mahajan, A. S.; Stegh, A. H. Spherical Nucleic Acids as Precision Therapeutics for the Treatment of Cancer—From Bench to Bedside. *Cancers* **2022**, *14* (7), 1615. https://doi.org/10.3390/cancers14071615.

(83) Mirkin, C. A.; Letsinger, R. L.; Mucic, R. C.; Storhoff, J. J. A DNA-Based Method for Rationally Assembling Nanoparticles into Macroscopic Materials. *Nature* **1996**, *382* (6592), 607. https://doi.org/10.1038/382607a0.

(84) Rosi, N. L.; Giljohann, D. A.; Thaxton, C. S.; Lytton-Jean, A. K. R.; Han, M. S.; Mirkin, C. A. Oligonucleotide-Modified Gold Nanoparticles for Intracellular Gene Regulation. *Science* **2006**, *312* (5776), 1027–1030. https://doi.org/10.1126/science.1125559.

(85) Seferos, D. S.; Prigodich, A. E.; Giljohann, D. A.; Patel, P. C.; Mirkin, C. A. Polyvalent DNA Nanoparticle Conjugates Stabilize Nucleic Acids. *Nano Lett.* **2009**, *9* (1), 308–311. https://doi.org/10.1021/nl802958f.

(86) Zheng, D.; Giljohann, D. A.; Chen, D. L.; Massich, M. D.; Wang, X.-Q.; Iordanov, H.; Mirkin, C. A.; Paller, A. S. Topical Delivery of siRNA-Based Spherical Nucleic Acid Nanoparticle Conjugates for Gene Regulation. *PNAS* **2012**, *109* (30), 11975–11980. https://doi.org/10.1073/pnas.1118425109.

(87) Jensen, S. A.; Day, E. S.; Ko, C. H.; Hurley, L. A.; Luciano, J. P.; Kouri, F. M.; Merkel, T. J.; Luthi, A. J.; Patel, P. C.; Cutler, J. I.; Daniel, W. L.; Scott, A. W.; Rotz, M. W.; Meade, T. J.; Giljohann, D. A.; Mirkin, C. A.; Stegh, A. H. Spherical Nucleic Acid Nanoparticle Conjugates as an RNAi-Based Therapy for Glioblastoma. *Science Translational Medicine* **2013**, *5* (209), 209ra152-209ra152. https://doi.org/10.1126/scitranslmed.3006839.

(88) Randeria, P. S.; Seeger, M. A.; Wang, X.-Q.; Wilson, H.; Shipp, D.; Mirkin, C. A.; Paller, A. S. siRNA-Based Spherical Nucleic Acids Reverse Impaired Wound Healing in Diabetic Mice by Ganglioside GM3 Synthase Knockdown. *PNAS* **2015**, *112* (18), 5573–5578. https://doi.org/10.1073/pnas.1505951112.

(89) Nemati, H.; Ghahramani, M.-H.; Faridi-Majidi, R.; Izadi, B.; Bahrami, G.; Madani, S.-H.; Tavoosidana, G. Using siRNA-Based Spherical Nucleic Acid Nanoparticle Conjugates for Gene Regulation in Psoriasis. *Journal of Controlled Release* **2017**, *268*, 259–268. https://doi.org/10.1016/j.jconrel.2017.10.034.

(90) Choi, C. H. J.; Hao, L.; Narayan, S. P.; Auyeung, E.; Mirkin, C. A. Mechanism for the Endocytosis of Spherical Nucleic Acid Nanoparticle Conjugates. *Proc Natl Acad Sci U S A* **2013**, *110* (19), 7625–7630. https://doi.org/10.1073/pnas.1305804110.

(91) Massich, M. D.; Giljohann, D. A.; Seferos, D. S.; Ludlow, L. E.; Horvath, C. M.; Mirkin, C. A. Regulating Immune Response Using Polyvalent Nucleic Acid−Gold Nanoparticle Conjugates. *Mol. Pharmaceutics* **2009**, *6* (6), 1934–1940. https://doi.org/10.1021/mp900172m.

(92) Seferos, D. S.; Giljohann, D. A.; Hill, H. D.; Prigodich, A. E.; Mirkin, C. A. Nano-Flares: Probes for Transfection and mRNA Detection in Living Cells. *J. Am. Chem. Soc.* **2007**, *129* (50), 15477–15479. https://doi.org/10.1021/ja0776529.

(93) Prigodich, A. E.; Seferos, D. S.; Massich, M. D.; Giljohann, D. A.; Lane, B. C.; Mirkin, C. A. Nano-Flares for mRNA Regulation and Detection. *ACS Nano* **2009**, *3* (8), 2147–2152. https://doi.org/10.1021/nn9003814.

(94) Radovic-Moreno, A. F.; Chernyak, N.; Mader, C. C.; Nallagatla, S.; Kang, R. S.; Hao, L.; Walker, D. A.; Halo, T. L.; Merkel, T. J.; Rische, C. H.; Anantatmula, S.; Burkhart, M.;

Mirkin, C. A.; Gryaznov, S. M. Immunomodulatory Spherical Nucleic Acids. *PNAS* **2015**, *112* (13), 3892–3897. https://doi.org/10.1073/pnas.1502850112.

(95) Banga, R. J.; Chernyak, N.; Narayan, S. P.; Nguyen, S. T.; Mirkin, C. A. Liposomal Spherical Nucleic Acids. *J Am Chem Soc* **2014**, *136* (28), 9866–9869. https://doi.org/10.1021/ja504845f.

(96) Zhu, S.; Xing, H.; Gordiichuk, P.; Park, J.; Mirkin, C. A. PLGA Spherical Nucleic Acids. *Advanced Materials* **2018**, *30* (22), 1707113. https://doi.org/10.1002/adma.201707113.

(97) Brodin, J. D.; Sprangers, A. J.; McMillan, J. R.; Mirkin, C. A. DNA-Mediated Cellular Delivery of Functional Enzymes. *J. Am. Chem. Soc.* **2015**, *137* (47), 14838–14841. https://doi.org/10.1021/jacs.5b09711.

(98) Cutler, J. I.; Zhang, K.; Zheng, D.; Auyeung, E.; Prigodich, A. E.; Mirkin, C. A. Polyvalent Nucleic Acid Nanostructures. *J. Am. Chem. Soc.* **2011**, *133* (24), 9254–9257. https://doi.org/10.1021/ja203375n.

(99) Barnaby, S. N.; Perelman, G. A.; Kohlstedt, K. L.; Chinen, A. B.; Schatz, G. C.; Mirkin, C. A. Design Considerations for RNA Spherical Nucleic Acids (SNAs). *Bioconjugate Chem.* **2016**, *27* (9), 2124–2131. https://doi.org/10.1021/acs.bioconjchem.6b00350.

(100) Giljohann, D. A.; Seferos, D. S.; Patel, P. C.; Millstone, J. E.; Rosi, N. L.; Mirkin, C. A. Oligonucleotide Loading Determines Cellular Uptake of DNA-Modified Gold Nanoparticles. *Nano Lett.* **2007**, *7* (12), 3818–3821. https://doi.org/10.1021/nl072471q.

(101) Narayan, S. P.; Choi, C. H. J.; Hao, L.; Calabrese, C. M.; Auyeung, E.; Zhang, C.; Goor, O. J. G. M.; Mirkin, C. A. The Sequence-Specific Cellular Uptake of Spherical Nucleic Acid Nanoparticle Conjugates. *Small* **2015**, *11* (33), 4173–4182. https://doi.org/10.1002/smll.201500027.

(102) Giljohann, D. A.; Seferos, D. S.; Prigodich, A. E.; Patel, P. C.; Mirkin, C. A. Gene Regulation with Polyvalent siRNA-Nanoparticle Conjugates. *J Am Chem Soc* **2009**, *131* (6), 2072–2073. https://doi.org/10.1021/ja808719p.

(103) Kumthekar, P.; Ko, C. H.; Paunesku, T.; Dixit, K.; Sonabend, A. M.; Bloch, O.; Tate, M.; Schwartz, M.; Zuckerman, L.; Lezon, R.; Lukas, R. V.; Jovanovic, B.; McCortney, K.; Colman, H.; Chen, S.; Lai, B.; Antipova, O.; Deng, J.; Li, L.; Tommasini-Ghelfi, S.; Hurley, L. A.; Unruh, D.; Sharma, N. V.; Kandpal, M.; Kouri, F. M.; Davuluri, R. V.; Brat, D. J.; Muzzio, M.; Glass, M.; Vijayakumar, V.; Heidel, J.; Giles, F. J.; Adams, A. K.; James, C. D.; Woloschak, G. E.; Horbinski, C.; Stegh, A. H. A First-in-Human Phase 0 Clinical Study of RNA Interference–Based Spherical Nucleic Acids in Patients with Recurrent Glioblastoma. *Science Translational Medicine* **2021**, *13* (584). https://doi.org/10.1126/scitranslmed.abb3945.

(104) Randeria, P. S.; Jones, M. R.; Kohlstedt, K. L.; Banga, R. J.; Olvera de la Cruz, M.; Schatz, G. C.; Mirkin, C. A. What Controls the Hybridization Thermodynamics of Spherical Nucleic Acids? *J. Am. Chem. Soc.* **2015**, *137* (10), 3486–3489. https://doi.org/10.1021/jacs.5b00670.

(105) Yamankurt, G.; Stawicki, R. J.; Posadas, D. M.; Nguyen, J. Q.; Carthew, R. W.; Mirkin, C. A. The Effector Mechanism of siRNA Spherical Nucleic Acids. *PNAS* **2020**, *117* (3), 1312–1320. https://doi.org/10.1073/pnas.1915907117.

(106) Hong, J.; Huang, Y.; Li, J.; Yi, F.; Zheng, J.; Huang, H.; Wei, N.; Shan, Y.; An, M.; Zhang, H.; Ji, J.; Zhang, P.; Xi, Z.; Du, Q.; Liang, Z. Comprehensive Analysis of Sequence-Specific Stability of siRNA. *FASEB J* **2010**, *24* (12), 4844–4855. https://doi.org/10.1096/fj.09-142398.

(107) Barnaby, S. N.; Lee, A.; Mirkin, C. A. Probing the Inherent Stability of siRNA Immobilized on Nanoparticle Constructs. *PNAS* **2014**, *111* (27), 9739–9744. https://doi.org/10.1073/pnas.1409431111.

(108) Massich, M. D.; Giljohann, D. A.; Schmucker, A. L.; Patel, P. C.; Mirkin, C. A. Cellular Response of Polyvalent Oligonucleotide−Gold Nanoparticle Conjugates. *ACS Nano* **2010**, *4* (10), 5641–5646. https://doi.org/10.1021/nn102228s.

(109) Fratoddi, I.; Venditti, I.; Cametti, C.; Russo, M. V. How Toxic Are Gold Nanoparticles? The State-of-the-Art. *Nano Res.* **2015**, *8* (6), 1771–1799. https://doi.org/10.1007/s12274-014-0697-3.

(110) Singh, P.; Pandit, S.; Mokkapati, V. R. S. S.; Garg, A.; Ravikumar, V.; Mijakovic, I. Gold Nanoparticles in Diagnostics and Therapeutics for Human Cancer. *International Journal of Molecular Sciences* **2018**, *19* (7), 1979. https://doi.org/10.3390/ijms19071979.

(111) Wu, X. A.; Choi, C. H. J.; Zhang, C.; Hao, L.; Mirkin, C. A. Intracellular Fate of Spherical Nucleic Acid Nanoparticle Conjugates. *J. Am. Chem. Soc.* **2014**, *136* (21), 7726–7733. https://doi.org/10.1021/ja503010a.

(112) Pei, D.; Buyanova, M. Overcoming Endosomal Entrapment in Drug Delivery. *Bioconjugate Chem.* **2019**, *30* (2), 273–283. https://doi.org/10.1021/acs.bioconjchem.8b00778.

(113) Huang, Z.; Callmann, C. E.; Wang, S.; Vasher, M. K.; Evangelopoulos, M.; Petrosko, S. H.; Mirkin, C. A. Rational Vaccinology: Harnessing Nanoscale Chemical Design for Cancer Immunotherapy. *ACS Cent. Sci.* **2022**, *8* (6), 692–704. https://doi.org/10.1021/acscentsci.2c00227.

(114) Ferrer, J. R.; Sinegra, A. J.; Ivancic, D.; Yeap, X. Y.; Qiu, L.; Wang, J.-J.; Zhang, Z. J.; Wertheim, J. A.; Mirkin, C. A. Structure-Dependent Biodistribution of Liposomal Spherical Nucleic Acids. *ACS Nano* **2020**, *14* (2), 1682–1693. https://doi.org/10.1021/acsnano.9b07254.

(115) Callmann, C. E.; Kusmierz, C. D.; Dittmar, J. W.; Broger, L.; Mirkin, C. A. Impact of Liposomal Spherical Nucleic Acid Structure on Immunotherapeutic Function. *ACS Cent. Sci.* **2021**, *7* (5), 892–899. https://doi.org/10.1021/acscentsci.1c00181.

(116) Sinegra, A. J.; Evangelopoulos, M.; Park, J.; Huang, Z.; Mirkin, C. A. Lipid Nanoparticle Spherical Nucleic Acids for Intracellular DNA and RNA Delivery. *Nano Lett.* **2021**, *21* (15), 6584–6591. https://doi.org/10.1021/acs.nanolett.1c01973.

(117) Wang, S.; Qin, L.; Yamankurt, G.; Skakuj, K.; Huang, Z.; Chen, P.-C.; Dominguez, D.; Lee, A.; Zhang, B.; Mirkin, C. A. Rational Vaccinology with Spherical Nucleic Acids. *Proceedings of the National Academy of Sciences* **2019**, *116* (21), 10473–10481. https://doi.org/10.1073/pnas.1902805116.

(118) Petrocca, F.; Lieberman, J. Promise and Challenge of RNA Interference–Based Therapy for Cancer. *JCO* **2011**, *29* (6), 747–754. https://doi.org/10.1200/JCO.2009.27.6287.

(119) Shim, M. S.; Kwon, Y. J. Efficient and Targeted Delivery of siRNA *in Vivo*. *The FEBS Journal* **2010**, *277* (23), 4814–4827. https://doi.org/10.1111/j.1742-4658.2010.07904.x.

(120) Ionita, P.; Volkov, A.; Jeschke, G.; Chechik, V. Lateral Diffusion of Thiol Ligands on the Surface of Au Nanoparticles: An Electron Paramagnetic Resonance Study. *Anal. Chem.* **2008**, *80* (1), 95–106. https://doi.org/10.1021/ac071266s.

(121) Kimling, J.; Maier, M.; Okenve, B.; Kotaidis, V.; Ballot, H.; Plech, A. Turkevich Method for Gold Nanoparticle Synthesis Revisited. *J. Phys. Chem. B* **2006**, *110* (32), 15700–15707. https://doi.org/10.1021/jp061667w.

(122) Demers, L. M.; Mirkin, C. A.; Mucic, R. C.; Reynolds, R. A.; Letsinger, R. L.; Elghanian, R.; Viswanadham, G. A Fluorescence-Based Method for Determining the Surface Coverage and Hybridization Efficiency of Thiol-Capped Oligonucleotides Bound to Gold Thin Films and Nanoparticles. *Anal. Chem.* **2000**, *72* (22), 5535–5541. https://doi.org/10.1021/ac0006627.

(123) Pfaffl, M. W. A New Mathematical Model for Relative Quantification in Real-Time RT-PCR. *Nucleic Acids Res.* **2001**, *29* (9), e45. https://doi.org/10.1093/nar/29.9.e45.

(124) Mitri, Z.; Constantine, T.; O'Regan, R. The HER2 Receptor in Breast Cancer: Pathophysiology, Clinical Use, and New Advances in Therapy. *Chemother Res Pract* **2012**, *2012*, 743193. https://doi.org/10.1155/2012/743193.

(125) Bartlett, D. W.; Davis, M. E. Insights into the Kinetics of siRNA-Mediated Gene Silencing from Live-Cell and Live-Animal Bioluminescent Imaging. *Nucleic Acids Res* **2006**, *34* (1), 322–333. https://doi.org/10.1093/nar/gkj439.

(126) Ruvinov, E.; Kryukov, O.; Forti, E.; Korin, E.; Goldstein, M.; Cohen, S. Calcium-siRNA Nanocomplexes: What Reversibility Is All About. *J Control Release* **2015**, *203*, 150–160. https://doi.org/10.1016/j.jconrel.2015.02.029.

(127) Goldshtein, M.; Forti, E.; Ruvinov, E.; Cohen, S. Mechanisms of Cellular Uptake and Endosomal Escape of Calcium-siRNA Nanocomplexes. *Int J Pharm* **2016**, *515* (1–2), 46–56. https://doi.org/10.1016/j.ijpharm.2016.10.009.

(128) Callmann, C. E.; Cole, L. E.; Kusmierz, C. D.; Huang, Z.; Horiuchi, D.; Mirkin, C. A. Tumor Cell Lysate-Loaded Immunostimulatory Spherical Nucleic Acids as Therapeutics for Triple-Negative Breast Cancer. *Proceedings of the National Academy of Sciences* **2020**, *117* (30), 17543–17550. https://doi.org/10.1073/pnas.2005794117.

(129) Teplensky, M. H.; Dittmar, J. W.; Qin, L.; Wang, S.; Evangelopoulos, M.; Zhang, B.; Mirkin, C. A. Spherical Nucleic Acid Vaccine Structure Markedly Influences Adaptive Immune Responses of Clinically Utilized Prostate Cancer Targets. *Advanced Healthcare Materials* **2021**, *10* (22), 2101262. https://doi.org/10.1002/adhm.202101262.

(130) Hurst, S. J.; Lytton-Jean, A. K. R.; Mirkin, C. A. Maximizing DNA Loading on a Range of Gold Nanoparticle Sizes. *Anal. Chem.* **2006**, *78* (24), 8313–8318. https://doi.org/10.1021/ac0613582.

(131) Vasher, M. K.; Yamankurt, G.; Mirkin, C. A. Hairpin-like siRNA-Based Spherical Nucleic Acids. *J. Am. Chem. Soc.* **2022**, *144* (7), 3174–3181. https://doi.org/10.1021/jacs.1c12750.

(132) Blanco, E.; Shen, H.; Ferrari, M. Principles of Nanoparticle Design for Overcoming Biological Barriers to Drug Delivery. *Nat Biotechnol* **2015**, *33* (9), 941–951. https://doi.org/10.1038/nbt.3330.

(133) Ouyang, B.; Poon, W.; Zhang, Y.-N.; Lin, Z. P.; Kingston, B. R.; Tavares, A. J.; Zhang, Y.; Chen, J.; Valic, M. S.; Syed, A. M.; MacMillan, P.; Couture-Senécal, J.; Zheng, G.; Chan, W. C. W. The Dose Threshold for Nanoparticle Tumour Delivery. *Nat. Mater.* **2020**, *19* (12), 1362–1371. https://doi.org/10.1038/s41563-020-0755-z.

(134) Hoshyar, N.; Gray, S.; Han, H.; Bao, G. The Effect of Nanoparticle Size on *in Vivo* Pharmacokinetics and Cellular Interaction. *Nanomedicine (Lond)* **2016**, *11* (6), 673–692. https://doi.org/10.2217/nnm.16.5.

(135) Longmire, M.; Choyke, P. L.; Kobayashi, H. Clearance Properties of Nano-Sized Particles and Molecules as Imaging Agents: Considerations and Caveats. *Nanomedicine* **2008**, *3* (5), 703–717. https://doi.org/10.2217/17435889.3.5.703.

(136) Sonavane, G.; Tomoda, K.; Makino, K. Biodistribution of Colloidal Gold Nanoparticles after Intravenous Administration: Effect of Particle Size. *Colloids and Surfaces B: Biointerfaces* **2008**, *66* (2), 274–280. https://doi.org/10.1016/j.colsurfb.2008.07.004.

(137) Hirn, S.; Semmler-Behnke, M.; Schleh, C.; Wenk, A.; Lipka, J.; Schäffler, M.; Takenaka, S.; Möller, W.; Schmid, G.; Simon, U.; Kreyling, W. G. Particle Size-Dependent and Surface Charge-Dependent Biodistribution of Gold Nanoparticles after Intravenous Administration. *European Journal of Pharmaceutics and Biopharmaceutics* **2011**, *77* (3), 407–416. https://doi.org/10.1016/j.ejpb.2010.12.029.

(138) Wang, J.; Liu, G. Imaging Nano–Bio Interactions in the Kidney: Toward a Better Understanding of Nanoparticle Clearance. *Angewandte Chemie International Edition* **2018**, *57* (12), 3008–3010. https://doi.org/10.1002/anie.201711705.

(139) Zhu, G. H.; Azharuddin, M.; Islam, R.; Rahmoune, H.; Deb, S.; Kanji, U.; Das, J.; Osterrieth, J.; Aulakh, P.; Ibrahim-Hashi, H.; Manchanda, R.; Nilsson, P. H.; Mollnes, T. E.; Bhattacharyya, M.; Islam, M. M.; Hinkula, J.; Slater, N. K. H.; Patra, H. K. Innate Immune Invisible Ultrasmall Gold Nanoparticles—Framework for Synthesis and Evaluation. *ACS Appl. Mater. Interfaces* **2021**, *13* (20), 23410–23422. https://doi.org/10.1021/acsami.1c02834.

(140) Zhao, Y.; Sultan, D.; Detering, L.; Luehmann, H.; Liu, Y. Facile Synthesis, Pharmacokinetic and Systemic Clearance Evaluation, and Positron Emission Tomography Cancer Imaging of ^{64}Cu–Au Alloy Nanoclusters. *Nanoscale* **2014**, *6* (22), 13501–13509. https://doi.org/10.1039/C4NR04569F.

(141) Park, S.; Aalipour, A.; Vermesh, O.; Yu, J. H.; Gambhir, S. S. Towards Clinically Translatable *in Vivo* Nanodiagnostics. *Nat Rev Mater* **2017**, *2* (5), 1–20. https://doi.org/10.1038/natrevmats.2017.14.

(142) Yu, M.; Xu, J.; Zheng, J. Renal Clearable Luminescent Gold Nanoparticles: From the Bench to the Clinic. *Angewandte Chemie International Edition* **2019**, *58* (13), 4112–4128. https://doi.org/10.1002/anie.201807847.

(143) Kang, H.; Rho, S.; Stiles, W. R.; Hu, S.; Baek, Y.; Hwang, D. W.; Kashiwagi, S.; Kim, M. S.; Choi, H. S. Size-Dependent EPR Effect of Polymeric Nanoparticles on Tumor Targeting. *Advanced Healthcare Materials* **2020**, *9* (1), 1901223. https://doi.org/10.1002/adhm.201901223.

(144) Huang, K.; Ma, H.; Liu, J.; Huo, S.; Kumar, A.; Wei, T.; Zhang, X.; Jin, S.; Gan, Y.; Wang, P. C.; He, S.; Zhang, X.; Liang, X.-J. Size-Dependent Localization and Penetration of Ultrasmall Gold Nanoparticles in Cancer Cells, Multicellular Spheroids, and Tumors *in Vivo*. *ACS Nano* **2012**, *6* (5), 4483–4493. https://doi.org/10.1021/nn301282m.

(145) Huo, S.; Jin, S.; Ma, X.; Xue, X.; Yang, K.; Kumar, A.; Wang, P. C.; Zhang, J.; Hu, Z.; Liang, X.-J. Ultrasmall Gold Nanoparticles as Carriers for Nucleus-Based Gene Therapy Due to Size-Dependent Nuclear Entry. *ACS Nano* **2014**, *8* (6), 5852–5862. https://doi.org/10.1021/nn5008572.

(146) Huo, S.; Chen, S.; Gong, N.; Liu, J.; Li, X.; Zhao, Y.; Liang, X.-J. Ultrasmall Gold Nanoparticles Behavior *in Vivo* Modulated by Surface Polyethylene Glycol (PEG) Grafting. *Bioconjugate Chem.* **2017**, *28* (1), 239–243. https://doi.org/10.1021/acs.bioconjchem.6b00488.

(147) Wu, M.; Guo, H.; Liu, L.; Liu, Y.; Xie, L. Size-Dependent Cellular Uptake and Localization Profiles of Silver Nanoparticles. *Int J Nanomedicine* **2019**, *14*, 4247–4259. https://doi.org/10.2147/IJN.S201107.

(148) Li, H.; Zhang, B.; Lu, X.; Tan, X.; Jia, F.; Xiao, Y.; Cheng, Z.; Li, Y.; Silva, D. O.; Schrekker, H. S.; Zhang, K.; Mirkin, C. A. Molecular Spherical Nucleic Acids. *Proceedings of the National Academy of Sciences* **2018**, *115* (17), 4340–4344. https://doi.org/10.1073/pnas.1801836115.

(149) Chinen, A. B.; Guan, C. M.; Ko, C. H.; Mirkin, C. A. The Impact of Protein Corona Formation on the Macrophage Cellular Uptake and Biodistribution of Spherical Nucleic Acids. *Small* **2017**, *13* (16), 1603847. https://doi.org/10.1002/smll.201603847.

(150) Sita, T. L.; Kouri, F. M.; Hurley, L. A.; Merkel, T. J.; Chalastanis, A.; May, J. L.; Ghelfi, S. T.; Cole, L. E.; Cayton, T. C.; Barnaby, S. N.; Sprangers, A. J.; Savalia, N.; James, C. D.; Lee, A.; Mirkin, C. A.; Stegh, A. H. Dual Bioluminescence and Near-Infrared Fluorescence Monitoring to Evaluate Spherical Nucleic Acid Nanoconjugate Activity *in Vivo*. *Proceedings of the National Academy of Sciences* **2017**, *114* (16), 4129–4134. https://doi.org/10.1073/pnas.1702736114.

(151) Levi-Kalisman, Y.; Jadzinsky, P. D.; Kalisman, N.; Tsunoyama, H.; Tsukuda, T.; Bushnell, D. A.; Kornberg, R. D. Synthesis and Characterization of Au_{102}(*p*-MBA)$_{44}$

Nanoparticles. *J. Am. Chem. Soc.* **2011**, *133* (9), 2976–2982. https://doi.org/10.1021/ja109131w.

(152) Girard, M.; Wang, S.; Du, J. S.; Das, A.; Huang, Z.; Dravid, V. P.; Lee, B.; Mirkin, C. A.; Cruz, M. O. de la. Particle Analogs of Electrons in Colloidal Crystals. *Science* **2019**, *364* (6446), 1174–1178. https://doi.org/10.1126/science.aaw8237.

(153) Elghanian, R.; Storhoff, J. J.; Mucic, R. C.; Letsinger, R. L.; Mirkin, C. A. Selective Colorimetric Detection of Polynucleotides Based on the Distance-Dependent Optical Properties of Gold Nanoparticles. *Science* **1997**, *277* (5329), 1078–1081. https://doi.org/10.1126/science.277.5329.1078.

(154) Zhang, S.; Li, J.; Lykotrafitis, G.; Bao, G.; Suresh, S. Size-Dependent Endocytosis of Nanoparticles. *Advanced Materials* **2009**, *21* (4), 419–424. https://doi.org/10.1002/adma.200801393.

(155) Li, X. Size and Shape Effects on Receptor-Mediated Endocytosis of Nanoparticles. *Journal of Applied Physics* **2012**, *111* (2), 024702. https://doi.org/10.1063/1.3676448.

(156) Choi, H. S.; Ipe, B. I.; Misra, P.; Lee, J. H.; Bawendi, M. G.; Frangioni, J. V. Tissue- and Organ-Selective Biodistribution of NIR Fluorescent Quantum Dots. *Nano Lett.* **2009**, *9* (6), 2354–2359. https://doi.org/10.1021/nl900872r.

(157) Wilhelm, S.; Tavares, A. J.; Dai, Q.; Ohta, S.; Audet, J.; Dvorak, H. F.; Chan, W. C. W. Analysis of Nanoparticle Delivery to Tumours. *Nat Rev Mater* **2016**, *1* (5), 1–12. https://doi.org/10.1038/natrevmats.2016.14.

(158) Distler, M. E.; Teplensky, M. H.; Bujold, K. E.; Kusmierz, C. D.; Evangelopoulos, M.; Mirkin, C. A. DNA Dendrons as Agents for Intracellular Delivery. *J. Am. Chem. Soc.* **2021**, *143* (34), 13513–13518. https://doi.org/10.1021/jacs.1c07240.

(159) Teplensky, M. H.; Distler, M. E.; Kusmierz, C. D.; Evangelopoulos, M.; Gula, H.; Elli, D.; Tomatsidou, A.; Nicolaescu, V.; Gelarden, I.; Yeldandi, A.; Batlle, D.; Missiakas, D.; Mirkin, C. A. Spherical Nucleic Acids as an Infectious Disease Vaccine Platform. *Proceedings of the National Academy of Sciences* **2022**, *119* (14), e2119093119. https://doi.org/10.1073/pnas.2119093119.

(160) Carpentier, G.; Berndt, S.; Ferratge, S.; Rasband, W.; Cuendet, M.; Uzan, G.; Albanese, P. Angiogenesis Analyzer for ImageJ — A Comparative Morphometric Analysis of "Endothelial Tube Formation Assay" and "Fibrin Bead Assay." *Sci Rep* **2020**, *10* (1), 11568. https://doi.org/10.1038/s41598-020-67289-8.

(161) IT'IS Foundation. Density. https://itis.swiss/virtual-population/tissue-properties/database/density/ (accessed 2022-07-26).

(162) Mcintosh, R. L.; Anderson, V. A Comprehensive Tissue Properties Database Provided for the Thermal Assessment of a Human at Rest. *Biophys. Rev. Lett.* **2010**, *05* (03), 129–151. https://doi.org/10.1142/S1793048010001184.

(163) Stefánsson, E.; Wilson, C. A.; Lightman, S. L.; Kuwabara, T.; Palestine, A. G.; Wagner, H. G. Quantitative Measurements of Retinal Edema by Specific Gravity Determinations. *Investigative Ophthalmology & Visual Science* **1987**, *28* (8), 1281–1289.

(164) Meckes, B.; Banga, R. J.; Nguyen, S. T.; Mirkin, C. A. Enhancing the Stability and Immunomodulatory Activity of Liposomal Spherical Nucleic Acids through Lipid-Tail DNA Modifications. *Small* **2018**, *14* (5), 1702909. https://doi.org/10.1002/smll.201702909.

(165) Ferrara, N. VEGF as a Therapeutic Target in Cancer. *OCL* **2005**, *69* (Suppl. 3), 11–16. https://doi.org/10.1159/000088479.

(166) Amadio, M.; Govoni, S.; Pascale, A. Targeting VEGF in Eye Neovascularization: What's New?: A Comprehensive Review on Current Therapies and Oligonucleotide-Based Interventions under Development. *Pharmacological Research* **2016**, *103*, 253–269. https://doi.org/10.1016/j.phrs.2015.11.027.

(167) Campochiaro, P. A. Retinal and Choroidal Neovascularization. *Journal of Cellular Physiology* **2000**, *184* (3), 301–310. https://doi.org/10.1002/1097-4652(200009)184:3<301::AID-JCP3>3.0.CO;2-H.

(168) Kearns, V. R.; Williams, R. L. Drug Delivery Systems for the Eye. *Expert Review of Medical Devices* **2009**, *6* (3), 277–290. https://doi.org/10.1586/erd.09.4.

(169) Eljarrat-Binstock, E.; Pe'er, J.; Domb, A. J. New Techniques for Drug Delivery to the Posterior Eye Segment. *Pharm Res* **2010**, *27* (4), 530–543. https://doi.org/10.1007/s11095-009-0042-9.

(170) Polat, O.; İnan, S.; Özcan, S.; Doğan, M.; Küsbeci, T.; Yavaş, G. F.; İnan, Ü. Ü. Factors Affecting Compliance to Intravitreal Anti-Vascular Endothelial Growth Factor Therapy in Patients with Age-Related Macular Degeneration. *Turk J Ophthalmol* **2017**, *47* (4), 205–210. https://doi.org/10.4274/tjo.28003.

(171) Ghasemi Falavarjani, K.; Nguyen, Q. D. Adverse Events and Complications Associated with Intravitreal Injection of Anti-VEGF Agents: A Review of Literature. *Eye (Lond)* **2013**, *27* (7), 787–794. https://doi.org/10.1038/eye.2013.107.

(172) Khar, R. K.; Jain, G. K.; Warsi, M. H.; Mallick, N.; Akhter, S.; Pathan, S. A.; Ahmad, F. J. Nano-Vectors for the Ocular Delivery of Nucleic Acid-Based Therapeutics. *Indian J Pharm Sci* **2010**, *72* (6), 675–688. https://doi.org/10.4103/0250-474X.84575.

(173) Pañeda, C.; Martínez, T.; Wright, N.; Jimenez, A. I. *Recent Advances in Ocular Nucleic Acid-Based Therapies: The Silent Era*; IntechOpen, 2012. https://doi.org/10.5772/48454.

(174) Xia, X.; Xiong, S.; Song, W.; Luo, J.; Wang, Y.; Zhou, R. Inhibition of Retinal Neovascularization by siRNA Targeting $VEGF_{165}$. *Mol Vis* **2008**, *14*, 1965–1973.

(175) Supe, S.; Upadhya, A.; Singh, K. Role of Small Interfering RNA (siRNA) in Targeting Ocular Neovascularization: A Review. *Experimental Eye Research* **2021**, *202*, 108329. https://doi.org/10.1016/j.exer.2020.108329.

(176) Tremblay, G.; Oldfield, P. Bioanalysis of siRNA and Oligonucleotide Therapeutics in Biological Fluids and Tissues. *Bioanalysis* **2009**, *1*, 595–609. https://doi.org/10.4155/bio.09.66.

(177) Lambert, V.; Lecomte, J.; Hansen, S.; Blacher, S.; Gonzalez, M.-L. A.; Struman, I.; Sounni, N. E.; Rozet, E.; de Tullio, P.; Foidart, J. M.; Rakic, J.-M.; Noel, A. Laser-Induced Choroidal Neovascularization Model to Study Age-Related Macular Degeneration in Mice. *Nat Protoc* **2013**, *8* (11), 2197–2211. https://doi.org/10.1038/nprot.2013.135.

(178) Kusmierz, C. D.; Bujold, K. E.; Callmann, C. E.; Mirkin, C. A. Defining the Design Parameters for *in Vivo* Enzyme Delivery Through Protein Spherical Nucleic Acids. *ACS Cent. Sci.* **2020**, *6* (5), 815–822. https://doi.org/10.1021/acscentsci.0c00313.

(179) Zou, S.; Tong, Q.; Liu, B.; Huang, W.; Tian, Y.; Fu, X. Targeting STAT3 in Cancer Immunotherapy. *Molecular Cancer* **2020**, *19* (1), 145. https://doi.org/10.1186/s12943-020-01258-7.

(180) Li, H. S.; Liu, C.; Xiao, Y.; Chu, F.; Liang, X.; Peng, W.; Hu, J.; Neelapu, S. S.; Sun, S.-C.; Hwu, P.; Watowich, S. S. Bypassing STAT3-Mediated Inhibition of the

Transcriptional Regulator ID2 Improves the Antitumor Efficacy of Dendritic Cells. *Science Signaling* **2016**, *9* (447), ra94–ra94. https://doi.org/10.1126/scisignal.aaf3957.

Vita

Matthew K. Vasher

1351 W Belmont Ave
Apt 2W
Chicago, IL 60657

(734) 417-4306
mkvasher@gmail.com
linkedin.com/in/mkvasher

Education

PhD in Biomedical Engineering 2022
Northwestern University, Evanston, IL
- Advisor: Dr. Chad A. Mirkin

Certificate in Management for Scientists and Engineers 2021
Kellogg School of Management, Northwestern University, Evanston, IL

BS in Biosystems Engineering 2017
Michigan State University, East Lansing, MI
- Biomedical Engineering concentration
- Honors College member

Research Experience

Graduate Research Assistant 2017–2022
Advisor: Dr. Chad A. Mirkin, Northwestern University
- Developed a novel hairpin-like architecture of siRNA-based spherical nucleic acid (SNA) for gene regulation therapy with higher active siRNA loading, greater stability, lower toxicity, and more durable therapeutic effect
- Led a project to develop biocompatible SNA constructs that can transport through the eye to treat retinal diseases and coordinated animal studies with a contract research organization
- Investigated the lower size limit of SNA properties by characterizing the behavior of ultrasmall SNAs
- Mentored 4 students

Undergraduate Research Assistant 2013–2017
Advisor: Dr. Evangelyn C. Alocilja, Michigan State University
- Collaborated with scientists from the Philippines, Mexico, and Peru to develop and implement diagnostic devices for low-resource communities
- Developed colorimetric and electrochemical nanoparticle-based biosensors for rapidly detecting pathogens at low concentrations
- Characterized novel optical properties of magnetic nanoparticle-pathogen interactions

Research and Development Intern 2016
Beckman Coulter, Inc., Miami, FL
- Conducted research with an R&D team to develop an automated blood preparation device for flow cytometers
- Presented project results and revenue projections to company executives

Manufacturing Operations Intern 2015
Beckman Coulter, Inc., Chaska, MN

- Implemented a design change for antibody purification resulting in an estimated $40,000 in annual savings
- Conducted risk analyses to evaluate and select design changes
- Worked with a team to utilize lean manufacturing principles to optimize production efficiency at a distribution center

Publications

Huang, Z; Callmann, C. E.; Wang, S.; **Vasher, M. K.**; Evangelopoulos, M.; Petrosko, S. H.; Mirkin, C. A. The Emergence of Rational Vaccinology: Harnessing the Power of Nanomaterial Design in Immunotherapy. *ACS Cent. Sci.* **2022**, *8* (6): 692–704.

Vasher, M. K.; Yamankurt, G.; Mirkin, C. A. Hairpin-like siRNA-Based Spherical Nucleic Acids. *J. Am. Chem. Soc.* **2022**, *144* (7): 3174–3181.

Baetsen-Young, A. M.; **Vasher, M. K.**; Matta, L. L.; Colgan, P.; Alocilja, E. C.; Day, B. Direct Colorimetric Detection of Unamplified Pathogen DNA by Dextrin-Capped Gold Nanoparticles. *Biosens. Bioelectron.* **2018**, *101*: 29–36.

Fernando, L. M,; **Vasher, M. K.**; Alocilja, E. C. A DNA-Based Nanobiosensor for the Rapid Detection of the Dengue Virus in Mosquito. *Int. J. Pharmacol. Pharm. Sci.* **2015**, *9* (12): 822–825.

Patents

Mirkin, C. A.; Yamankurt, G.; **Vasher, M. K.** Hairpin-like Oligonucleotide-Conjugated Spherical Nucleic Acid. **2020**, U.S. Patent Application PCT/US2020/021275.

Poster Presentations and Talks

Vasher, M. K.; Evangelopoulos, M.; Mirkin, C. A. Spherical Nucleic Acids for Delivering siRNA Into the Eye. *Biomedical Engineering Society (BMES) Annual Meeting* **2021**, Orlando, FL.

Vasher, M. K.; Yamankurt, G.; Mirkin, C. A. Hairpin-like siRNA-Based Spherical Nucleic Acids for Enhanced siRNA Duplex Delivery. *BMES Annual Meeting* **2020**, Virtual Conference.

Vasher M. K.; Alocilja, E. C. Dengue Virus Detection Using a Biosensor. *College of Agriculture and Natural Resources Research Round-Up* **2015**, East Lansing, MI. Awarded third place.

Vasher M. K.; Alocilja, E. C. Detecting Pathogens Using a DNA-Based Biosensor. *University Undergraduate Research and Arts Forum (UURAF)* **2015**, East Lansing, MI. Awarded first place.

Teaching Experience

Graduate Teaching Assistant 2020
BME 303/403: Quantitative Systems Physiology, Northwestern University
- Assisted Dr. Casey J. Ankeny in teaching over 70 students
- Helped transition the course to a virtual format during the COVID-19 pandemic
- Held weekly recitations and office hours
- Graded assignments and helped write exams
- Recognized with Biomedical Engineering Teaching Assistant Award Honorable Mention

Undergraduate Teaching Assistant 2017
BE 444/844: Biosensors for Medical Diagnostics, Michigan State University
- Assisted Dr. Evangelyn C. Alocilja in teaching over 30 students
- Served as substitute lecturer
- Graded assignments and guided students through projects

Undergraduate Teaching Assistant 2015
BE 101: Introduction to Biosystems Engineering, Michigan State University
- Assisted Dr. Bradley P. Marks in teaching over 90 students
- Provided career advice and curriculum guidance
- Held office hours and graded assignments

Leadership

Nanomedicine Subgroup Leader 2021–2022
Mirkin Lab, Northwestern University
- Managed 20 graduate students and postdocs through life science-based nanotechnology projects
- Supervised collaborations, manuscript preparation, mentor assignments, and instrument responsibilities
- Organized and led weekly subgroup presentations and scientific discussions
- Recruited graduate students and postdocs to the subgroup through interviews, discussions, and recruitment events in collaboration with faculty and staff
- Mentored new graduate students and postdocs to acclimate them to the lab

Data Coordinator 2020–2022
Northwestern University Center of Cancer Nanotechnology Excellence (CCNE)
- Compiled, organized, and managed data from nanomedicine projects funded by an $11.7 million NIH grant into an online database of nanomaterials (caNanoLab) to foster collaboration between nanotechnology labs and communicate results to the National Cancer Institute

Lab Manager 2016–2017
Alocilja Lab, Michigan State University
- Managed research projects, lab operations, and finances
- Oversaw reagent orders, equipment installation and maintenance, and hazardous waste disposal
- Trained and mentored 6 undergraduate research assistants

Community Involvement

Mentor 2018–2022
Science Club, Science In Society, Northwestern University
- Mentored underserved Chicago middle school students through semester-long science projects
- One of my mentees won first prize in their school science fair and competed at the regional level

Diversity Committee Member 2020–2021
Biomedical Engineering Graduate Students (BMEGS)
- Implemented specific, quantifiable goals for improving diversity, equity, and inclusion at Northwestern University
- Organized monthly department-wide discussions on topics of inclusion and equity

Mentor 2020–2021
EvanSTEM, District 65
- Mentored underserved Evanston middle school students through semester-long coding projects

Professional Development

American Association for the Advancement of Science (AAAS) Catalyzing Advocacy in Science and Engineering (CASE) Workshop 2018
AAAS Headquarters, Washington, D.C.
- Applied for and obtained institutional support to represent Northwestern University at a 4-day science policy workshop
- Advocated to Members of Congress for increased scientific research funding

Tau Beta Pi (Engineering Honor Society) Member 2014 – present

Honors, Fellowships, and Awards

Fellowship in Leadership 2022
- Collaborated with faculty, staff, and students to study and develop leadership strategies

International Institute for Nanotechnology (IIN) Outstanding Researcher Award 2021
- Awarded for exceptional contributions to the field of nanotechnology

Biomedical Engineering Teaching Assistant Award Honorable Mention 2021
- Recognized for distinguished contributions to student learning in Northwestern's Biomedical Engineering department, awarded for TA work in BME 303/403: Quantitative Systems Physiology

Ryan Fellowship 2019–2022
- Awarded to exceptional graduate students dedicated to the exploration of fundamental nanoscale science and to advancing this knowledge into practical applications of benefit to society

Professional Development Scholarship 2017
- Awarded by Northwestern University's Biomedical Engineering department for academic performance

Board of Trustees' Award 2017

- Awarded for graduating from Michigan State University with a perfect 4.0 GPA, ranking 1st in my class of 5,547

Graduation from Michigan State University with High Honors 2017

- Recognized for graduating in the top 6% of the class

A.W. Farrall Scholarship 2016

- The most prestigious scholarship awarded by Michigan State University's Biosystems Engineering department, based on academic achievement and leadership

Undergraduate Research Scholarship 2015–2016

- Research funding for 3 semesters awarded by Michigan State University's College of Agriculture and Natural Resources through a competitive application process

UURAF Grand Prize 2015

- First place poster presentation and research paper out of 700+ presenters

Professorial Assistantship 2013–2015

- Research funding for 4 semesters awarded for 36 ACT score and academic achievement

Distinguished Freshman Scholarship 2013

- Full tuition scholarship awarded from 2013 Michigan State University Alumni Distinguished Scholarship (ADS) Competition, ranked in top 3% of test scores out of ~1,200 invited competitors